



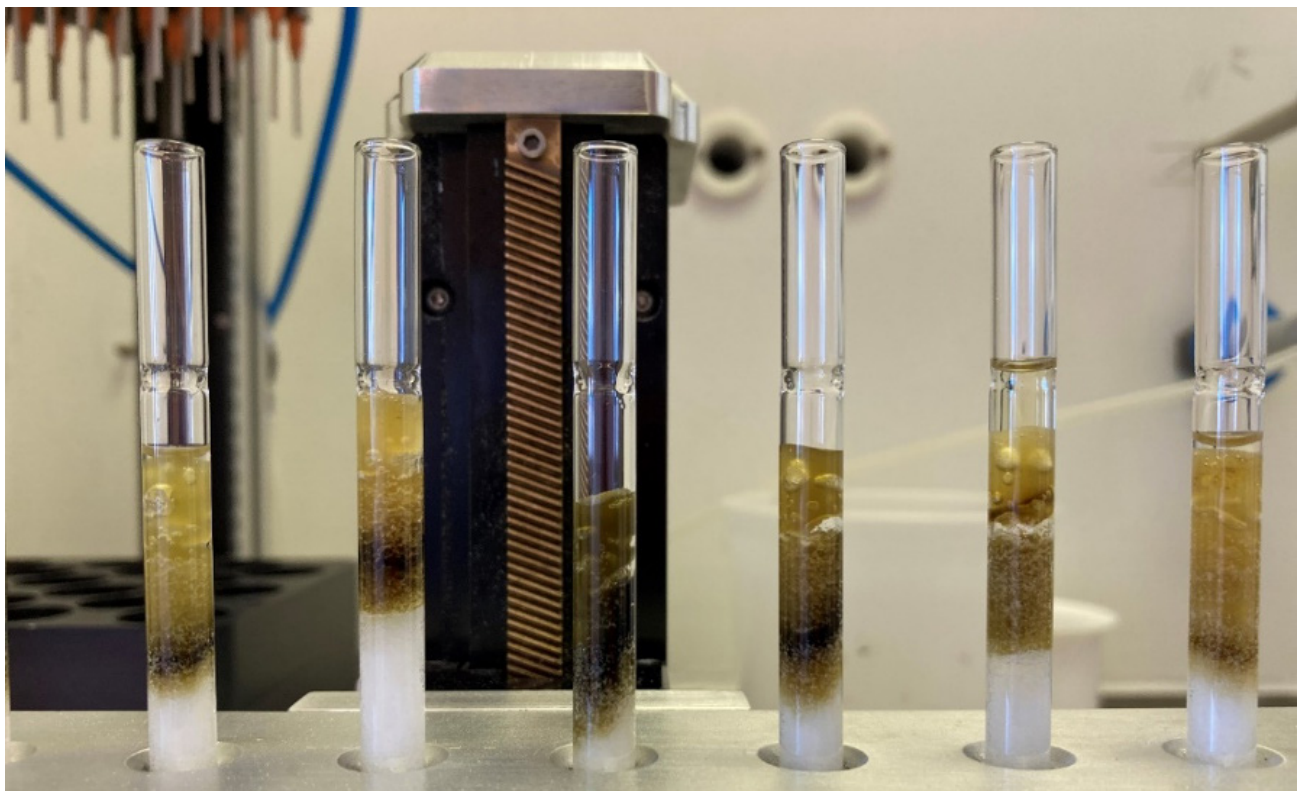
Stockholm
University

Bachelor Thesis

Degree Project in
Geochemistry 15 hp

Late Holocene climate and environmental reconstruction of Sumatra using organic geochemical proxies

Yolanda Liane Schankat



Stockholm 2022

Department of Geological Sciences
Stockholm University
SE-106 91 Stockholm

Late Holocene climate and environmental reconstruction of Sumatra using organic geochemical proxies

Yolanda Liane Schankat

Abstract

The branched and isoprenoid glycerol dialkyl glycerol tetraethers (br- resp. isoGDGTs) in a sediment core of lake Maninjau, West Sumatra, Indonesia, have been studied in this work. GDGTs are microbial derived membrane spanning lipids, which are providing information about past temperatures, pHs and other environmental conditions (oxygenation, humidity, etc.) through empirical distribution-based proxies and corresponding calibrations. The lake Maninjau is located in the Indo-Pacific Warm Pool (IPWP), which has a sea surface temperature above 28 °C and is supplying a large amount of latent heat and moisture to the atmosphere. The IPWP plays an important role in the global climate system and is affected by climate phenomena like the El Niño-Southern Oscillation (ENSO) and the Indian Monsoon. Improved insight and understanding of the climate dynamics of this globally important region is hampered by a lack of paleoclimate data. The radiocarbon analysis allowed the dating of the sediment core to a basal age of 2660-2340 cal yr BP. The MBT'_{5ME} proxy, which based on the methylation of the brGDGTs and the resulting mean annual air temperature reconstruction is mainly controlled by the ratio of un- and monocyclized tetra- to pentamethylated brGDGTs. The temperature reconstruction according to the MBT'_{5ME} proxy shows a warming trend of 1.63 °C over 2500 cal yr BP, whereas the temperature reconstruction according to another proxy based on H-shaped brGDGTs, does not. It is under discussion whether a temperature increase in the last 2500 cal yr BP in the southern latitudes close to the equator can be assumed at all. All pH reconstructions according to different variations of the cyclization of branched tetraether lipids (CBT proxy) show a slight increase of the pH value towards the sediment top with an average of 1.36 fluctuation over the studied 2500 cal yr BP. The lake surface temperature reconstructed by a proxy based on the extent of cyclization of isoprenoid tetraether lipids (TEX_{86}) shows no significant trend. An increase in the BIT index towards the sediment surface indicates an increased influence of terrestrial brGDGTs. This is possibly due to erosion in the lake Maninjau as a result of increased human activities, especially intensive aquaculture use. In summary, this study provides information about the distribution of GDGTs in lake Maninjau sediment and the applicability of temperature reconstructions by brGDGTs, H-GDGTs and isoGDGTs and other GDGTs based proxies. This study is one of the first investigations on the distribution of GDGTs in equatorial Asian lakes and thus can provide a contribution of paleoclimate and paleoenvironmental data for further studies.

Keywords

GDGTs
Mean annual air temperature
Lake surface temperature
Lake water pH
Lake Maninjau

Zusammenfassung

In dieser Arbeit wurden verzweigte und isoprenoide Glycerin-dialkyl-glycerin-tetraetherlipide (br- bzw. isoGDGTs) in einem Sedimentkern des Sees Maninjau, West-Sumatra, Indonesien, untersucht. GDGTs sind mikrobielle, membranumspannende Lipide, die durch empirische Verteilungsproxies und entsprechende Kalibrierungen Informationen über vergangene Temperaturen, pH-Werte und andere Umweltbedingungen (Sauerstoffgehalt, Feuchtigkeit usw.) liefern. Der See Maninjau liegt im Indo-Pazifischen Warmpool (IPWP), der eine Meeresoberflächentemperatur von über 28 °C aufweist und eine große Menge an latenter Wärme und Feuchtigkeit an die Atmosphäre abgibt. Der IPWP spielt somit eine wichtige Rolle im globalen Klimasystem und wird von Klimaphänomenen, wie der El-Niño-Southern Oscillation (ENSO) und dem indischen Monsun beeinflusst. Ein besserer Einblick und ein besseres Verständnis der Klimadynamik dieser weltweit wichtigen Region wird durch einen Mangel an Paläoklimadaten erschwert. Die Radiokohlenstoffanalyse ermöglichte die Datierung des Sedimentkerns auf ein Alter von 2660-2340 cal yr BP. Der MBT'_{5ME} Proxy, der auf der Methylierung der brGDGTs und der daraus resultierenden Rekonstruktion der mittleren jährlichen Lufttemperatur basiert, wird hauptsächlich durch das Verhältnis von un- und monozyklisierten tetra- zu pentamethylierten brGDGTs gesteuert. Die Temperaturrekonstruktion nach dem MBT'_{5ME} Proxy zeigt einen Erwärmungstrend von 1.63 °C über 2500 cal yr BP, während die Temperaturrekonstruktion nach einem anderen auf H-förmigen brGDGTs basierenden Proxy dies nicht tut. Fraglich ist, ob ein Temperaturanstieg in den letzten 2500 cal yr BP in den südlichen, äquatornahen Breiten überhaupt angenommen werden kann. Alle pH Rekonstruktionen nach verschiedenen Varianten der Zyklisierung von verzweigten Tetraetherlipiden (CBT-Proxy) zeigen einen leichten Anstieg des pH-Wertes zur Sedimentoberfläche mit einer durchschnittlichen Schwankung von 1.36 über den untersuchten Zeitraum von 2500 cal yr BP. Die Oberflächentemperatur des Sees, rekonstruiert durch einen Proxy, der auf dem Ausmaß der Zyklisierung von isoprenoiden Tetraetherlipiden (TEX₈₆) basiert, zeigt keinen eindeutigen Trend. Ein Anstieg des BIT Indexes zur Sedimentoberfläche deutet auf einen erhöhten Einfluss von terrestrischen brGDGTs hin. Dies ist möglicherweise auf die Erosion in den See Maninjau infolge der zunehmenden menschlichen Aktivitäten, insbesondere der intensiven Aquakultur, zurückzuführen. Zusammenfassend liefert diese Arbeit Informationen über die Verteilung von GDGTs im Sediment des Sees Maninjau und die Anwendbarkeit von Temperaturrekonstruktionen mittels brGDGTs, H-GDGTs und isoGDGTs sowie anderen GDGTs basierenden Proxies. Diese Studie ist eine der ersten Untersuchungen über die Verteilung von GDGTs in äquatorialen asiatischen Seen und kann einen Beitrag zu Paläoklima- und Paläoumweltdaten für weitere Studien leisten.

Acknowledgements

I would like to express special thanks to my supervisor Prof. Dr. Eva Lehndorff from the Department of Soil Ecology at the University of Bayreuth, who supported and encouraged me to write my Bachelor's thesis during a semester abroad in Stockholm and made this collaboration possible. Furthermore, I would like to thank my supervisors from Stockholm University Prof. Dr. Rienk Smittenberg and Petter Hällberg for their support, advice and for being available for any questions. I am grateful to have had the opportunity to get an introduction to paleoclimate and paleoenvironmental research, into laboratory and scientific work. Thanks to Julia Steinbach and Björn Eriksson for their help with laboratory and IT questions and Elisabeth Däcker for the organisation. Also, thanks to the entire Department of Geosciences and especially the IGV's geochemistry group at Stockholm University for the welcoming atmosphere during my two semesters there. I have positive memories of my time there.

Table of contents

Abstract.....	I
Keywords	I
Zusammenfassung.....	II
Acknowledgements	III
Abbreviations	VIII
1. Introduction and Goal of the Thesis.....	1
2. Background.....	3
2.1 GDGTs	3
2.1.1 Branched GDGTs	3
2.1.2 Isoprenoid GDGTs.....	5
2.1.3 GMGTs	6
2.2 About Lakes.....	6
2.3 Lake Sediments	6
3. Site Description	7
3.1 Lake Maninjau	7
3.2 Current Climate	8
4. Material and Methodology	9
4.1 Subsampling and Sample Preparation	9
4.2 Lipid Extraction	10
4.3 Fractionations	10
4.4 Sub-sample Preparation for HPLC-APCI-MS Analyses	10
4.5 HPLC-APCI-MS Analysis and Quantifications.....	10
4.6 Chronology.....	11
4.7 Paleotemperature and Paleoenvironmental Proxy Calculations.....	11
5. Results.....	14
5.1 Maninjau Lake Sediment Core Description	14
5.2 Depth-Age Model and Sedimentation	15
5.3 Distribution of GDGTs in Lake Maninjau.....	16
5.3.1 Fractional Abundance of brGDGTs	16
5.3.2 Fractional Abundance of brGMGTs.....	17
5.3.3 Fractional Abundance of isoGDGTs	17
5.3.4 Differences between the two HPLC-APCI-MS Measurements	18
5.4 Derived Proxies of Branched Tetraether	19
5.4.1 Methylation of Branched Tetraether.....	19
5.4.2 Mean Annual Air Reconstruction according to the MBT Proxy	20
5.4.3 Cyclization of Branched Tetraether	20
5.4.4 pH Reconstruction according to the CBT Proxy.....	21
5.4.5 Impact of Soil Organic Matter	22

5.4.6	Impact of Isomerization.....	23
5.5	Derived Proxies of Isoprenoid Tetraethers	23
5.5.1	Tetraether Index of 86 Carbons	23
5.5.2	Lake Surface Temperature Reconstruction according to the TEX ₈₆ Proxy.....	24
5.5.3	Impacts on the TEX ₈₆ Proxy	25
6.	Discussion.....	26
6.1	Interpretation of Branched Tetraethers Proxies	26
6.1.1	Fractional Abundance of brGDGTs in relation to MBT' _{5ME}	26
6.1.2	Fractional Abundance of brGMGTs in relation to brGMGTI.....	27
6.1.3	Mean Annual Air Temperature Reconstructions according to the MBT' _{5ME} Proxy	29
6.1.4	Fractional Abundance of brGDGTs in relation to CBT.....	30
6.1.5	pH Reconstructions according to the CBT Proxy	32
6.1.6	Impact of Soil Organic Matter	33
6.1.7	Impact of Isomerization.....	34
6.2	Interpretation of Isoprenoid Tetraethers Proxies.....	35
6.2.1	Fractional Abundance of isoGDGTs according to TEX ₈₆ Proxy.....	35
6.2.2	Lake Surface Temperature Reconstructions according to the TEX ₈₆ Proxy ...	35
6.3	Constraints on the Results.....	38
6.4	Relevance for the Lake Maninjau	38
7.	Conclusion and Future Prospects.....	39
	References.....	IX
	Appendix	XVIII
	Declaration	XXVII

List of Tables and Figures

Table 1: Settings of the TSQ Quantum mass spectrometer	11
Table 2: ¹⁴ C radiocarbon data from three samples of lake Maninjau sediment core.....	15
Table 3: MBT' _{5ME} proxy	XVIII
Table 4: brGMGTI proxy	XIX
Table 5: CBT proxy	XX
Table 6: CBT' _{5ME} proxy.....	XXI
Table 7: CBT _{peat} proxy	XXIII
Table 8: CBT' proxy.....	XXIV
Table 9: TEX ₈₆ proxy	XXV
Figure 1: Indo-Pacific Warm Pool (IPWP).....	1
Figure 2: Chemical structure formula of brGDGTs.....	4
Figure 3: Chemical structure formula of isoGDGTs	5
Figure 4: Chemical structure formula of brGMGTs and isoGMGTs.....	6
Figure 5: Map of Sumatra, Indonesia and the study location lake Maninjau.....	8
Figure 6: Average temperatures of Maninjau over the course of the year	9
Figure 7: Picture of the Man-18-44A sediment core from the lake Maninjau	15
Figure 8: a) Depth-age model, b) Sedimentation rate	16
Figure 9: Fractional abundance of the detected brGDGTs.....	17
Figure 10: Fractional abundance of the detected brGMGTs	17
Figure 11: Fractional abundance of the detected isoGDGTs and one isoGMGT.....	18
Figure 12: Cross plots of the fractional abundance of the GDGTs	19
Figure 13: a) MBT' _{5ME} index, b) brGMGTI index.....	19
Figure 14: Mean air temperature reconstructions according to MBT' _{5ME} and brGMGTI.....	20
Figure 15: Cyclization of branched tetraethers calculated through different CBT proxies.....	21
Figure 16: pH reconstructions according to CBT proxies	22
Figure 17: a) BIT index, b) brGDGT/isoGDGT ratio	22
Figure 18: a) The isomerization index IR _{6ME} , b) IBT index.....	23
Figure 19: The distribution of the TEX ₈₆ proxy	24
Figure 20: Lake surface water reconstruction according to TEX ₈₆ proxy	25
Figure 21: a) Methane index, b) GDGT-0/crenarchaeol	25
Figure 22: The fractional abundance of brGDGTs plotted against the MBT' _{5ME} proxy.....	27
Figure 23: The fractional abundance of three brGMGTs plotted against brGMGTI proxy.....	28

Figure 24: The fractional abundance of three brGMGTs plotted against MBT' _{5ME} proxy	28
Figure 25: Mean annual air temperature reconstructions plotted against ¹⁴ C age	30
Figure 26: The fractional abundance of brGDGTs plotted against the CBT proxy	32
Figure 27: a) Relation between IR _{6ME} and MBT' _{5ME} , b) Relation between IBT and MBT' _{5ME} ..	34
Figure 28: a) Relation between IR _{6ME} and CBT, b) Relation between IBT and CBT	35
Figure 29: The fractional abundance of isoGDGTs plotted against TEX ₈₆ proxy	35
Figure 30: a) Relation BIT and TEX ₈₆ , b) Relation br-/isoGDGT and TEX ₈₆	36

Abbreviations

A.	Appendix
ALST	Annual lake surface temperature
AMS	Accelerator mass spectrometer
AOM	Anaerobic oxidation of methane
APCI	Atmospheric pressure chemical ionization
BIT index	Branched to isoprenoid tetraether index
Cal yr BP	Calibrated years before present, before 1950
CBT	Cyclization of branched tetraether
CE	Common Era
DCM	Dichloromethane
ECMWF	European Centre for Medium-Range Weather Forecasts
ENSO	El Niño-Southern Oscillation
FA	Fractional abundance
GDGTs	Glycerol dialkyl glycerol tetraether
GMGTs	Glycerol monoalkyl glycerol tetraethers
HEX	Hexane
HILIC	Hydrophilic interaction liquid chromatography
HPLC	High performance liquid chromatography
IBT	Isomerization of branched tetraethers
IPA	Isopropyl alcohol
IPPs	Isopentyl pyrophosphates
IPWP	Indo-Pacific Warm Pool
IR	Isomerization ratio
IRMS	Isotope ratio mass spectrometry
ITCZ	Intertropical Convergence Zone
LST	Lake surface temperature
MAAT	Mean annual air temperature
Man-1	First HPLC-APCI-MS measurement of the Man-18-44A samples
Man-2	Second HPLC-APCI-MS measurement of the Man-18-44A samples
MAT	Mean air temperature
MBT	Methylation of branched tetraether
MeOH	Methanol
MI	Methane index
MS	Mass spectrometer
NMR	Nuclear magnetic resonance
PTFE	Polytetrafluoroethylene
Ref	Relative centrifugal force
SD	Standard deviation
SRB	Sulphate reducing bacteria
SST	Sea surface temperature
TEX ₈₆	Tetraether index of 86 carbons
TLE	Total liquid lipid
\bar{x}	Mean

1. Introduction and Goal of the Thesis

The study of past climatic conditions is crucial to better understand past climates through reconstructions and to better predict future ones. The investigation of paleoclimate within the Indo-Pacific Warm Pool (IPWP), which covers an area of $> 30 \times 10^6 \text{ km}^2$, is critical because it plays an important role in the global climate system (Figure 1), (De Deckker 2016). It provides a large amount of latent heat and moisture that rises to higher atmospheric layers via deep atmospheric convection. The IPWP is defined as having sea surface temperatures (SST) above 28°C and is also described as the "steam engine" of the world (Dang et al. 2020; Chabangborn et al. 2018; Hällberg et al. 2022a). The IPWP is located between Southeast Asia and Australia in the eastern Indian Ocean and the western Pacific Ocean, which includes the studied lake Maninjau (Figure 1).

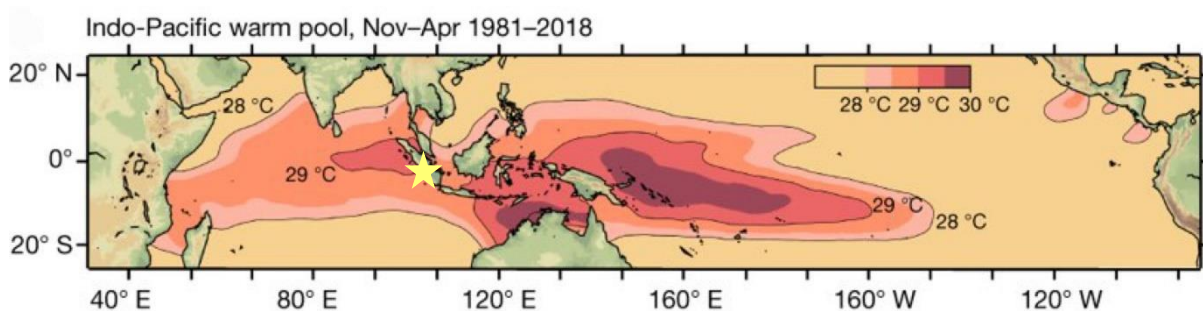


Figure 1: Indo-Pacific Warm Pool (IPWP) expansion with average sea surface temperatures from April to November in the period 1981-2018 (Roxy et al. 2019). The seawater area with sea surface temperature (SST) above 28°C includes parts of the western Pacific Ocean and the eastern Indian Ocean. The yellow star marks the location of lake Maninjau.

The IPWP is influenced by the Indian Monsoon and the El Niño-Southern Oscillation (ENSO), which affects Sumatra in the form of droughts or heavy rainfall, but directly and indirectly affects half the global population. The IPWP is also influenced by the twice-yearly latitudinal shift of the Intertropical Convergence Zone (ITCZ), which causes fluctuations in the Walker circulation, and the monsoon systems and also affects ENSO (Hällberg et al. 2022a). The ITCZ is where of southern and northern hemisphere trade winds convergence. Another important aspect of the tropical climate is, the East Asian monsoon system, which transports a lot of heat energy and moisture to the higher latitudes, and this also significantly affects the rainfall pattern on Sumatra (Chabangborn and Wohlfarth 2014). Over the last decades, the IPWP has doubled in size during 1981-2018 compared to 1900-1980 (Roxy et al. 2019). The increased variability of ENSO, among other things, may lead to a change in the hydrological cycle and increases possibilities for droughts (Liu et al. 2019; Cai et al. 2018). These would enhance the risk of forest fires and possibly turn a carbon sink into a source (Dommain et al. 2014). A variety of climatic interactions have feedback effects on each other, which only makes it more important to study past climate. During the Early and Middle Holocene, warming of the western equatorial thermocline in the Pacific is thought to have been associated with an increase in the W-E thermal gradient, resulting in a strengthening of the Walker circulation and a reduction in ENSO activity (Rosenthal et al. 2013; Marcott et al. 2013). On the other hand, the equatorial Pacific W-E gradient was reduced by greenhouse warming in the 20th century and presumably, the Walker circulation slowed down and the ENSO variability increased (Liu et al. 2019; Cai et al. 2018; Cai et al. 2019). In the case of Sumatra, in El-Niño years, the low-pressure area near the ground over South-East Asia transforms into a high-pressure area near

the ground. As a result of the equalization of the pressure areas, rather dry weather conditions prevail compared to normal conditions. The convection and cloud formation that normally occurs in South-East Asia is much reduced. The lower cloud cover tends to provide warmer temperatures, as shortwave solar radiation can reach the earth's surface unimpeded. Cloud cover reflects, in part, the shortwave radiation coming from the sun and thus has the consequence of lower surface temperatures. This would be the case with a low-pressure area near the ground over South-East-Asia, as it would be the case under "normal conditions" or in La-Niña years.

A lot of climate reconstructions have been made from ice sheets and deep-sea sediments, but there is a lack of research from continental equatorial areas to study the history of the IPWP, ENSO and Indian Monsoon (Otto-Bliesner et al. 2006; Blome et al. 2012; Loomis et al. 2017). Many paleoclimate reconstructions depend on the stable isotopic composition of carbonates (speleothems, deep-sea sediments) or ice, but others use lipid biomarker proxies. Under lipid biomarkers, organic molecular fossils are understood, which were components of former living organisms of e.g., plants, bacteria or archaea and are preserved in sediment or soil (Castañeda and Schouten 2011). Their molecular remains, such as plant waxes or membrane lipids, can be used as indicators of certain processes, organisms or abiotic and biotic conditions (Killips and Killips 2005). Organic geochemical proxies developed from lipid biomarkers are widely used in paleoclimate and paleoenvironmental research. In this thesis, glycerol dialkyl glycerol tetraethers (GDGTs) extracted and analysed from lacustrine sediment from Sumatra are used as lipid biomarkers. Based on the distribution of microbially derived GDGTs, proxies are applied and paleoclimate and paleoenvironmental data are generated. GDGTs have the potential to record past temperature changes and reconstruct environmental conditions.

The aim of this work was to produce a climatic and environmental reconstruction of the late Holocene of Sumatra. Using organic geochemical proxies based on a sediment core from lake Maninjau, a reconstruction of about 2500 cal yr BP was created. It was also investigated if the lake biomarkers recorded the significantly increasing anthropogenic activities around the lake in modern times. Through subsampling and lipid extraction, an organic chemical lipid biomarker analysis was performed. The relative distribution of microbial derived GDGTs was investigated and analysed by HPLC-APCI-MS analysis.

Among other aspects, in this thesis the temperature behaviour in the late Holocene on Sumatra is studied. Global proxy records of the late Holocene suggest a long-term cooling trend of the global ocean surface (Liu et al. 2014). For instance, by using different proxies, such as alkenone distributions, and Mg/Ca ratios and $\delta^{18}\text{O}$ values of foraminifera, a cooling trend of the SST can be observed for the Mediterranean Sea, Gulf of Mexico, northern Atlantic and the Labrador Sea before Newfoundland in the late Holocene (Marriner et al. 2022; Richey et al. 2011; Ayache et al. 2018; Orme et al. 2021). A long-term SST cooling in the global mean of 0.08 °C per 1000 years was detected over the Holocene (Kaufman et al. 2020). The SST cooling trend can be associated with the variation of solar forcing, which results from orbital variations (Milankovitch cycles) due to the changing gravitational attractions between the planets (Berner et al. 2011). But there is a discrepancy between the proxy records, which calculate a long-term cooling trend, and climate models, which simulate a global long-term warming trend, also described as the "Holocene temperature conundrum" (Liu et al. 2014). Nevertheless, from this, it can be a hypothesis that terrestrial temperatures on Sumatra also follow a cooling trend and decrease over the last 2500 years BP, as is the case for SST in the late Holocene in the examples given.

2. Background

2.1 GDGTs

Glycerol dialkyl glycerol tetraethers (GDGTs) are membrane spanning lipids of microbial origin. They are among the most abundant and ubiquitously occurring lipids on Earth (Schouten et al. 2013). They are composed of two carbon chains, which are bound on both ends to glycerol by ether bonds (Schouten et al. 2007). They vary in the number of cyclopentane rings and in the amount and position of methyl groups (De Jonge et al. 2013). The GDGTs can be divided into two main groups, the bacterial synthesised branched GDGTs (brGDGTs) (Figure 2) and the archaeal synthesised isoprenoid GDGTs (isoGDGTs) (Figure 3), which are distinguished by their carbon skeletal structure. They occur in almost all types of environments including soil, peat, lacustrine water column and sediments, modern hot springs, loess, stalagmites, marine water column and deeply buried sediments (Sinninghe Damsté et al. 2009; Yang et al. 2011; Schouten et al. 2000; Schouten et al. 2003; Schouten et al. 2007; Huguet et al. 2012). GDGTs are used as lipid biomarkers to study past climates and are therefore an important tool in paleoenvironmental and paleoclimate research (Baxter et al. 2021). Conclusions on past temperatures and pH values are possible, as the GDGT distribution in the membrane of bacteria and archaea responds to growth conditions, likely mainly temperature and pH values. As environmental conditions change, the membrane composition changes to maintain functions such as membrane permeability (Qin et al. 2015).

The lipid composition of GDGTs is quite well known by now (De Jonge et al. 2013; Schouten et al. 2013). (Weijers et al. 2006a), concluded a bacterial origin based on the stereochemistry of the glycerol moieties. *Acidobacterium solibacter usitatus*, Proteobacteria, Chlorobi and among others could be identified as a brGDGT producing bacteria (Chen et al. 2022; Halamka et al. 2022; Raberg et al. 2021; Van Bree et al. 2020). For a long time, the origin of brGDGTs was assumed to be purely terrestrial, and the occurrence of brGDGTs in lakes was explained by the erosion of soils from the catchment area that were washed into the lake (Blaga et al. 2009). Production of in situ brGDGTs could later be verified in several lakes (Van Bree et al. 2020; Liang et al. 2022; Baxter et al. 2021). But the abundance of brGDGTs in terrestrial systems is clearly higher than in marine or lacustrine settings (Schouten et al. 2013). The source of the isoGDGTs synthesising archaea could be identified as ammonium oxidising archaea of the phylum Thaumarchaeota (Bale et al. 2019). Previously, only isoGDGT synthesising archaea in extreme environments were assumed. Now isoGDGTs synthesising archaea have been detected in mesophilic marine and lacustrine environments and not exclusively in environments with extreme pH values and high salinity (Schouten et al. 2013).

2.1.1 Branched GDGTs

A subclassification of GDGTs are the bacterially synthesised brGDGTs with a 1,2-sn-glycerol stereochemistry (Figure 2). The different brGDGTs vary in the number of cyclopentane rings on the straight alkyl core chains, which are formed by internal cyclization (Sinninghe Damsté et al. 2000). The investigated brGDGTs have 0-2 cyclopentane rings, which are described by the letters a-c (a = absence of cyclopentane rings/uncyclized, b = 1 cyclopentane ring/monocyclized, c = 2 cyclopentane rings/bicyclized) in abbreviated notation. Furthermore, a distinction is made between tetra-, penta- and hexamethylated brGDGTs, which are abbreviated with the roman numerals I-III. If the position of the methyl group varies, it is referred to as an isomer of the respective brGDGT and marked with a prime notation. This work is divided into isomers with the methyl groups at different carbon atoms. For the tetramethylated

brGDGTs, the methyl groups are located on both chains at the 13th and 16th carbon, isomers are not known. In the case of pentamethylated brGDGTs, the methyl groups are on one chain at the central 13th and 16th carbon atoms and on the other alkyl chain at the 5th, 13th and 16th carbon atom. 6-methyl isomers have one methyl group at the 6th carbon instead of at the 5th carbon atom, designated as 6-methyl GDGTs and in shorthand notation provided with a prime notation (e.g., IIa'). In hexamethylated brGDGTs, the methyl groups of both chains are located at the 5th, 13th and 16th carbon. In the case of the 6-methyl brGDGTs isomers, both methyl groups of both chains are located on the 6th carbon (e.g., IIIa'). There is also a known isomer with one methyl group on the 5th and the other on the 6th carbon (e.g., IIIa'') (Weber et al. 2015). The last isomer variant investigated in the work is the one with a methyl group on the 7th carbon (IIIa''').

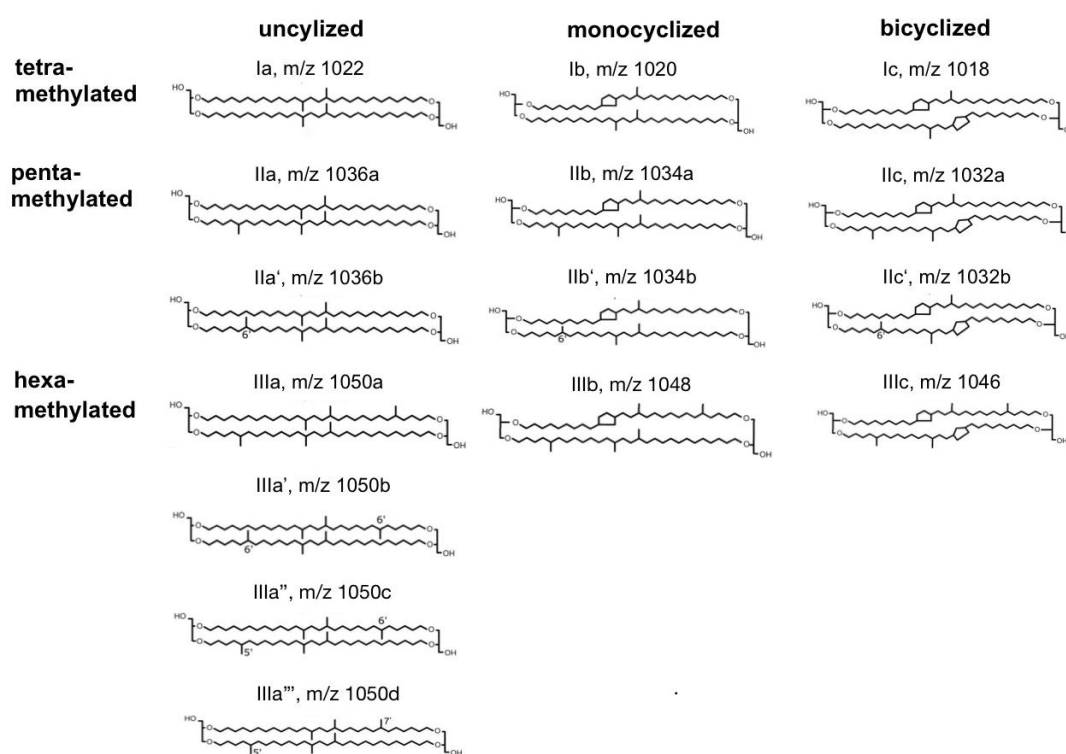


Figure 2: Chemical structure formula of brGDGTs and their mass-to-charge ratios (m/z). Figure redrawn from (Ratray and Smittenberg 2020).

BrGDGTs were discovered in 1979 in the 47-48 million year old Messel shale (Chappe et al. 1979; UNESCO World Heritage 2022). Detailed knowledge was later obtained on the basis of mass spectrometry, nuclear magnetic resonance (NMR) spectroscopy and by released products after chemical degradation (Sinninghe Damsté et al. 2000; Schouten et al. 2000). GDGTs play a crucial role in the physiology of the bacterial membrane and can be influenced by many external factors (Raberg et al. 2022). The investigated brGDGTs with mass over charge ratios (m/z) 1018-1050 are abundant in mesophilic, terrestrial settings, such as soil and peat (Naafs et al. 2019). Originally, it was hypothesised that the empirical relationships between the brGDGTs distribution and the transformation parameters were a physiological adaptation of the original bacteria to the fluctuations in external temperature and pH (Weijers et al. 2007). However, recent studies show that brGDGT distribution is also related to changes in microbial community composition, which would make brGDGT distribution an indirect indicator of environmental parameters (De Jonge et al. 2019; De Jonge et al. 2021; Weber et

al. 2018; Wu et al. 2021; Van Bree et al. 2020). It is essential for the accuracy and reliability of the results to find out whether microorganisms react to changing environmental conditions with a direct physiological response, such as a change in membrane structure, or with an indirect restructuring of the microbial community (De Jonge et al. 2021). BrGDGTs have been found to be abundant in the anoxic part of peat, suggesting that synthesis by anaerobic bacteria is likely (Weijers et al. 2006a), however their omnipresence also in oxic conditions indicates that this is facultative (Schouten et al. 2013).

2.1.2 Isoprenoid GDGTs

In contrast to brGDGTs, isoGDGTs are synthesised by archaea with 2,3-sn-glycerol stereochemistry (Figure 3). Archaea synthesise isoGDGTs rather than straight carbon skeletons (Schouten et al. 2013). IsoGDGTs differ in the number of cyclopentane rings, as can be seen in (Figure 3). Isomers differ in the position of the ring and are marked with a prime notation (not shown). Furthermore, crenarchaeol and a crenarchaeol regioisomer with four cyclopentane moieties and one cyclohexane moiety exist.

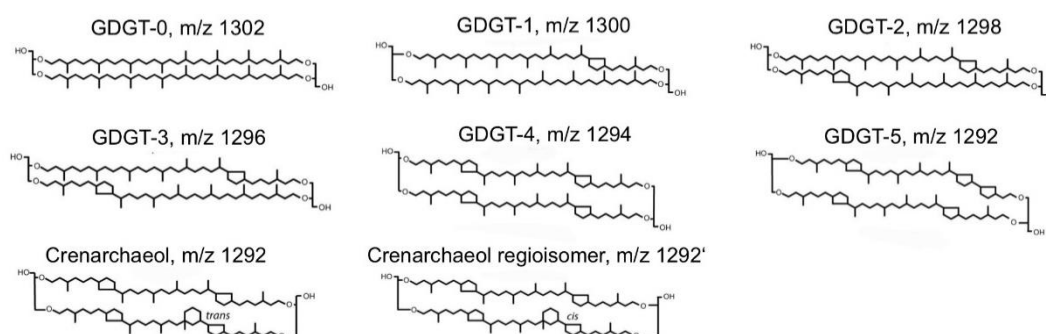


Figure 3: Chemical structure formula of isoGDGTs and their mass-to-charge ratios (m/z). Figure redrawn from (Ratray and Smittenberg 2020).

GDGTs-0 to -8 were first identified in extremophilic archaea by NMR spectroscopy by (De Rosa et al. 1977; Rosa and Gambacorta 1988). However, (Heathcock et al. 1985) had identified the stereochemistry of GDGT-0. In subsequent decades, isoGDGTs were found to be produced by a wide range of archaea and to be ubiquitous in natural settings (Schouten et al. 2013; Schouten et al. 2000; Pearson and Ingalls 2013). GDGT-0 is one of the most commonly occurring GDGTs, it can be found in all archaeal groups except the halophilic ones (Schouten et al. 2013). Among the GDGT-0 synthesising archaea are some methanotrophs that perform anaerobic methane oxidation (AOM), found for example in carbonates (Pape et al. 2005). GDGTs-1-4 have been cultivated in the archaeal subgroup Thaumarchaeota and are found ubiquitously in the environment (Sinninghe Damsté et al. 2012; Kim et al. 2008; Kim et al. 2012; Schouten et al. 2008a). However, they usually occur in much lower abundance than GDGT-0 and crenarchaeol (Pancost et al. 2001).

GDGTs with more than five cyclopentane rings are mainly found in high temperature environments, such as hot springs (Schouten et al. 2007). Crenarchaeol belongs to the most ubiquitous GDGTs (Sinninghe Damsté et al. 2002). The cyclohexane moiety in addition to the four cyclohexane rings is a feature that has not been found in any previously archaeal GDGTs (Sinninghe Damsté et al. 2002). Notably, crenarchaeol and the crenarchaeol regioisomer is biosynthesised by ammonia oxidising Thaumarchaeota (Schouten et al. 2013; Sinninghe Damsté et al. 2002), and its presence can thus be indicative of oxic conditions (Naafs et al. 2019).

Many Thaumarchaeota are often chemolithoautotrophic and derive their energy, for example, from the oxidation of ammonia. As nitrifiers, they make an important contribution to the nitrogen cycle (Inglis and Tierney 2020). The chemical composition of the Thaumarchaeota membrane regulates so that its physical properties are best adapted to a specific temperature (Sinninghe Damsté et al. 2018).

2.1.3 GMGTs

Glycerol monoalkyl glycerol tetraethers (GMGTs) are a group of membrane spanning lipids where the two biphytanic skeletons are covalently linked (Figure 4). Because of their shape, they are also called H-shaped GDGTs (H-GDGTs). The link is located between a methyl group and the aliphatic chain, but the exact position is still unknown (Morii et al. 1998; Baxter et al. 2021). It is hypothesised that the carbon link between the two chains increases the archaeal membrane stability of the GMGTs and is an adaptation to higher temperatures (Morii et al. 1998; Schouten et al. 2008a). The GMGTs also vary in the degree of methylation GMGTs and are divided into branched GMGTs (brGMGTs) and isoprenoid GMGTs (isoGMGTs) (Baxter et al. 2021). IsoGMGTs were first discovered in culture for extremophile Euryarchaeota and Thaumarchaeota in 1998 (Morii et al. 1998). In the last decade, brGMGTs have been gradually detected (Liu et al. 2012; Naafs et al. 2019). In natural settings, GMGTs were first found synthesised by archaea under extreme environmental conditions (Morii et al. 1998). Later, GMGTs were also found in normal lacustrine and marine sediments, suggesting that certain non-extremophilic archaea also synthesise GMGTs (Schouten et al. 2008b).

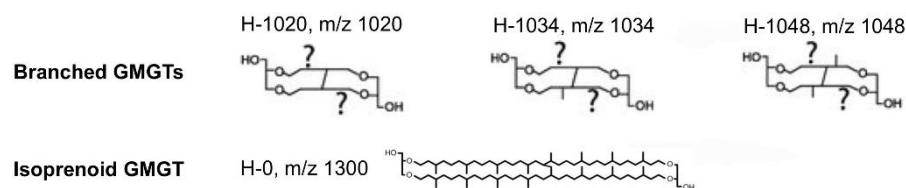


Figure 4: Chemical structure formula of brGMGTs and isoGMGTs and their mass-to-charge ratios (m/z). Figure redrawn from (Naafs et al. 2018; Rattray and Smittenberg 2020).

2.2 About Lakes

Lake sediments are often used as records of past environmental and climate changes. To interpret these records, some limnological knowledge is also required. Tropical lakes can be thermally stratified, typically consisting of a shallow, warm upper surface layer, the epilimnion, the underlying middle layer where the temperature declines rapidly, the metalimnion, and a deeper, cooler water body, the hypolimnion (Bouvet de la Maisonneuve et al. 2019). Complete mixing of the water layers can happen up to twice a year but typically less frequently or not at all in tropical areas (Bouvet de la Maisonneuve et al. 2019). The lake water level increases due to precipitation, inflow from the watershed and decreases due to outflow and evaporation. The concentrations of oxygen and nutrients are an important factor in the description of the lake, on which phytoplankton production and the trophic relationships that build on it depends (Bouvet de la Maisonneuve et al. 2019).

2.3 Lake Sediments

Lake sediments can provide paleoclimatic and paleoenvironmental data and contribute to reconstructing and better understanding variations and interactions like the monsoon, ENSO,

floods and droughts (Bouvet de la Maisonneuve et al. 2019). Generally, sediment is defined as particles resulting from weathering of rocks, biological material, such as plant residue materials or dead organisms and chemical deposits developed by a sedimentation process (Akmal et al. 2021). In lake sediments, signs of geological processes, such as volcanic eruptions, floods or landslides, and environmental changes, such as climate change, land use change and other human activities can also be archived (Beck 2009; Waldmann et al. 2011; Smith et al. 2013; Kremer et al. 2012; Coviaga et al. 2018). There is often also high organic matter storage in lake sediments, where possible lipid biomarkers such as GDGTs can be found (Cohen 2003). GDGTs can be found in many natural settings, but care must be taken that patterns and correlations in the abundance of GDGTs cannot be applied to all environments. For example, in small lakes, the occurrence of Thaumarchaeota is often very low compared to marine settings and larger lakes (Powers et al. 2010). In soil, the distribution of GDGTs is mainly determined by mean annual air temperature and pH, whereas in lake sediment the influences are similar (Russell et al. 2018). The chemical and physical limnology influences the distribution of microorganisms in the water column and the sediment in the lake (Powers et al. 2010). Particularly in deep tropical lakes, it should be noted that due to the stable stratification of the warmer water column, the lake is often never completely mixed because of the low seasonal temperature fluctuations, and this can lead to a permanent anoxic hypolimnion, which affects the type and distribution of microorganisms (Powers et al. 2010).

3. Site Description

3.1 Lake Maninjau

The caldera lake Maninjau (0°19'S 100°12'E) is one of the largest lakes of Sumatra (Bouvet de la Maisonneuve et al. 2019) (Figure 5). It is located in the Indonesian Highlands of West Sumatra. The lake was formed by the volcanic activity of Mount Maninjau Purba about 60,000 years ago (Akmal et al. 2021). There are still some active volcanoes in the area (e.g., Singgalang, Marapi, Talang), because the active Sumatran strike slip fault runs along it. Thus, the bathymetry of lake Maninjau mostly resulted from volcanic processes (Bouvet de la Maisonneuve et al. 2019). The water surface of lake Maninjau is 459 m above normal zero (Lehmusluoto 1997). The surface area of the lake is 99.5 km² and has a maximum depth of 169 m and an average depth of 100 m (Bouvet de la Maisonneuve et al. 2019; Akmal et al. 2021). There is an outlet to the west at Muko Muko through the Antukan (Sikikis) River (Lehmusluoto 1997) but there is no major inflow into the lake, so it is mainly recharged by precipitation (Cohen 2003).

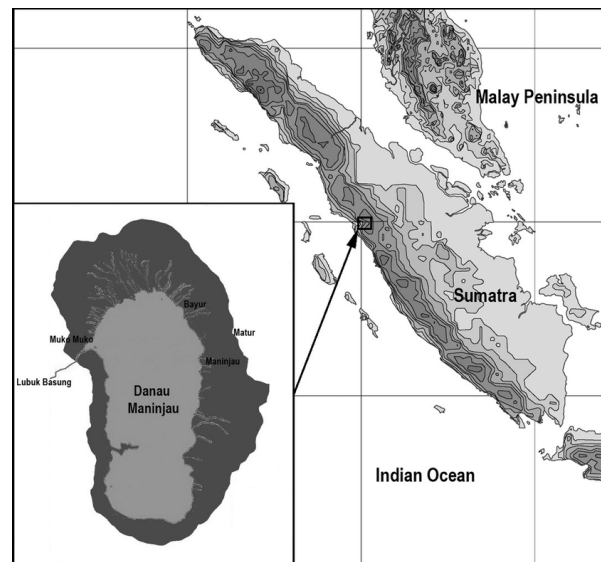


Figure 5: Map of Sumatra, Indonesia and the study location lake Maninjau (Milto and Bezman-Moseyko 2021).

The sediments of lake Maninjau are characterised by caldera collapse material that erodes from the sides and accumulates at the bottom of the lake (Prasetyo et al. 2022; Cohen 2003). The sediments of lake Maninjau are characterized by iron, silica and titanium (Prasetyo et al. 2022; Akmal et al. 2021). Since sediments only enter the lake through surface runoff or wind transport, the sedimentation rate is low (Bouvet de la Maisonneuve et al. 2019). (Bouvet de la Maisonneuve et al. 2019) estimates the minimum water residence time to be about 50 years with the assumptions of annual precipitation of 3122 mm/yr on average in Bukittinggi, located 30 km from lake Maninjau (Climate-data Bukittinggi 2022) and thus a minimum inflow of 0.3 km³/yr is implied.

Since 1992, the water quality in lake Maninjau has decreased due to an increase in nutrient inputs and organic material (Junaidi 2014). The degradation came mainly with the development of aquaculture and the since then developing infrastructures such as settlements, tourism, and hydropower. Between 2008 and 2009, the number of fish cages increased by 300 % for economic reasons, which had a significant impact on water quality (Yodfiatfinda 2017). 2012 exceeded the carrying capacity of the number of swimming-net fish cages again with a as result that the water quality degraded even more (Junaidi 2014). Lake Maninjau is vulnerable to eutrophication due to low water flow in and out of it and the increasing infrastructure and economic use of the lake (Bouvet de la Maisonneuve et al. 2019). The lake is also threatened by algae blooming, which can be attributed to the high population density, nearby agriculture, and fish farming (Bouvet de la Maisonneuve et al. 2019). Algae blooming reduces light penetration and oxygen levels. The first signs of cultural eutrophication were observed already in 1997 (Lehmusluoto 1997). Particularly striking is the green colour of the water and the total absence of fish record during the onset of the dry season (Bouvet de la Maisonneuve et al. 2019).

3.2 Current Climate

The current annual average temperature at lake Maninjau is 22.6 °C averaged from 21.6 °C (Climate-data Maninjau 2022) and 23.5 °C (Weatherspark Maninjau 2022) (Figure 6). The higher average annual temperature for (Climate-data Maninjau 2022) is because temperature data since 1991 and for (Weatherspark Maninjau 2022) already since 1956 are taken into

account. The temperature is relatively constant over the year with a fluctuation of $< 2\text{ }^{\circ}\text{C}$ in the average temperature.

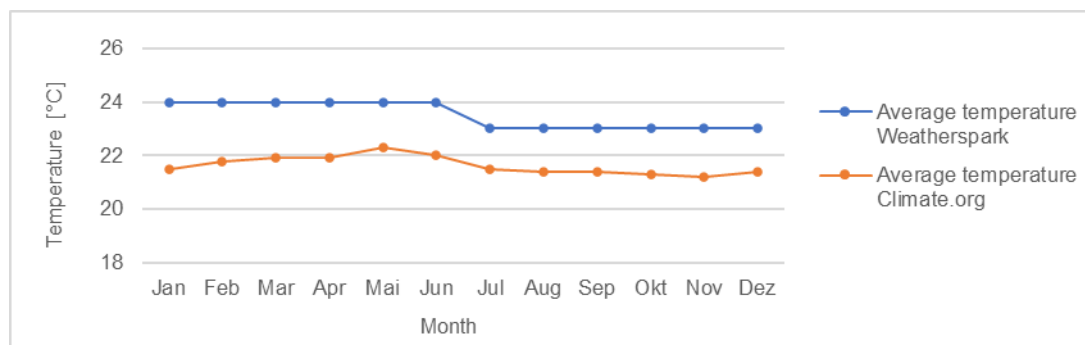


Figure 6: Average temperatures of Maninjau over the course of the year from 1956-2022 (blue line) (Weatherspark Maninjau 2022). The data are obtained from two weather stations Airport weather stations, Sultan Syarif Kasim International Airport, Riau, Indonesia (METAR), since 2011 and NOAA's Integrated Surface Database (ISD), since 1956. (Climate-data Maninjau 2022) provided average temperatures from 1991-2021 (orange line) based on ECMWF data.

Looking at the temperatures of Maninjau over the course of the year, no seasons can be identified, but the precipitation distribution shows variations over the year. November is the highest precipitation month with an average of 395 mm and the lowest precipitation month is June with an average of 189 mm over the period 1956-2022 (Weatherspark Maninjau 2022). Precipitation falls on average 19.2 days in November and 9.8 days in June (Weatherspark Maninjau 2022). Independent information on pH values, alkalinity, or dissolved oxygen content of Maninjau seawater are not known.

4. Material and Methodology

4.1 Subsampling and Sample Preparation

The lake sediment being studied was taken from lake Maninjau in Sumatra by Caroline Bouvet de la Maisonneuve's group from Nanyang Technological University in Singapore and with the assistance from Dr. Hamdi Rifai and his students from Padang State (University Negeri Padang) in Indonesia in 2019. The lake sediment core Man-18-44A of 42 cm was divided into 50 different samples. The division was based on different layers, which resulted in subdivisions of 0.3-1 cm thickness. The layers differed in colour or structure. The divided samples of lake Maninjau were stored in pre-cleaned 40 ml vials covered with perforated aluminium foil in freezer at $-18\text{ }^{\circ}\text{C}$ overnight. The samples were then freeze dried for 2.5 days by using a Scan Vac Cool Safe freeze dryer. Through the process, water was removed from the samples by reducing the pressure, the water passes from the frozen phase into the gaseous phase and thus evaporates. The conditions for this were achieved by a vacuum pump resulting in a vacuum of around 1 mbar, while a cooling coil held at $-102\text{ }^{\circ}\text{C}$ trapped the water vapour. The freeze-dried samples were ground into a fine powder using a Retsch-Mill. The grinding process was carried out at half power for 4 minutes. In addition, the samples were weighed. $2/3$ of the samples were used for the following laboratory steps and $1/3$ were stored.

4.2 Lipid Extraction

Lipid extraction was carried out using a mixture of dichloromethane (DCM) and methanol (MeOH) in a ratio of 9:1. The total 10 ml mixture added to each sample was mixed for a few seconds with the aid of a vortex and then sonicated for 10 min without heat. The sonication facilitates the extraction of lipids by mixing the particles with the added solution through ultrasonic sound waves. In order to extract the lipids, the samples were centrifuged in an Eppendorf 5810R centrifuge at 800 rcf (relative centrifugal force, unit of gravity) for 10 min at 6 °C. Care was taken to ensure that the individual sample holders were balanced to within 0.05 g, which was achieved by adding hexane (HEX) after the sonication. After centrifugation, the supernatant, the total liquid extract (TLE) was transferred to new vials. As soon as there was not enough space left in the vials with the TLE, the solvents were evaporated using a in the blow-down system with a gentle stream of nitrogen gas and with heating to 25 °C. The steps described in this section were repeated four times. After the fourth repetition, the supernatant was transparent and had no longer the same colour as before.

4.3 Fractionations

The dried samples were dissolved with DCM (< 1 ml) by swirling and then pre-combusted silica gel (deactivated with 5 % water) was added until the liquid was completely absorbed. The DCM was removed by gentle heating at 25 °C. The samples were then placed on the top of prepared glass columns. These consisted of glass pipettes half filled with 95 % deactivated silica gel and a stopper of cotton wool prerinsed with hexane and DCM. First, the non-polar hydrocarbons were eluted with hexane as the eluent (referred to as fraction F1). This was followed by the elution of slightly polar compounds like alkenones and fatty acid methyl esters by a mixture of DCM and hexanes in a 1:1 ratio (F2 referred to as fraction). Finally, a more polar fraction containing the GDGTs, sterols, etc. were eluted from the silica gel columns with a 1:1 mixture of DCM and MeOH (F3 referred to as fraction). The eluted fractions were collected in 4 ml vials. The eluent was added to the samples until the 4 ml vials were full.

4.4 Sub-sample Preparation for HPLC-APCI-MS Analyses

F3 samples were carefully dried under N₂ in the blow-down system at 25 °C and dissolved with a mixture of hexane and isopropyl alcohol (IPA) in a ratio of 99:1, vortexed and the residues were rinsed out three times with it. The samples were filtered using a syringe fitted with a 0.45 µm PTFE filter and filled into 2 ml vials. To concentrate the samples, they were dried under N₂ flow in the blown-down system at 25 °C and filled up with 1 ml HEX:IPA (99:1).

4.5 HPLC-APCI-MS Analysis and Quantifications

For the analysis of the extracted samples of the lake sediment core Man-18-44A, a high performance liquid chromatography, coupled with TSQ Quantum Access Max Triple Quadrupole mass spectrometer via an atmospheric pressure chemical ionization (APCI) ion source was used. This HPLC-APCI-MS apparatus combines the separation of individual substances based on their polarity and other physicochemical interaction like adsorption between the mobile and solid phase by chromatography with mass spectrometry to determine the mass-to-charge ratio. The interface between chromatography and the MS is carried out by APCI. For this purpose, the analytes are chemically ionised at atmospheric pressure and via a corona discharge needle, after which the ions are led into the mass spectrometer using

charged surfaces, lenses and vacuum. In the mass spectrometer the mass-to-charge ratio can be recorded by a detector via the deflection of the flight path of the ions by a quadropole. The results are displayed in ion chromatograms with a mass spectra.

Two HPLC-APCI-MS sequences of the prepared 50 sediment samples were performed. For the first analysis (Man-1), 10 microlitres were injected at a HPLC column with a temperature of 30 °C and a run time of 70 min. For the second measurement (Man-2), the method was changed to an injection of 20 microlitres at a higher temperature of 45 °C and a run time of 70 min. The GDGTs were analysed using the method by (Hopmans et al. 2016), except for using a flow of 0.3 ml/min and a slightly adjusted solvent gradient, on a Dionex/Thermo Scientific UltiMate3000 HPLC (equipped with two Acquity UPLC HILIC columns, 2.1 x 150 mm) connected to a TSQ Quantum Access Max Triple Quadrupole mass spectrometer and APCI ion source. GDGTs were scanned using m/z windows for tetra-, penta- and hexamethylated brGDGTs and one window for isoGDGTs: 1017-1023, 1031-1037, 1045-1051 and 1290-1304 (Table 1).

Table 1: Settings of the TSQ Quantum mass spectrometer after GDGTs were detected. Scanning was done after five center masses [m/z] with corresponding scan width [cm] and scan time [min].

Center mass [m/z]	Scan width [cm]	Scan time [min]
653.000	2.500	0.066
1020	7.500	0.200
1034	7.500	0.200
1048	7.500	0.200
1297	15.000	0.400

The relative abundances of isoGDGTs and brGDGTs were manually integrated using the Xcalibur software package. The identification of the individual GDGTs was based on the relative retention times and the mass spectra. The detection limit was set with a signal-to-background noise ratio of 3:1. The height of the peaks was measured in volts and the width of the peaks in seconds, so that the unit of the resulting area is volt seconds [$V*s$]. The integration and quantification of the chromatographic peaks was done according to the integration method described in the literature and the relative retention times of the respective GDGTs (Hopmans et al. 2016; Naafs et al. 2018; Baxter et al. 2019; Rattray and Smittenberg 2020; De Jonge et al. 2014).

4.6 Chronology

Three radiocarbon samples from the lake sediment cores Man-18-44A were available to create a depth-age model. The samples were 13 cm, 38 cm and 40 cm deep and were dated from the Nanyang Technological University, Singapore at the Beta Analytic Inc laboratory in Miami. The radiocarbon age can be dated by direct measurement of the present ^{14}C amount. The calculation of the isotope ratio $^{14}C/^{13}C/^{12}C$ determined by an NEC accelerator mass spectrometer (AMS) and isotope ratio mass spectrometry (IRMS). The error of radiocarbon dating of one sigma is ± 30 years (Table 2).

4.7 Paleotemperature and Paleoenvironmental Proxy Calculations

In order to draw conclusions about temperature, pH and terrestrial organic matter from the distribution of the different GDGTs, the following geochemical proxies are used. These were developed on field-based empirical observations. The relative amount of methyl branches is

expressed by the methylation index of branched tetraethers (MBT'_{5ME}), which shows the ratio of uncyclized tetramethylated to uncyclized penta- and hexamethylated brGDGTs (De Jonge et al. 2014) (1).

$$MBT'_{5ME} = \frac{Ia + Ib + Ic}{Ia + Ib + Ic + IIa + IIb + IIc + IIIa} \quad (1)$$

To provide inferences about paleotemperature, the following calibrations for mean air temperature (MAT) and mean annual air temperature (MAAT) are used. MAT developed by (De Jonge et al. 2014) (2), $MAAT_{soil}$ by (Naafs et al. 2017b) (3), $MAAT_{peat}$ by (Naafs et al. 2017a) (4) and $MAAT_{lake}$ by (Russell et al. 2018) (5).

$$MAT [^{\circ}C] = -8.57 + 31.45 * MBT'_{5ME} \quad (2)$$

$$MAAT_{soil} [^{\circ}C] = 40.01 * MBT'_{5ME} - 15.25 \quad (3)$$

$$MAAT_{peat} [^{\circ}C] = 52.18 * MBT'_{5ME} - 23.05 \quad (4)$$

$$MAAT_{lake} [^{\circ}C] = -1.21 + 32.42 * MBT'_{5ME} \quad (5)$$

(Baxter et al. 2019) detected a correlation between the distribution of brGMGTs and MAAT in East African lakes, resulting in a new index (brGMGTI) (6). This index represents the ratio of the three brGMGTs showing a positive correlation with MAAT in the numerator and the two GMGTs showing a negative correlation in the denominator.

$$brGMGTI = \frac{(H - 1020c) + (H - 1034a) + (H - 1034c)}{(H - 1020a) + (H - 1020c) + (H - 1034a) + (H - 1034c) + (H - 1048)} \quad (6)$$

The calibration matching the brGMGTI index to reconstruct the temperature (Baxter et al. 2019) (7).

$$MAAT_{brGMGTI} = 2.86 + 26.5 * brGMGTI \quad (7)$$

To represent the cyclization of the branched tetraethers (CBT), different CBT indices were used. On the basis that the number of cyclopentane moieties correlates with pH, CBT (Weijers et al. 2007) (8), CBT'_{5ME} (De Jonge et al. 2014) (10), CBT_{peat} (Naafs et al. 2017a) (12), CBT' (De Jonge et al. 2014) (14) were generated. With the specific calibrations for the reconstruction of pH, which are as follows: pH_{CBT} (De Jonge et al. 2014) (9), pH'_{5ME} (De Jonge et al. 2014) (11), pH_{peat} (Naafs et al. 2017a) (13) and $pH_{surface\ water}$ (Russell et al. 2018) (15).

$$CBT = -\log\left(\frac{Ib + IIb + IIb'}{Ia + IIa + IIa'}\right) \quad (8)$$

$$pH_{CBT} = 7.9 - 1.97 * CBT \quad (9)$$

$$CBT'_{5ME} = -\log\left(\frac{Ib + IIb}{Ia + IIa}\right) \quad (10)$$

$$pH'_{5ME} = 7.84 - 1.73 * CBT'_{5ME} \quad (11)$$

$$CBT_{peat} = \log \left(\frac{Ib + IIa' + IIb + IIb' + IIIa'}{Ia + IIa + IIIa} \right) \quad (12)$$

$$pH_{peat} = 2.49 * CBT_{peat} + 8.07 \quad (13)$$

$$CBT' = \log \left(\frac{Ic + IIa' + IIb' + IIc' + IIIa' + IIIb' + IIIc'}{Ia + IIa + IIIa} \right) \quad (14)$$

$$pH_{surface\ water} = 8.59 + 2.65 * CBT' \quad (15)$$

For the estimation of input of terrestrial organic matter into lacustrine sediments the BIT index was calculated (Hopmans et al. 2004) (16). This index quantifies the brGDGTs versus the isoGDGT crenarchaeol.

$$BIT = \frac{Ia + IIa + IIa' + IIIa + IIIa'}{Ia + IIa + IIa' + IIIa + IIIa' + crenarchaeol} \quad (16)$$

The ratio of brGDGT to isoGDGTs is an extended version of the BIT index that can be used to estimate the terrestrial impact of organic matter (Naehler et al. 2012) (17). In contrast to the BIT index, the brGDGT/isoGDGT ratio represents the brGDGTs to additional isoGDGTs and not only to crenarchaeol.

$$\frac{brGDGTs}{isoGDGTs} = \frac{Ia + Ib + Ic + IIa + IIb + IIc + IIIa}{(GDGT - 0) + (GDGT - 1) + (GDGT - 2) + (GDGT - 3) + cren. + cren.regioisomer} \quad (17)$$

The isomerization of the brGDGTs is considered by the IR_{6ME} index (Yang et al. 2015) (18). Only 6-methyl isomers are considered here.

$$IR_{6ME} = \frac{IIa' + IIb' + IIIa' + IIIb' + IIIc'}{IIa + IIa' + IIb + IIb' + IIc + IIc' + IIIa + IIIa' + IIIb + IIIb' + IIIc + IIIc'} \quad (18)$$

The IBT index also reflects the isomerization of the branched tetraethers but only the isomer formation of uncyclized pentamethylated GDGTs (IIa) and uncyclized hexamethylated GDGTs (IIIa) (Ding et al. 2015) (19).

$$IBT = -\log \left(\frac{IIa' + IIIa'}{IIa + IIIa} \right) \quad (19)$$

The tetraether index of 86 carbons (TEX₈₆) is based on the distribution of four isoGDGTs, including the crenarchaeol isomer (Schouten et al. 2002) (20). With suitable calibrations, the index can provide information about the sea surface temperature (SST). This is defined by a later retention time than crenarchaeol and occurs in much lower abundance than the crenarchaeol (Sinninghe Damsté et al. 2018). The two most abundant isoGDGTs crenarchaeol and GDGT-0 are excluded from the TEX₈₆ definition to avoid their overprinting on the index. GDGT-0 is also excluded for the reason that it was thought that it would be sourced by methanogenic Euryarchaeota, which are living in anoxic sedimentary environments and potentially disturbing the temperature signal (Schouten et al. 2002). A calibration to SST

(Schouten et al. 2002) (21) and an annual lake surface temperature (ALST) (Powers et al. 2010) (22) is used.

$$TEX_{86} = \frac{(GDGT - 2) + (GDGT - 3) + \text{crenarchaeol regio isomer}}{(GDGT - 1) + (GDGT - 2) + (GDGT - 3) + \text{crenarchaeol regio isomer}} \quad (20)$$

$$SST [^{\circ}C] = \frac{TEX_{86} - 0.28}{0.015} \quad (21)$$

$$ALST [^{\circ}C] = -10.4 + 50.8 * TEX_{86} \quad (22)$$

(Kim et al. 2010) recommend applying the SST^H calibration above temperatures of 15 °C SST (23).

$$SST^H [^{\circ}C] = 68.4 * (\log(TEX_{86})) + 38.6 \quad (23)$$

The methane index (MI) is composed of the relative distribution of isoGDGTs with one, two and three rings compared to crenarchaeol and crenarchaeol regioisomer (Zhang et al. 2011) (24).

$$MI = \frac{(GDGT - 1) + (GDGT - 2) + (GDGT - 3)}{(GDGT - 1) + (GDGT - 2) + (GDGT - 3) + \text{crenarchaeol} + \text{cren. regioisomer}} \quad (24)$$

The following statistical operations were used: average (\bar{x}) (25) and standard deviation (SD) (26).

$$\bar{x} = \frac{1}{n} \sum_{i=1}^n x_i \quad (25)$$

$$SD = \sqrt{\frac{\sum_{i=1}^n (x - \bar{x})^2}{(n - 1)}} \quad (26)$$

5. Results

5.1 Maninjau Lake Sediment Core Description

The sediment core from lake Maninjau (Man-18-44A) is 42 cm long in total (Figure 7). 0 cm corresponds to the upper rim and 42 cm to the lower rim. The core was kept in at 4 °C Stockholm University and was shaped like a quarter of a 42 cm long cylinder. At first view, the core has an even structure and is composed of a colour spectrum of brown-green-grey and black. The different layers, which can be between a few millimetres (0.3 mm) and centimetres (2 cm) wide, could be clearly identified, which is why the classification was made as best as possible based on the colour and structure of the layers.



Figure 7: Picture of the Man-18-44A sediment core from the lake Maninjau, West-Sumatra Indonesia with a length of 42 cm. 0 cm corresponds to the top of the sediment and 42 cm to the bottom of the sediment.

The top 1.3 cm of sediment was made up of heterogeneous material, both in texture and colour, ranging from light to dark brown. Between 3.3-3.7 cm there was a reddish layer suggesting iron oxides. A similar conspicuous layer of light-yellow material was found between 4.5-5.5 cm. In the section between 10.5 and 11.5 cm was a clump, 4 mm in size of fibrous greyish material in an otherwise uniform dark grey layer. Between 11.5-12.4 cm, the discovery was made of a presumably organic, black material, like a piece of tree bark. At 17 cm, finely structured, white, hard material appeared, which could not be identified under the microscope. Sporadically, in a less large quantity, it was also found in the upper layers up to 7.5 cm. In the core sediment section between 18.9-20.9 cm a few sand grains were found in an otherwise dark grey layer. The material of the different layers between 21.4-24.8 cm were coarser structured than the sediment section of 24.8-28.6 cm, which consisted of clearly finer material. In the previously mentioned section, there was also a noticeable light grey layer at 25.8-26.3 cm. In the segment of lake sediment from 29-34.1 cm, there was a change in the sediment structure that could be clearly distinguished from the upper and lower sections. The structure was clearly coarser-grained, but the particles were not exactly separated individually but often coherent. At 30 cm, the grainy structure was even orange. The structure described was unique in the whole sediment core. After the change in structure, a grey layer followed at 34.1-35.1 cm, with finer material and red spots, which could indicate iron oxides. Between 36.1-36.8 cm, a wood-like piece about 0.5 mm in size appeared. At 37.7-36.8 cm there was a particularly light grey layer with a yellowish colour gradient. In the section mentioned and, also in the following centimetres, the material was conspicuously fine, reminding of clay structure. The end of the sediment core from lake Maninjau is a dark brownish-green layer with a somewhat coarser structure.

5.2 Depth-Age Model and Sedimentation

Three radiocarbon dates were obtained (Table 2), which gave a basal age of 2660-2340 cal yr BP (two sigma range), allowing a basic depth-age model (Figure 8a). The calculated sedimentation rate over this period averages about 0.32 mm/yr (Figure 8b).

Table 2: ^{14}C radiocarbon data from three samples of lake Maninjau sediment core Man-18-44A at 13, 38 and 40 cm with dated ages (BP) with a two-sigma range (given in minimum and maximum dated ^{14}C age) and an error of ± 30 . Analysed from the Nanyang Technological University, Singapore at the Beta Analytic Inc laboratory in Miami.

Depth [cm]	^{14}C age	Error	Cal age BP (2 sigma range)	
			Min	Max
13	80	30	261	27
38	1870	30	1869	1713
40	2380	30	2666	2340

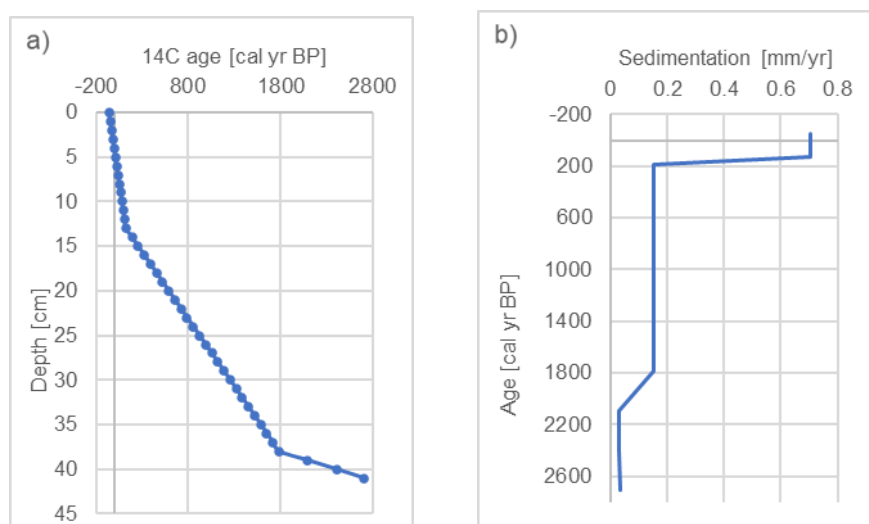


Figure 8: a) Depth-age model, b) Sedimentation rate calculated from three ¹⁴C data of the sediment core Man-18-44A of the lake Maninjau. The depth-age model reaches back to a basal age of 2660-2340 cal yr BP. The sedimentation rate in this period is about 0.32 mm/yr.

5.3 Distribution of GDGTs in Lake Maninjau

Through the HPLC-APCI-MS measurements, the following brGDGTs (Ia, Ib, Ic, IIa, IIb, IIc, IIa', IIb', IIc', IIIa, IIIb, IIIc, IIIa', IIIa'', IIIa'''), brGMGTs H-1020a, H-1020b, H-1020c, H-1034a, H-1034b, H-1034c, H-1048, isoGDGTs-0, -1, -2, -3, -4, -5, crenarchaeol, crenarchaeol regioisomer and one isoGMGT H-0 were identified and quantified.

5.3.1 Fractional Abundance of brGDGTs

In the case of both runs of the HPLC-APCI-MS of the Man-18-44A samples, the tetramethylated brGDGTs are the abundant, making up 59.35 % for measurement round Man-1 and 58.49 % for measurement round Man-2 (Figure 9). These are followed by the pentamethylated brGDGTs with 38.18 % for Man-1 and 35.2 % for Man-2. The smallest sum of the fractional abundance of the most methylated, the hexamethylated brGDGTs, at 5.47 % for Man-1 and 6.31 % for Man-2. The most abundant brGDGT in both runs is the uncyclized 5-methyl tetramethylated brGDGT Ia with 44.92 % at Man-1 and 44.4 % at Man-2. There are differences in the second most abundant between the two runs. In Man-1, it is the monocyclized 5-methyltetramethylated GDGT Ib with 13.68 % and in Man-2 the uncyclized 6-methyl pentamethylated brGDGT IIa' with 14.56 %. The third most abundant is the other one, Man-1 IIa' with 13.5 % and Man-2 Ib with 13.35 %. The same brGDGTs were found in both runs, even if in part in different amounts.

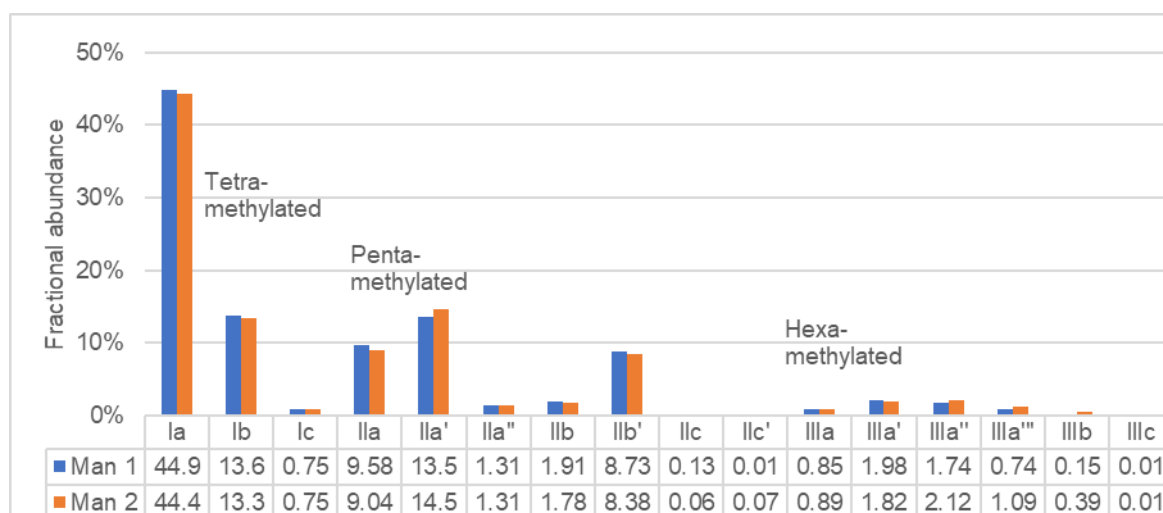


Figure 9: Fractional abundance of the detected brGDGTs from the two HPLC-APCI-MS measurements of the lake Maninjau sediment core Man-18-44A Man-1 (blue) and Man-2 (orange).

5.3.2 Fractional Abundance of brGMGTs

In contrast to the brGDGTs, the fractional abundance of the brGMGTs does not differ so much (Figure 10). The most abundant brGMGT is H-1020c with 35.64 % in Man-1 and with 37.71 % in Man-2. Second and third most abundant are H-1034b and H-1034c. It should be observed that the isomer H-1020c is more abundant than H-1020a.

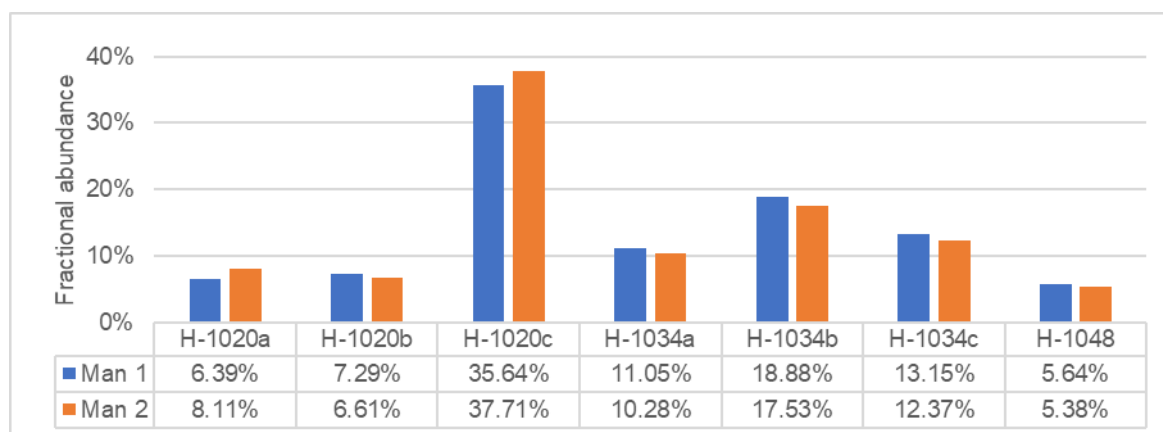


Figure 10: Fractional abundance of the detected brGMGTs from the two HPLC-APCI-MS measurements of the lake Maninjau sediment core Man-18-44A Man-1 (blue) and Man-2 (orange).

5.3.3 Fractional Abundance of isoGDGTs

Looking at the isoGDGTs, the most abundant isoGDGT is crenarchaeol with 59.91 % in Man-1 and 58.32 % in Man-2 (Figure 11). This is followed by the uncyclized GDGT-0 at Man-1 with 26.80 % and at Man-2 with 27.48 % and the third most abundant is the bicyclized GDGT isomer GDGT-3' for Man-1 with 3.09 % and at Man-2 with 3.15 %. In contrast to the brGDGTs, not all searched isoGDGTs are found. In run two (Man-2) with increased injection and increased temperature, no GDGT-4, and no isomer GDGT-4' are found. Possibly, the retention times of crenarchaeol and GDGT-4 shifted towards each other so that the peaks coeluted, and they cannot be separated by mass, since both have an m/z of 1292.

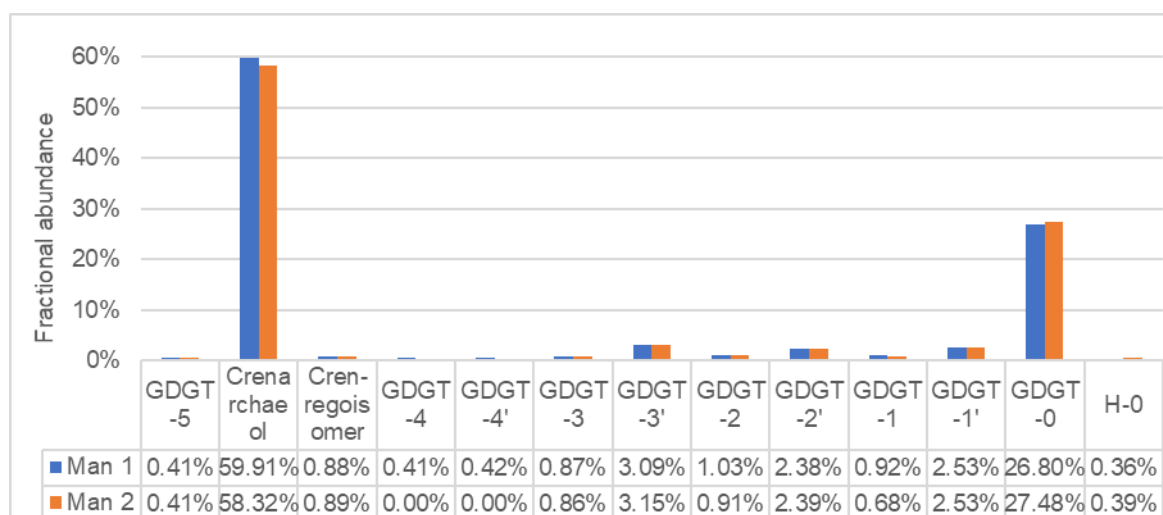


Figure 11: Fractional abundance of the detected isoGDGTs and one isoGMGT from the two HPLC-APCI-MS measurements of the lake Maninjau sediment core Man-18-44A Man-1 (blue) and Man-2 (orange).

5.3.4 Differences between the two HPLC-APCI-MS Measurements

Because in the first run Man-1 of the HPLC-APCI-MS only a small amount of GDGTs could be found in the top sediment sample (0-0.3 cm), the injection at the HPLC column was increased from 10 to 20 microlitres in the replicate Man-2. But at the end, no GDGTs could be detected in the top sediment sample (0-0.3 cm) of measurement Man-2. Also, the temperature differed between Man-1 30 °C and Man-2 45 °C. This resulted in the retention time of the individual peaks tending to be about 0.8 seconds earlier in the replicate Man-2.

Looking in detail at the HPLC-APCI-MS runs, some results of some GDGTs are almost identical e.g., crenarchaeol, as shown in the cross plot in (Figure 12). However, others are very different. The largest deviations between the two measurements are listed as cross plots in (Figure 12). For the brGDGTs IIc, the relative amount is higher for Man-1 than for Man-2. Strikingly, for the belonging isomer IIc', the distribution is the opposite. In Man-1, IIc' was found in only one sample, but in Man-2 in 16 of 50 samples. IIa'' and IIIa does not show such a big different distribution, the fractional abundance is on average slightly higher in Man-2 than in Man-1. The differences within the GMGTs are smaller, for example, the fractional abundance is more similar in the brGMGTs, as the cross plot of H-Ia demonstrates.

In general, most disagreements are due to non-detection versus detection in either Man-1 or Man-2. Often the reason is that the detected amounts are close to the detection limit of the signal-to-background noise ratio of 3:1. It is possible that the instrument has become dirtier during use, resulting in more background noise, and making it more difficult to detect the GDGTs. This must be taken into account when interpreting the applied proxies. However, the increased non-detection of brGDGTs and isoGDGTs is more likely to occur in the top centimetre samples.

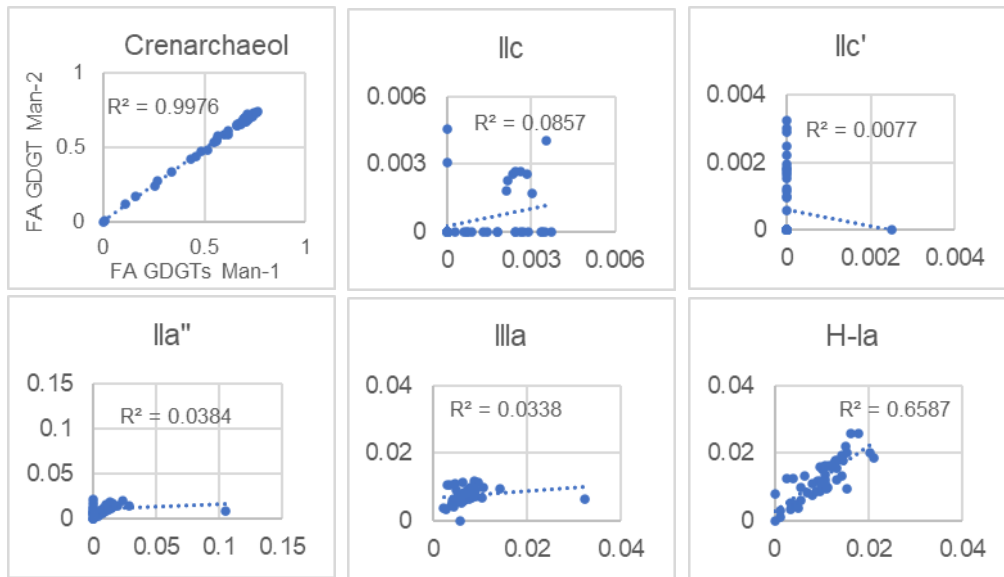


Figure 12: Cross plots of the fractional abundance of the GDGTs of the two HPLC-APCI-MS measurements of the lake Maninjau sediment core Man-18-44A Man-1 and Man-2 plotted against each other. The results of Man-1 are plotted on the x-axis and those of Man-2 on the y-axis. Examples of similar FA of both measurements (Crenarchaeota, H-Ia) and different FA (Ilc, Ilc', Ila'', Ila) are shown.

5.4 Derived Proxies of Branched Tetraether

5.4.1 Methylation of Branched Tetraether

The MBT'_{5ME} proxy, which relates the tetramethylated brGDGTs in relation to the penta- and hexamethylated brGDGTs, shows average values over the complete sediment depth for both measurements of $\bar{x} = 0.8311$ (Figure 13a, A.: Table 3). According to a personal note from R.H. Smittenberg (2022), through previous measurements of the MBT proxy, the instrumental error for MAAT reconstructions can be assumed to be 0.25 °C for all data. The MBT'_{5ME} values slightly increase towards the top of the sediment. The brGMGTI index, which represents the distribution of the brGMGTs, in contrast does not show any trend even course with mean values of both runs of $\bar{x} = 0.8251$ (Figure 13b, A.: Table 4).

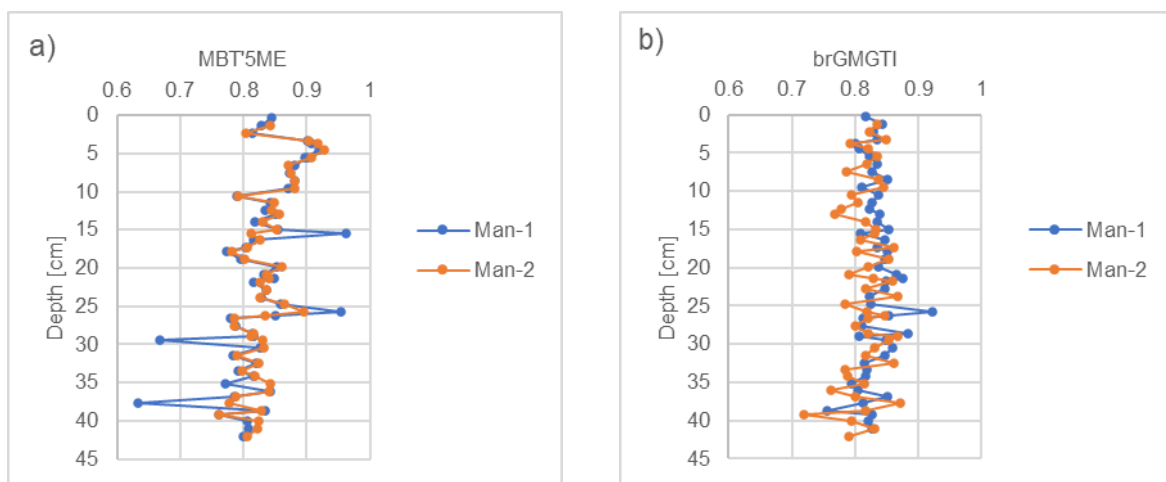


Figure 13: a) MBT'_{5ME} index, b) brGMGTI index plotted over the depth of the sediment core Man-18-44A from the lake Maninjau from the HPLC-APCI-MS measurements Man-1 (blue) and Man-2 (orange). MBT'_{5ME} index based on the distribution of brGDGTs (De Jonge et al. 2014) and brGMGTI index based on the distribution of brGMGTs (Baxter et al. 2019).

5.4.2 Mean Annual Air Reconstruction according to the MBT Proxy

The four temperature reconstructions of the lake sediment core Man-18-44A for the different MAAT calibrations based on the MBT_{5ME} index show a similar pattern (Figure 14). A minimal increase of in temperature of 1.63 °C can be seen from the bottom of the sediment core towards the top of the sediment core for MAT_{5ME}, MAAT_{soil}, MAAT_{peat} and MAAT_{lake}. The four temperature calibrations according to the MBT_{5ME} index have a fluctuation of 8.58 °C on average. Apart from four exceptions in the measurement Man-1, both measurements show very similar values. The trend of the MAAT calibration of the brGMGTI index, which is based on the distribution of GMGTs, does not show a significant warming trend towards the surface of the sediment, unlike the MAAT calibrations based on MBT_{5ME}. Also, for the brGMGTI methylation index, the measurement Man-2 shows a clearer course than Man-1 with some greater variation in the results. Note that the calibration maximum is for MAAT_{lake} at 31.21 °C and for MAAT_{brGMGTI} at 29.18 °C. However, with maximum calculated temperatures of 28.77 °C for MAAT_{lake} and 26.3 °C for MAAT_{brGMGTI}, the saturation is not reached.

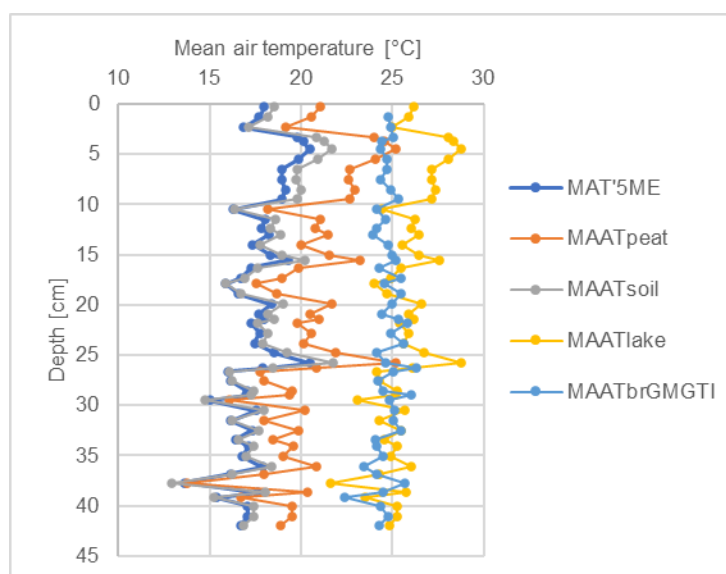


Figure 14: Mean air temperature reconstructions according to MBT_{5ME} and brGMGTI proxy plotted over the depth of the sediment core Man-18-44A from the lake Maninjau from the HPLC-APCI-MS measurements Man-1 and Man-2. MAT_{5ME} (De Jonge et al. 2014), MAAT_{peat} (Naafs et al. 2017a), MAAT_{soil} (Naafs et al. 2017b), MAAT_{lake} (Russell et al. 2018) are according to MBT_{5ME} proxy and MAAT_{brGMGTI} (Baxter et al. 2019) according to brGMGTI proxy. A slight increase in calibrated temperature towards the top of the sediment can be seen.

5.4.3 Cyclization of Branched Tetraether

All different variants of the CBT index represent the cyclization of the brGDGTs (Figure 15). The CBT and CBT_{5ME} index variants consider only tetra- and pentamethylated GDGTs, but CBT_{5ME} only 5-methyl GDGTs and CBT additionally 6-methyl GDGTs. Nevertheless, both show a similar course, a slight increase towards the top with slightly higher values for CBT_{5ME}. The average of both measurements for CBT $\bar{x} = 0.4611$ (A.: Table 5) and for CBT_{5ME} $\bar{x} = 0.5457$ (A.: Table 6). The CBT_{peat} proxy and CBT' proxy, which in addition to CBT also considers hexamethylated GDGTs, also show a slight increase towards the top but with significantly lower values for CBT_{peat} $\bar{x} = (-0.1428)$ (A.: Table 7) and for CBT' $\bar{x} = (-0.3537)$ (A.: Table 8).

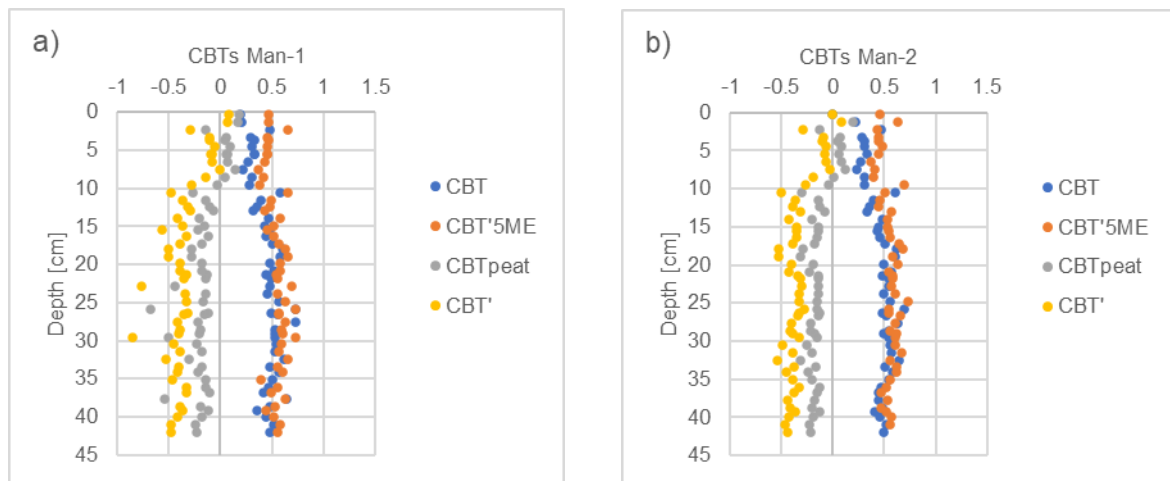


Figure 15: Cyclization of branched tetraethers calculated through different CBT proxies variations plotted over the depth of the sediment core Man-18-44A from the lake Maninjau from the HPLC-APCI-MS measurements a) Man-1 and b) Man-2. CBT (Weijers et al. 2007), CBT'_{5ME} (De Jonge et al. 2014), CBT_{peat} (Naafs et al. 2017a), CBT' (De Jonge et al. 2014).

5.4.4 pH Reconstruction according to the CBT Proxy

Through the changes of the corresponding CBT indexes a minimal increase in pH can be seen from the bottom of the sediment core towards the top of the sediment core (Figure 16). Like the proxies themselves, the reconstructed, estimated pH values according to the CBT and CBT'_{5ME} index are very similar. For all calibrations, the pH value increases towards the top of the sediment. The difference between the values reconstructed at the bottom, the oldest and the youngest at the sediment top is in the mean of both HPLC-APCI-MS runs for pH_{CBT} 0.57, $\text{pH}'_{5\text{ME}}$ 0.14, pH_{peat} 1.00 and $\text{pH}_{\text{surface water}}$ 1.43.

The average values over the entire sediment core is for pH_{CBT} $\bar{x} = 6.99$ and for $\text{pH}'_{5\text{ME}}$ $\bar{x} = 6.90$. Whereas the pH calibration developed for peat shows a higher reconstructed average pH value with $\bar{x} = 7.71$ and the pH calibration developed for surface water has an average of $\bar{x} = 8.01$. All pH reconstructions according to different CBT proxies show a slight increase of the pH value upwards with an average of 1.36 fluctuation.

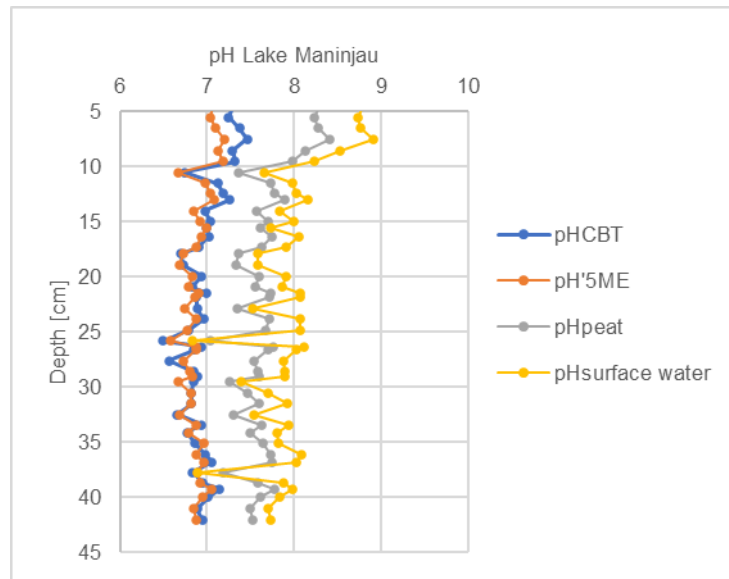


Figure 16: pH reconstructions according to CBT proxies plotted over the depth of the sediment core Man-18-44A from the lake Maninjau from the HPLC-APCI-MS measurements Man-1 and Man-2. pH_{CBT} calibration (De Jonge et al. 2014) according to CBT proxy, pH'_{5ME} (De Jonge et al. 2014) according to CBT_{5ME} proxy, pH_{peat} (Naafs et al. 2017a) according to CBT_{peat} proxy and $pH_{surface\ water}$ (Russell et al. 2018) according to CBT' proxy.

5.4.5 Impact of Soil Organic Matter

The relative abundance of brGDGTs versus crenarchaeol expressed by the BIT index shows a significant increase in the upper 10 cm of the sediment for Man-1 and Man-2, respectively (Figure 17a). An increase of the ratio of br-/isoGDGTs, which expresses the relative abundance of brGDGTs versus additional isoGDGTs including crenarchaeol, can also be seen in the upper 10 cm for Man-1 and Man-2, although not as strong as for the original BIT index (Figure 17a, b). An increase in the ratio of br-/isoGDGTs in the upper 10 cm probably means that the brGDGTs are more dominant than in the deeper layers in the sediment.

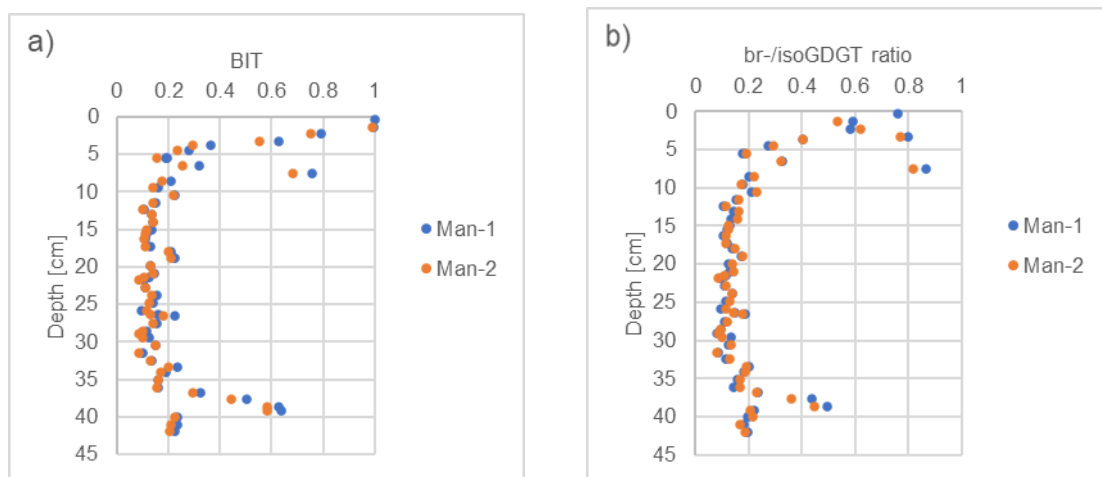


Figure 17: a) BIT index, b) brGDGT/isoGDGT ratio plotted over the depth of the sediment core Man-18-44A from the lake Maninjau from the HPLC-APCI-MS measurements Man-1 (blue) and Man-2 (orange). BIT sets brGDGTs in relation to crenarchaeol (Hopmans et al. 2004) and br-/isoGDGT ratio in relation to other isoGDGTs (Naehler et al. 2012). Elevated values can indicate terrestrial influence or in situ production of brGDGTs.

5.4.6 Impact of Isomerization

The IR_{6ME} isomerization index, which relates 5-methylated to 6-methylated brGDGTs, low values indicate a dominance of 5-methylated brGDGTs over 6-methylated GDGTs (Figure 18a). For the Man-1 samples 92 % of all IR_{6ME} values and for Man-2, all values are above a value IR_{6ME} 0.5, suggesting a dominance of 6-methylated brGDGTs compared to 5-methylated GDGTs, which slightly increases towards the surface of the sediment.

The IBT isomerization index only reflects the isomerization of uncyclized penta- and hexamethylated brGDGTs for the 5-methyl and the 6-methyl GDGTs. The IBT values over the sediment depth are opposite to the IR_{6ME} index but have the same meaning (Figure 18b). A decrease of the IBT values, as it can easily be seen at the top of the sediment, indicates that the relative proportion of the 6-methylated brGDGT tends to increase. But overall, it is noteworthy that the regularity of the progression of both indices for the replicate measurement Man-2 is better than for Man-1. The larger injection in the HPLC-APCI-MS measurement of Man-1 could be a reason for the different results compared to Man-2.

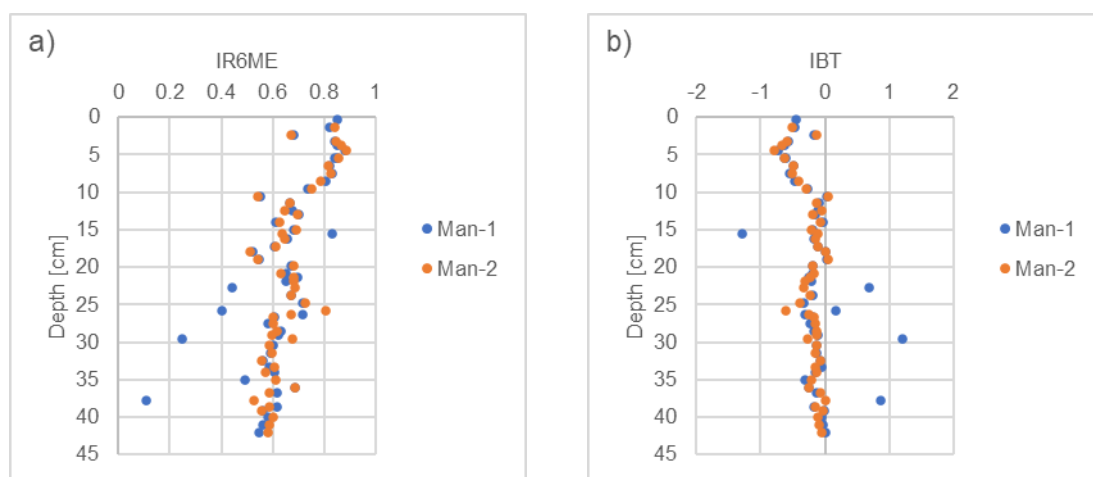


Figure 18: a) The isomerization index IR_{6ME} , b) IBT index plotted over the depth of the sediment core Man-18-44A from the lake Maninjau from the HPLC-APCI-MS measurements Man-1 (blue) and Man-2 (orange). IR_{6ME} (Yang et al. 2015) and IBT (Ding et al. 2015) show both an increase in 6-methyl isomers compared to 5-methyl brGDGTs towards the sediment top.

5.5 Derived Proxies of Isoprenoid Tetraethers

5.5.1 Tetraether Index of 86 Carbons

The TEX_{86} proxy compares different cyclized isoGDGTs and enables a reconstruction of the surface water temperature through corresponding calibrations (Schouten et al. 2002). Except for the uppermost and the lowermost 10 cm, the course of the TEX_{86} values is uniform and shows no significant trend (Figure 19). The mean value of both measurements over the complete sediment core are $\bar{x} = 0.7581$ (A.: Table 9).

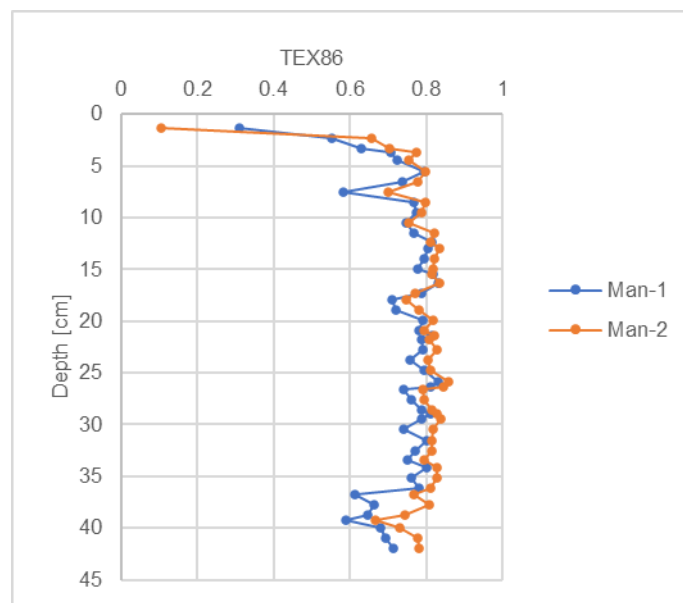


Figure 19: The distribution of the TEX_{86} proxy (Schouten et al. 2002) plotted over the depth of the sediment core Man-18-44A from the lake Maninjau from the HPLC-APCI-MS measurements Man-1 (blue) and Man-2 (orange). Apart from the outliers, there is a slight decrease in the TEX_{86} values towards the top of the sediment.

5.5.2 Lake Surface Temperature Reconstruction according to the TEX_{86} Proxy

From the distribution of isoGDGT, the lake surface temperature can be deduced with the help of the TEX_{86} proxy (Figure 20). The TEX_{86} proxy relates four isoGDGT, including crenarchaeol regioisomer. It is defined by a later retention time than crenarchaeol and occurs in much lower abundance than the main crenarchaeol (Sinninghe Damsté et al. 2018).

All three temperature calibrations SST^H , SST, and ALST show a similar trend even if in slightly shifted temperature ranges. The calibration developed for explicit annual lake surface temperature by (Powers 2010) shows the lowest values with an average of both HPLC-APCI-MS runs with 28.11 °C for the ALST calibration. The average temperature value for the SST calibration from (Schouten et al. 2002) according to the TEX_{86} proxy is 31.87 °C. (Kim et al. 2010) recommends the use of SST^H calibration above 15 °C, which was explicitly developed for higher temperatures. The average SST^H is 29.95 °C. Overall, the range of the reconstructed SST according to TEX_{86} is noticeably large. The temperature deviations reconstructed through TEX_{86} proxy in the upper centimetres and from < 36 cm upwards are due to a low presence of GDGT-1.

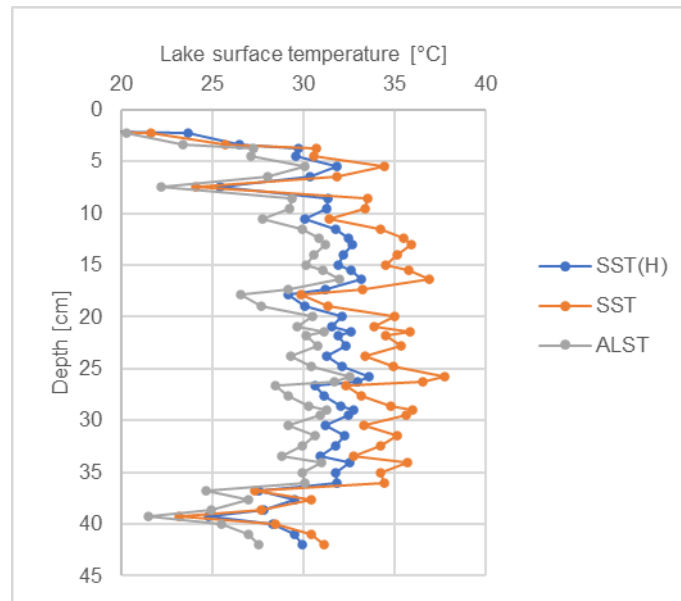


Figure 20: Lake surface water reconstruction according to TEX_{86} proxy plotted over the depth of the sediment core Man-18-44A from the lake Maninjau from the HPLC-APCI-MS measurements Man-1 and Man-2. The calibrations SST^H (Kim et al. 2010), SST (Schouten et al. 2002) and ALST (Powers et al. 2010) are according to TEX_{86} proxy. Apart from the outliers, there is a slight decrease in the reconstructed LST towards the top of the sediment.

5.5.3 Impacts on the TEX_{86} Proxy

The values of the methane index are low with an average of Man-1 $\bar{x} = 0.0589$ and Man-2 $\bar{x} = 0.0517$. Apart from a few exceptions, all values are below 0.1. Over the entire length of the sediment core, no significant differences can be observed between Man-1 and Man-2 (Figure 21a). To investigate the influence of archaea involved in the methane cycle and thus to determine an influence on the TEX_{86} signal, the ratio of GDGT-0 to crenarchaeol can be determined (Figure 21b). If the ratio is > 2 it can be assumed that there is a possible influence of methanogenic AOM archaea (Blaga et al. 2009). The results show that for Man-1 90 % of the values are below 2 and for Man-2 89.8 %.

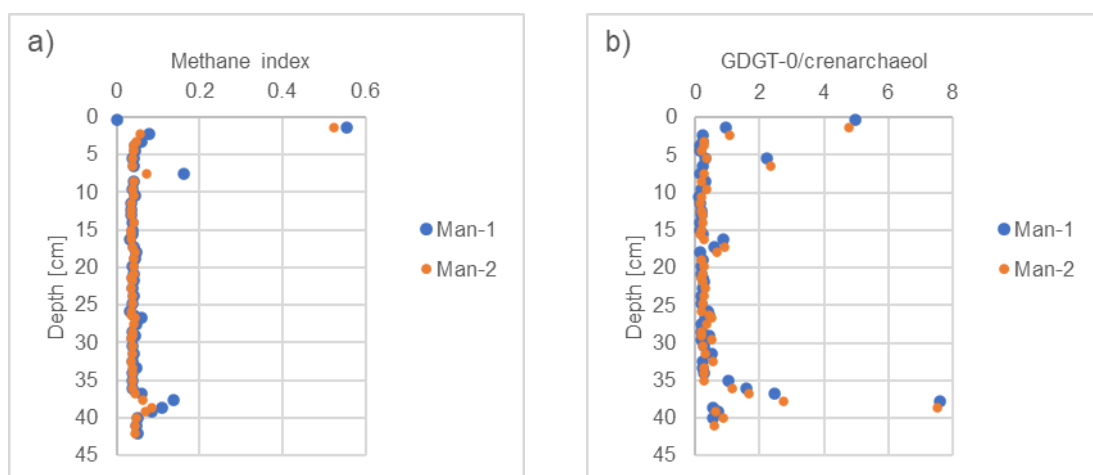


Figure 21: a) Methane index, b) GDGT-0/crenarchaeol plotted over the depth of the sediment core Man-18-44A from the lake Maninjau from the HPLC-APCI-MS measurements Man-1 (blue) and Man-2 (orange). The low values of the Methane index (Zhang et al. 2011) and the ratio of GDGT-0/crenarchaeol (Blaga et al. 2009) indicate no influence of methanogenic AOM archaea.

6. Discussion

6.1 Interpretation of Branched Tetraethers Proxies

6.1.1 Fractional Abundance of brGDGTs in relation to MBT'_{5ME}

To find out which brGDGTs are most important for changes in the MBT'_{5ME} index, the fractional abundance (FA) calculated according to the methylation set of (Raberg et al. 2021) are plotted against the MBT'_{5ME} index (Figure 22). The calculation of these sets is done for uncyclized, monocyclized and bicyclized brGDGTs. An example methylation set for the uncyclized brGDGTs is given (27):

$$FA_{Ia} = \frac{Ia}{\sum 5 - methyl\ uncyclized\ brGDGTs} = \frac{Ia}{(Ia + IIa + IIIa)} \quad (27)$$

There is a positive correlation between the FA of Ia and Ib and MBT'_{5ME} (Figure 22). This is not unexpected, as the MBT'_{5ME} index reflects the ratio of tetramethylated to penta- and hexamethylated. (Raberg et al. 2021) concluded that for all tetramethylated brGDGTs there is a strong linear relation to the MBT'_{5ME} index. The uncyclized and monocyclized tetramethylated Ia and Ib show a strong linear correlation with correlation coefficient for Man-1 ($R^2 = 0.92$) and for Man-2 ($R^2 = 0.93$). But for the tetramethylated bicyclized brGDGT Ic, no clear trend can be seen. One reason for this could be that the relative abundance is generally low and IIc and IIIc were almost not found over the entire depth of the Man-18-44A lake sediment core, suggesting that bicyclized tetramethylated brGDGTs are not important for MBT'_{5ME} reconstructions in this Sumatran lake.

In contrast to tetramethylated brGDGTs a negative correlation to MBT'_{5ME} can be observed for the 5-methyl pentamethylated brGDGTs IIa and IIb. (Raberg et al. 2021) concluded that all 5-methyl pentamethylated brGDGTs show a linear negative correlation to MBT'_{5ME} . This can be confirmed by the results presented, except for IIc, where the distribution gives unusable results. It can be inferred that the FA of the 5-methyl pentamethylated brGDGTs decreases with increasing temperature. For the 5-methyl hexamethylated brGDGTs IIIa, IIIb, IIIc, no significant correlation with a change in temperature is seen. (Raberg et al. 2021) came to the same conclusion with the suggestion that the FA of the 5-methyl hexamethylated ones is too weak for accurate results. Also, the FA 6-methyl isomers of the penta- and hexamethylated brGDGTs show no clear trend with changing MBT'_{5ME} . In summary, it can be concluded that in the case of the investigated samples, the MBT'_{5ME} is mainly determined by the ratio of un- and monocyclized tetra- to pentamethylated brGDGTs.

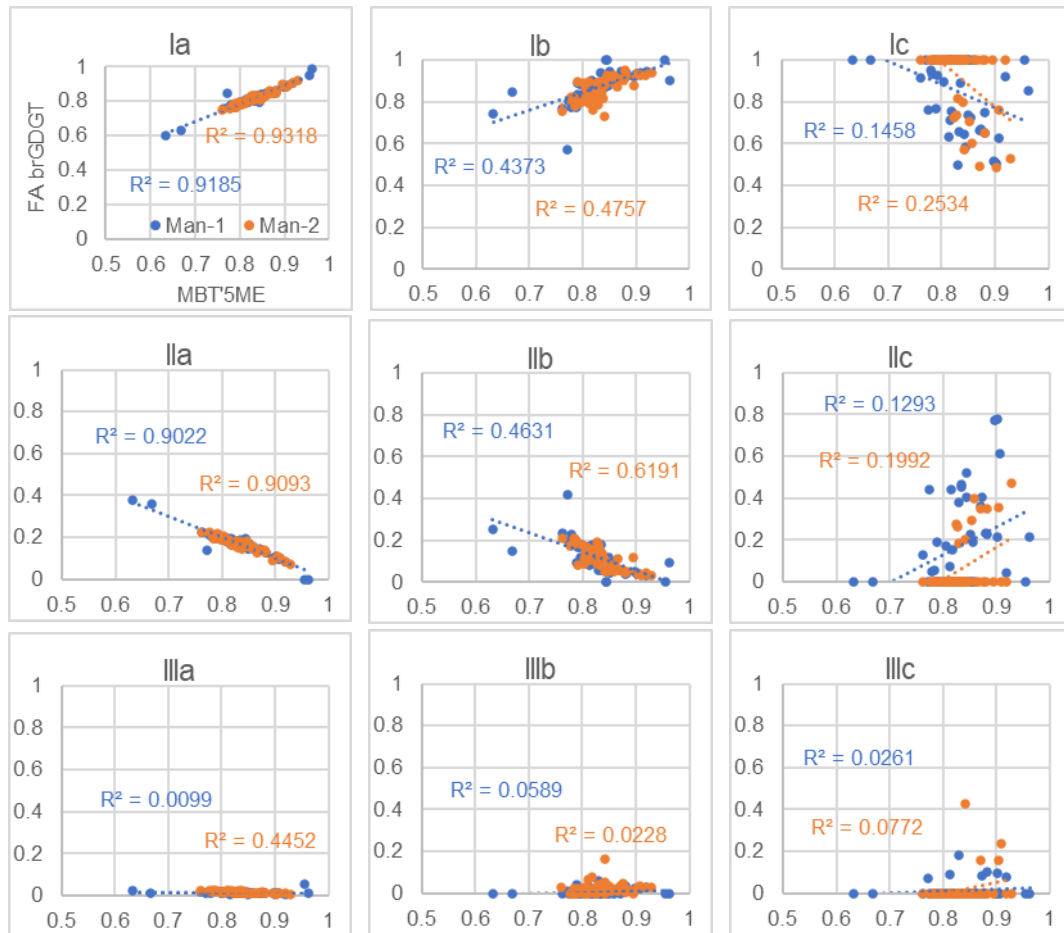


Figure 22: The fractional abundance of brGDGTs plotted against the MBT'_{5ME} proxy. The y-axis shows the brGDGTs FA of from the HPLC-APCI-MS measurements Man-1 (blue) and Man-2 (orange) calculated by the methylation set of (Raberg et al. 2021) and the x-axis shows the MBT'_{5ME} proxy (De Jonge et al. 2014). The correlation coefficient (R^2) and linear trend lines allow correlations to be identified easily.

6.1.2 Fractional Abundance of brGMGTs in relation to brGMGTI

The same calculation was applied to the brGMGTs and plotted against brGMGTI (Figure 23). As with MBT'_{5ME} , the temperature can then also be estimated from the brGMGTI results through calibrations. The calculation of the FA of the brGMGT was carried out with the basis of methylation sets based on the calculation of (Raberg et al. 2021). The calculation of these sets is done for tetramethylated, pentamethylated and hexamethylated brGMGTs (28). Below the example of H-1020a is given:

$$FA_{H-1020a} = \frac{(H - 1020a)}{((H - 1020a) + (H - 1034a) + (H - 1048))} \quad (28)$$

The uncyclized and monocyclized tetramethylated brGDGTs Ia and Ib show a linear positive correlation to MBT'_{5ME} (Figure 22). These results do not translate to the GMGTs (Figure 23). Especially not for H-1020a, which is comparable to the chemical structure of the brGDGT Ia. On the other hand, H-1034a shows a positive correlation with brGMGTI with correlation coefficient for Man-1 ($R^2 = 0.44$) and for Man-2 ($R^2 = 0.48$), like the corresponding brGDGT Ib to MBT'_{5ME} . Nevertheless, all other investigated GMGTs show no correlation to the brGMGTI index calculated from lake Maninjau.

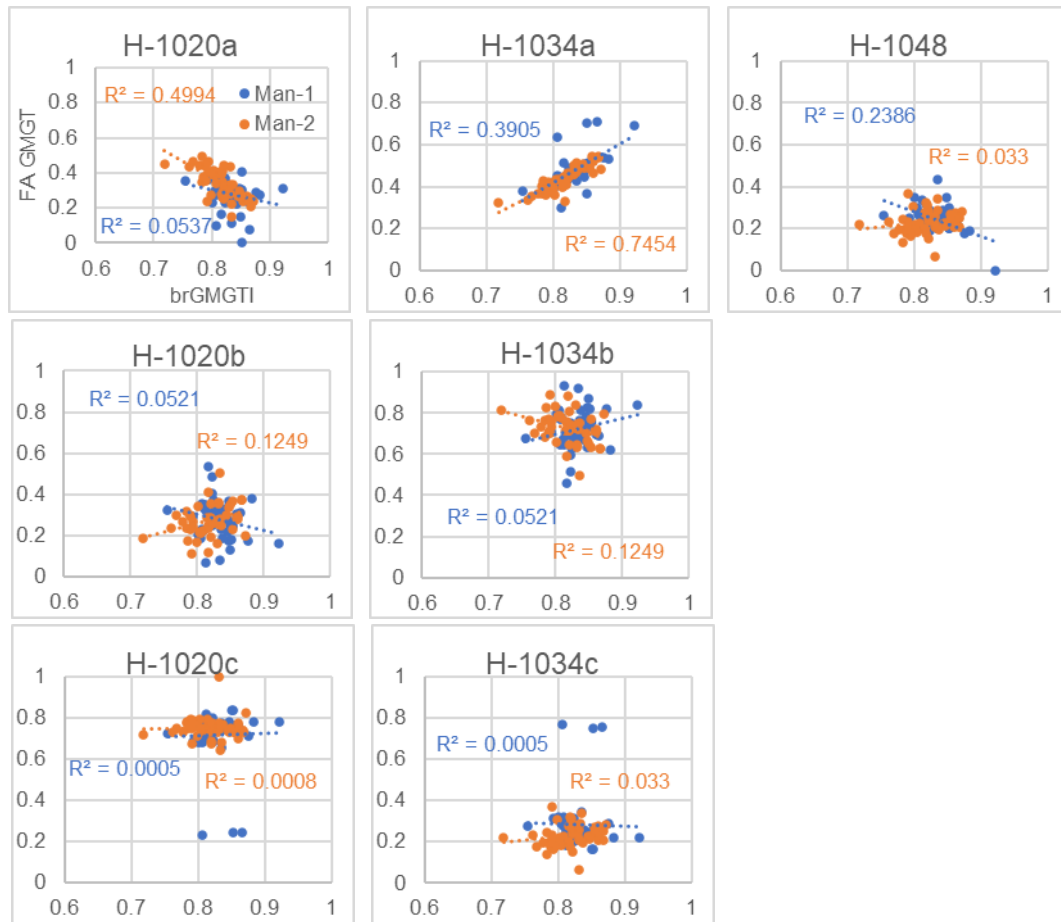


Figure 23: The fractional abundance of three brGMGTs plotted against brGMGTI proxy from the HPLC-APCI-MS measurements Man-1 (blue) and Man-2 (orange). The y-axis shows the brGMGT FA calculated through the equation (29) and the x-axis the brGMGTI proxy (Baxter et al. 2019). The correlation coefficient (R^2) and linear trend lines allow correlations to be identified easily.

The brGMGTs do not correlate significantly with the MBT'_{5ME} proxy (Figure 24). Thus, unlike the brGDGTs, the brGMGT abundances do not correlate with the temperature derived from the MBT'_{5ME} proxy.

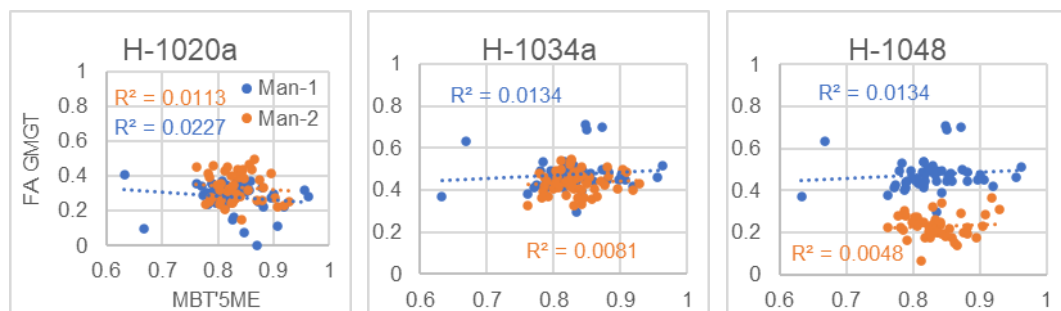


Figure 24: The fractional abundance of three brGMGTs plotted against MBT'_{5ME} proxy from the HPLC-APCI-MS measurements Man-1 (blue) and Man-2 (orange). The y-axis shows the brGMGT FA calculated through the equation (29) and the x-axis the MBT'_{5ME} proxy (De Jonge et al. 2014). The correlation coefficient (R^2) and linear trend lines allow correlations to be identified easily.

6.1.3 Mean Annual Air Temperature Reconstructions according to the MBT'_{5ME} Proxy

The reconstruction of the different mean annual air temperatures from the distribution of the brGDGTs of the measurements Man-1 and Man-2 are depending on the calculated MBT'_{5ME} index (Figure 13a). From the formula of the MBT'_{5ME} index, an increase of the tetramethylated brGDGTs Ia, Ib, Ic compared to the penta- and hexamethylated brGDGTs indicates an increase of the MBT'_{5ME} values and consequently an increase of MAAT. The slight increase in MBT'_{5ME} values and thus MAAT are mainly due to an increase in uncyclized and monocyclized tetramethylated brGDGT Ia, Ib. Also, from the calculated methylation set (Figure 22) according to the plotting style of (Raberg et al. 2021), it is evident that with increasing MBT'_{5ME} values and from this the temperature, the abundance of the two mentioned tetramethylated brGDGTs increases. The strong positive correlation of the FA of Ia to the MBT'_{5ME} index and to the temperature was also found in other studies and can therefore be confirmed (De Jonge et al. 2014; Russell et al. 2018).

As shown by the methylation sets of brGDGTs (Figure 22) and brGMGTs (Figure 23), the observed correlations between methylation and FA of brGDGTs are not transferable to brGMGTs. There is a negative correlation between temperature and methylation of GMGTs found by (De Jonge et al. 2014), which would be the opposite of the correlation between GDGTs and MBT'_{5ME} . This can only be confirmed with limitations for H-1034b, which shows a decrease in FA with increasing temperature (Figure 23). It is remarkable that in contrast to the MAAT calibrations obtained from the results of the brGDGT distribution, the $MAAT_{brGMGT}$ calibration from the brGMGTs does not show any trend towards temperature increase, despite the earlier findings by Baxter in another tropical lake (Baxter et al. 2019) (Figure 14). The relation of the FA of the brGMGTs against the MBT'_{5ME} index shows no correlation, indicating that the brGMGTs do not respond to a temperature change according to the proxies (Figure 24).

The MAAT reconstruction from the distribution of the brGDGTs shows, even if not quite clear and not quite steady, temperature increase (Figure 25). In contrast to the MAAT reconstruction according to MBT'_{5ME} , which shows a fluctuation of more than 8 °C over the period considered and a warming trend towards the top of the sediment of 1.63 °C. However, it is to be questioned generally whether, in the period of 2500 cal yr BP in the southern latitudes close to the equator, where Sumatra is to be found, a temperature rise is to be expected at all. If one leaves out of consideration first that the rapid warming induced by increasing anthropogenic greenhouse gases. The hypothesis proposed at the beginning, which assumes a temperature decline even until the end of the little ice age (1450-1850 CE) of terrestrial temperatures on Sumatra, cannot be supported by the reconstructed MAAT according to the MBT'_{5ME} proxy. Global proxy records suggest a cooling in marine and terrestrial temperature during the late Holocene, whereas climate models simulate a global long-term warming trend, which would be consistent with Maninjau's MAAT reconstruction (Liu et al. 2014).

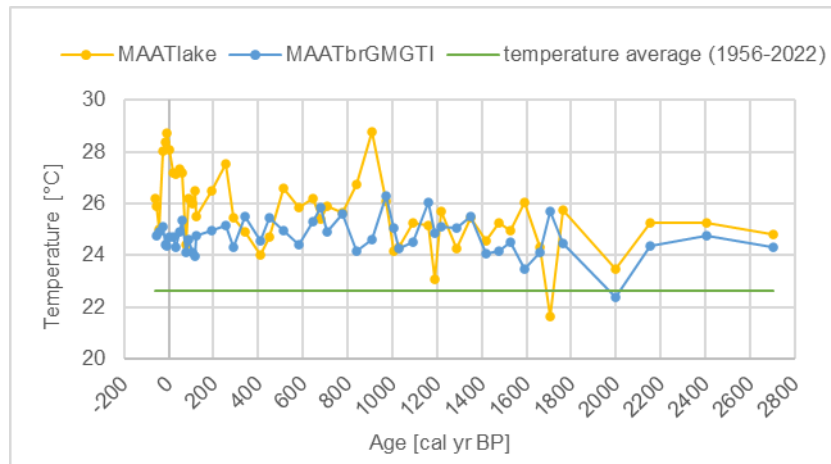


Figure 25: Mean annual air temperature reconstructions plotted against ^{14}C age. The y-axis shows the ^{14}C dated age from basal 2660-2340 cal yr BP and the x-axis shows the temperature reconstructions $\text{MAAT}_{\text{lake}}$ and $\text{MAAT}_{\text{brGMGTI}}$ according to $\text{MBT}'_{5\text{ME}}$ and brGMGTI proxy resulted from both HPLC-APCI-MS Maninjau measurements of Man-1 and Man-2. The green line indicates the temperature average (1956-2022) of Maninjau (Weatherspark Maninjau 2022; Climate-data Maninjau 2022).

A change in climatic conditions including temperature, can be influenced by various large-scale climatic events. Influences on climatic conditions in the IPWP include the annual shift of the ITCZ to the south and north, the changing Walker circulation, and trade winds, which affect the Indian Monsoon and thus ENSO phenomena (Niedermeyer et al. 2014; De Deckker 2016). In the case of the Maninjau lake sediment core, each of the 50 samples corresponds to a dated average time period of 54 years. Thus, climatic changes caused by ENSO, which occur in a sub-decadal manner, cannot be recorded. Thus, the observed long-term warming trend for Sumatra in the case of the Man-18-44A sediment core should have other causes, such as changes in orbital insolation, volcanic forcing, or changes in the mean Walker circulation or ocean dynamics. In summary, the warming trend of the MAAT reconstruction of Sumatra according to the $\text{MBT}'_{5\text{ME}}$ proxy does not match with the global proxy temperature reconstruction (Liu et al. 2014; Kaufman et al. 2020). However, our data suggests the opposite to global reconstructions, and a different temperature trend or a steady temperature on Sumatra in the late Holocene can therefore not be excluded. Due to the general lack of temperature reconstructions for the late Holocene in South-East Asia, the temperature development there can not yet be answered conclusively.

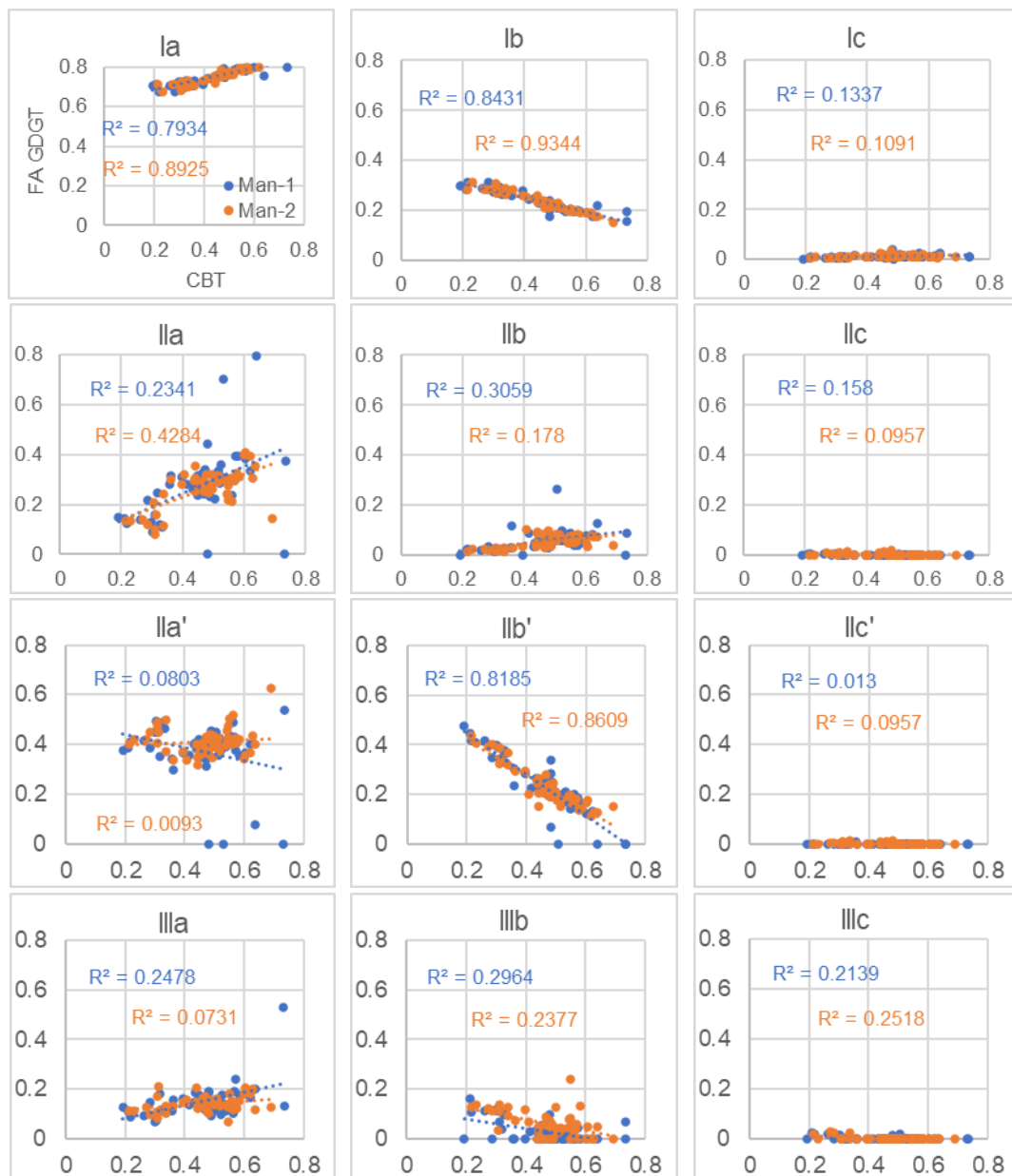
6.1.4 Fractional Abundance of brGDGTs in relation to CBT

In order to show the correlation between the cyclization of brGDGTs and CBT proxy, the representation method of the FA of the brGDGTs, the so-called cyclization set (Raberg et al. 2021), was used. The cyclization set calculated for tetra-, penta- and hexamethylated brGDGTs is related to the CBT proxy of (Weijers et al. 2007). This allows to find out which compounds contribute most to the CBT proxy and supposedly react most strongly to pH, assuming a relationship between CBT and pH. A calculation example is given for a uncyclized brGDGTs (29):

$$FA_{IIIa} = \frac{IIIa}{\sum \text{hexamethylated brGDGTs}} = \frac{IIIa}{(IIIa + IIIb + IIIc + IIIa' + IIIa'' + IIIa''')} \quad (29)$$

The plots show noticeable results for two out of four monocyclized brGDGTs Ib, Ib' (Figure 26). These brGDGTs correlates linearly negative with CBT. For the tetramethylated

monocyclized brGDGT Ib with the correlation coefficients for Man-1 ($R^2 = 0.84$) and for Man-2 with ($R^2 = 0.93$), a clear correlation can be seen between FA and CBT. Insufficient correlations can be observed for cyclized brGDGTs Ic, IIc, IIc', IIIc and IIb and IIIb. The abundance of the hexamethylated ones are probably very low, as they were not found in every analysed sample to draw significant conclusions. The conclusion of (Raberg et al. 2021) that with a decreasing CBT values and the resulting higher pH values all cyclized brGDGTs occur in higher abundance can be confirmed for the monocyclized except for IIb, which shows a weak negative correlation. For the 5-methyl uncyclized tetra-, penta- and hexamethylated brGDGTs Ia, IIa, IIIa, an increase in FA with the CBT proxy can be seen. On the other hand, the 6-methyl uncyclized isomers IIa', IIIa' do not show a clear correlation. In conclusion, the abundance of bicyclized brGDGTs increases with decreasing CBT proxy with results in higher pH (Figure 26).



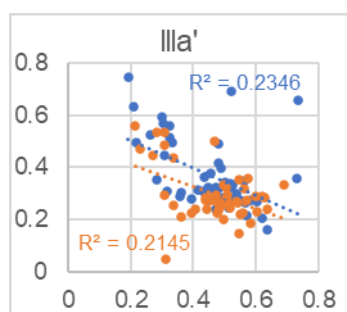


Figure 26: The fractional abundance of brGDGTs plotted against the CBT proxy. The y-axis shows the brGDGT FA calculated by the cyclization set of (Raberg et al. 2021) and the x-axis the CBT proxy (Weijers et al. 2007) from the HPLC-APCI-MS measurements Man-1 (blue) and Man-2 (orange). Thereby, low CBT values correspond to a low reconstructed pH value. The correlation coefficient (R^2) and linear trend lines allow correlations to be identified easily.

6.1.5 pH Reconstructions according to the CBT Proxy

Through the different CBT proxies the cyclization is considered and with the respective calibration the pH value can be reconstructed. (Weijers et al. 2007) indicated that the degree of cyclization and the degree of the methylation are linked to pH; higher numbers of cyclopentane rings should be found more likely at higher pH values. The Maninjau results show that the monocyclized brGDGTs Ib, IIb' a negative correlation between FA and the CBT proxy (Figure 26), which confirm the hypothesis of (Weijers et al. 2007).

But it cannot be confirmed that in general, a negative correlation between cyclization and CBT, corresponding likely to increasing pH, since the most highly cyclized brGDGTs, those with two cyclopentane rings, do not show a correlation (Figure 26). Thus, the statement (Weijers et al. 2007) of the positive correlation between cyclization and pH, which was found in soils, can only be partially confirmed. In the Maninjau results, the behaviour to CBT proxy differs from monocyclized to bicyclized brGDGTs, so the simple relationship between cyclization and CBT, and thus supposedly pH, does not hold.

Remarkably, as mentioned above, a negative correlation to CBT is found for IIb' but none for IIb (Figure 26). Based on this result, it seems that an increase in pH according to a decreasing CBT proxy does not have the same effect on 5-methyl and 6-methyl brGDGTs. (De Jonge et al. 2014) suspected a common biological source on the basis that 5-methyl and 6-methyl cyclopentane containing brGDGTs both presented a positive correlation to pH value; this cannot be confirmed here. However, it could be assumed that the community of 6-methyl-producing bacteria is shifting towards higher pH.

In studies on the surface sediment of East African lakes, only weak correlations were found between pH and the cyclization of brGDGTs (Tierney et al. 2010). Also, (Baxter et al. 2019) found that the correlation between cyclization and pH was not evident. This makes it not surprising that with the Maninjau results, the negative correlation between cyclization and CBT proxy can only be confirmed with constraints. Also, a negative correlation between methylation and pH value was found, although much weaker than the correlation between methylation and pH (Weijers et al. 2007). The Maninjau results show slight positive correlations for the FA of pentamethylated brGDGTs IIa, IIb and for the hexamethylated IIIa to CBT (Figure 26). For these brGDGTs the statement (Weijers et al. 2007) can be confirmed, since the FA of the components increases with decreasing (reconstructed) pH.

Based on the observed correlations between FA of the brGDGTs and the pH_{CBT} calibration of (De Jonge et al. 2014) and the CBT proxy variant (Weijers et al. 2007) can be considered most suitable for the Maninjau samples. This includes the brGDGTs Ib and IIb', which

represent the strongest correlation to CBT (Figure 26). The CBT_{peat} proxy (Naafs et al. 2019) also includes Ib and IIb' but even bicyclized brGDGTs Ic and IIc', which do not yield significant results in the Maninjau measurements. The Maninjau results show a slight increase in pH according to the CBT proxy from the bottom to the top of the sediment (Figure 16). Independent pH measurements are not known, in order to make a statement about the validity of the pH value reconstructions.

It has been found that the CBT proxy is also dependent on alkalinity (Schoon et al. 2013). A high alkalinity increases the FA of the uncyclized brGDGTs. When comparing the FA, the uncyclized brGDGTs are more frequent than those with cyclopentane rings (Figure 9). This result could indicate high alkalinity, which may have increased over the last 30 years due to increasing anthropogenic influences through the influx of ions as nutrients and increased organic algal production (Zhang et al. 2016). Due to the algae's photosynthesis, dissolved inorganic carbon is taken up from the water (carbonate equilibria), which increases the alkalinity (Schlesinger and Bernhardt 2020).

6.1.6 Impact of Soil Organic Matter

The BIT represents the relative abundance of the brGDGTs to the isoGDGT crenarchaeol to show the influence of terrestrial organic matter into lacustrine sediments. (Hopmans et al. 2004) showed that results close to 1 are characteristic for soil and peat samples and results close to 0 for marine sediments, which can be transferred with restrictions to lacustrine sediments. The ratio of br-/isoGDGTs is an extended variant, where brGDGTs are compared to isoGDGTs up to 3 cyclopentane moieties, crenarchaeol and crenarchaeol regioisomer. The rather low values of BIT index and of the br-/isoGDGT ratio on average indicate a relatively low terrestrial influence (Figure 17). The results of both indices show an increase in values in the upper 10 cm of the sediment core. There are two possible explanations for this, either terrestrial influence has increased over the period of these sediment deposits or brGDGTs have increased due to in situ production. The latter is unlikely, as presumably increased BIT and br-/isoGDGT ratio would tend to show in the whole sediment core if brGDGTs were produced in situ (Tierney and Russell 2009; Tierney et al. 2012; Sinninghe Damsté et al. 2012). When considering all GDGTs, there is an increase in the FA of the brGDGTs and no decrease in the FA of the isoGDGTs towards the top. This must be considered that the high BIT and br-/isoGDGT ratio values are not entirely caused by an increase in uncyclized brGDGTs alone.

Increased terrestrial influence could be due to erosion from enhanced anthropogenic influences, the use of lake Maninjau for economic use by aquaculture since 1992 (Junaidi 2014). Another possible reason for increased erosion and then terrestrial organic matter introduced by surface runoff is increased rainfall, which on Sumatra is influenced by ENSO and the Indian Monsoon. This could be identified as a reason for high brGDGTs for the East African Lake Challa (Verschuren et al. 2009). Due to the fact that lake Maninjau has no major inflows, an increased input of brGDGTs by rivers flowing into the lake is unlikely (Cohen 2003). Increased rainfall could be a possible reason for the elevated BIT and br-/isoGDGT ratio values in the lower part of the sediment cores between 35-40 cm (Figure 17). A possible reason, as mentioned, would be increased erosion during this period of sediment deposition due to increased rainfall. Another cause of erosion is human perturbation, such as deforestation or agricultural land use.

6.1.7 Impact of Isomerization

The isomerization of the brGDGTs can be determined using the IR_{6ME} index, which represents the ratio between 5- and 6-methyl brGDGTs, and the IBT index, which considers only uncyclized 5- and 6-methyl brGDGTs. From the results of the IR_{6ME} index it can be concluded that penta- and hexamethylated brGDGTs with the methyl group at the 6th carbon dominate over those with the methyl group at the 5th carbon, this ratio increases towards the top of the sediment (Figure 18a). The results of the IBT index show that even with the uncyclized brGDGTs alone, the 6-methyl brGDGTs dominate and even increase towards the surface of the sediment (Figure 18b). One explanation why the HPLC-APCI-MS measurements show a clearer trend at Man-2 than at Man-1 is probably due to inaccurate integration, as it only affects single values.

Both the results of the temperature reconstruction and the pH reconstruction, show a slight trend towards higher values towards the surface. Thus, there could be a link to isomerization. The results could indicate that at elevated temperature and/or at elevated pH there is a tendency for more 6-methyl brGDGTs to be formed. Verification of the correlation of the isomerization indices and the $MAAT_{lake}$ calibration (Russell et al. 2018) according to MBT'_{5ME} proxies (De Jonge et al. 2014) show strong correlations to the two proxies IR_{6ME} and IBT for Man-1 and Man-2 (Figure 28).

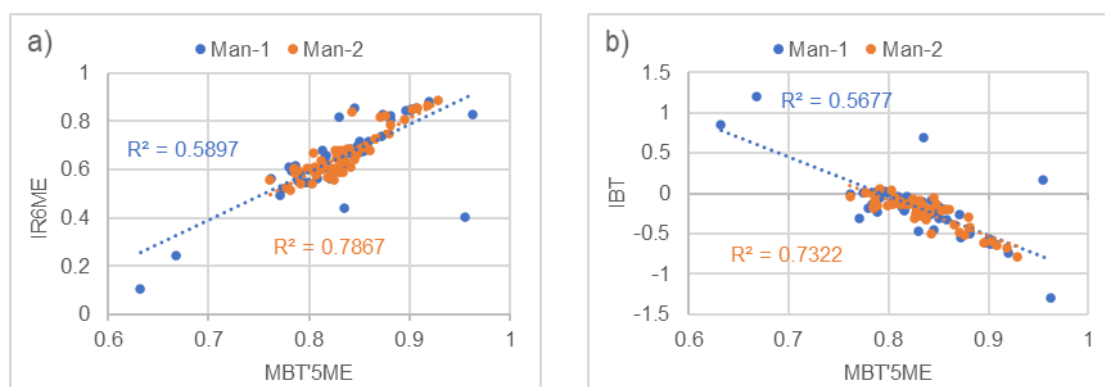


Figure 27: a) Relation between IR_{6ME} and MBT'_{5ME} , b) Relation between IBT and MBT'_{5ME} of both HPLC-APCI-MS Maninjau measurements of Man-1 (blue) and Man-2 (orange). Based on the definition of the IR_{6ME} (Yang et al. 2015) and IBT index (Ding et al. 2015) both correlations indicate increased 6-methyl brGDGT isomer formation with increased MBT'_{5ME} proxy (De Jonge et al. 2014).

Correlations between the isomerization indices and the CBT proxy (Weijers et al. 2007) can also be observed (Figure 28). Due to the negative logarithmic definition of the CBT formula, a negative correlation between the isomerisation indices and CBT results in a positive correlation to the pH (8). A positive correlation between pH and IR_{6ME} was also found for soil samples (Yang et al. 2015) and also for peat samples (Naafs et al. 2017b). In this case, the correlation between the IR_{6ME} and the CBT value is the better correlation (Figure 28a). But it shows that isomerization correlates better with MBT'_{5ME} than with CBT. Thus, it can be concluded that the isomerization of the brGDGTs is critical for temperature and pH reconstruction. Thus, it should be noted that the 6-methyl isomers are taken into account in the development of respective proxies for pH and temperature. Also of interest would be the effect of other isomers, such as 5/6-methyl or 7-methyl, which could be studied by a suitably defined proxies to pH value and temperature. Today's knowledge especially about isomers other than 6-methyl is too limited to obtain accurate results.

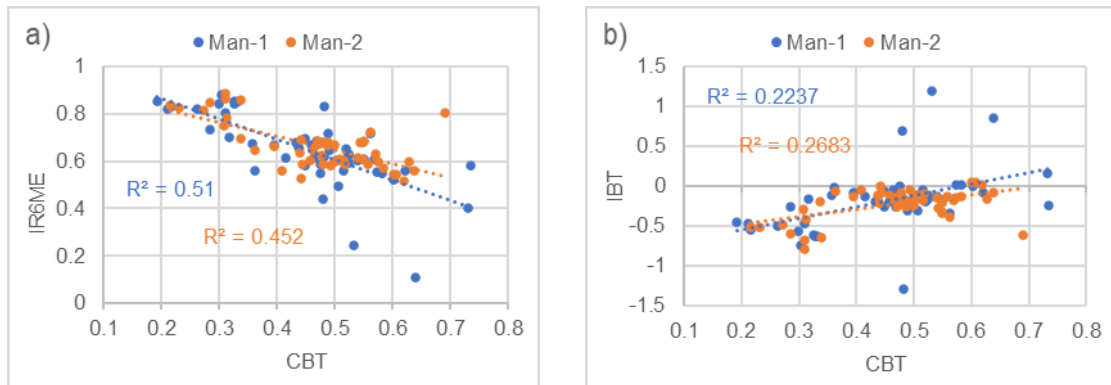


Figure 28: a) Relation between IR_{6ME} and CBT, b) Relation between IBT and CBT of both HPLC-APCI-MS Maninjau measurements of Man-1 (blue) and Man-2 (orange). Based on the definition of IR_{6ME} (Yang et al. 2015) and IBT (Ding et al. 2015) both correlations indicate increased 6-methyl brGDGT isomer formation with decreased CBT proxy (Weijers et al. 2007).

6.2 Interpretation of Isoprenoid Tetraethers Proxies

6.2.1 Fractional Abundance of isoGDGTs according to TEX_{86} Proxy

An investigation of a correlation between the FA of the isoGDGTs and the TEX_{86} proxy provides information on which component has the greatest impact on the TEX_{86} values and thus supposedly determines the derived ALST (Figure 29).

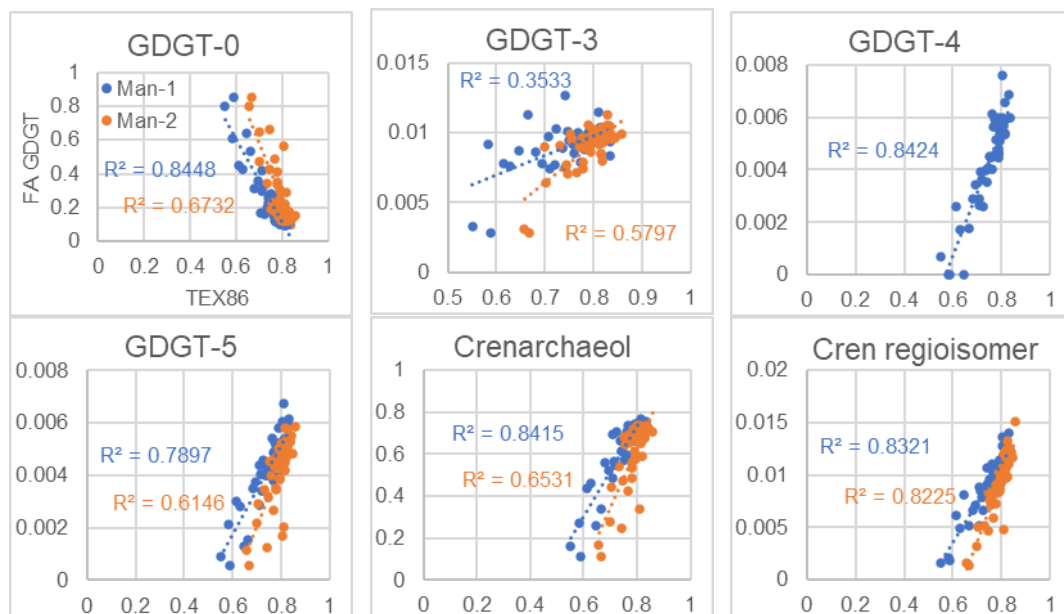


Figure 29: The fractional abundance of isoGDGTs plotted against TEX_{86} proxy. The y-axis shows the isoGDGT FA and the x-axis the TEX_{86} proxy (Schouten et al. 2002) from the HPLC-APCI-MS measurements Man-1 (blue) and Man-2 (orange). The correlation coefficient (R^2) and linear trend lines allow correlations to be identified easily.

6.2.2 Lake Surface Temperature Reconstructions according to the TEX_{86} Proxy

From the tetraether proxy TEX_{86} the sea surface temperature and accordingly, the lake surface temperature can be calculated and serves as a paleothermometer. The reconstruction from the different calibrations calculated lake surface temperatures shows no clear trend (Figure 20). Presumably, as for MAAT, no real trend for warming in the region of Sumatra and in the time period is to be expected. But the observation can be made that all compounds used

in the TEX_{86} proxy contribute significantly (Figure 29). Based on the positive correlation between TEX_{86} proxy and the multiple cyclized isoGDGTs and the negative correlation especially of the uncyclized GDGT-0 to TEX_{86} proxy. The positive correlation was detected between the number of cyclized rings and temperature by (Schouten et al. 2002).

A negative linear relationship between TEX_{86} and BIT, as found by (Inglis and Tierney 2020), can be observed in the Maninjau results (Figure 30a). Also a negative correlation to the additional calculated ratio of br-/isoGDGTs (Figure 30b). (Inglis and Tierney 2020) assume a possible oxic degradation of the sediments if the negative relationship between TEX_{86} and BIT with low TEX_{86} values. This is not the case for the Maninjau samples. In deep tropical lakes, such as lake Maninjau with an average water depth of 100 m, there is often no turnover of the water layers resulting in a permanent anoxic hypolimnion (Akmal et al. 2021; Powers et al. 2010). So probably no oxic degradation can be expected in lake Maninjau.

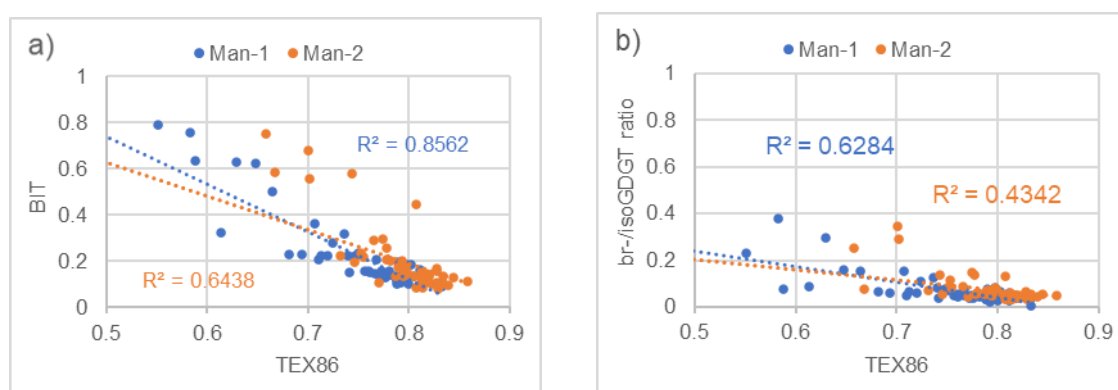


Figure 30: a) Relation BIT and TEX_{86} , b) Relation br-/isoGDGT and TEX_{86} of both HPLC-APCI-MS Maninjau measurements of Man-1 (blue) and Man-2 (orange). In case BIT (Hopmans et al. 2004) and br-/isoGDGT (Naehler et al. 2012) to TEX_{86} a negative linear correlations can be found.

The reconstruction must be considered critically, because especially the large difference of the individual LST is remarkable. Clearly not feasible are the reconstructed LSTs for the most recent period, which were obtained from the isoGDGT distribution of the upper sediment samples. Temperatures well below 25 °C can be considered unrealistic. Recent, studies have measured water temperatures for lake Maninjau average 27.2 °C in the epilimnion (Santoso et al. 2021), surface water temperatures between 28.0-29.0 °C (Henny and Nomosatryo 2016), or temperatures range from 28.1-32.9 °C (Komala et al. 2019). With the information from the measured values, it can be presumed that the ALST calibration (Powers et al. 2010), which was explicitly developed for lakes and thus differs from the other calibrations used, is the most appropriate with average values of 27.19 °C for Man-1 and 29.09 °C for Man-2.

In the sediment samples where lower ALST according to the TEX_{86} proxy were found, high BIT values and br-/isoGDGT ratios were found. The high BIT values and br-/isoGDGT ratios could also indicate a high influence of terrestrial organic matter, which is a restriction for the application of the TEX_{86} proxy and therefore it is not surprising how it is the case in the upper 10 cm and between 35-40 cm of the sediment cores (Weijers et al. 2006b). At BIT values > 0.3, the influence of TEX_{86} proxy reconstructed temperature is estimated to be > 2 °C (Weijers et al. 2006b).

High values (> 0.3) of the methane index would also be a restriction for the use of TEX_{86} , as a larger contribution of methanogenic archaea could bias the SST and LST calibrations (Zhang et al. 2011) (Figure 21a). Since almost all Maninjau values are < 0.1, no restriction to use of the TEX_{86} proxy can be assumed. Low MI values suggest that isoGDGTs are synthesized by

non-methanotrophic Thaumarchaeota (Zhang et al. 2011). This inference comes from the fact that crenarchaeol is not synthesized by methanotrophic Euryarchaeota but by non-methanotrophic Thaumarchaeota. As soon as the ratio of crenarchaeol and crenarchaeol regioisomer to GDGT-1, -2 and 3 is correspondingly high, low MI values are obtained. The results of the methane index indicate anaerobic oxidation of methane (AOM) performing archaea are not prevalent, which would be a restriction for the application of the TEX₈₆ proxy. The ratio of GDGT-0 to crenarchaeol is < 0.2 in only a few cases, which would affect the TEX₈₆ proxy signal by AOM archaea (Blaga et al. 2009) (Figure 21b). These results imply a low or insignificant influence of AOM archaea, confirming the conclusion from the MI.

(Qin et al. 2015) found an influence of different oxygen concentrations on TEX₈₆ proxies. Pure culture studies of archaea in low-oxygen environments, which affect lipid biosynthesis, were linked to high TEX₈₆ values (Qin et al. 2015). The enhanced synthesis of GDGT-2 and GDGT-3 at the expense of GDGT-1 under oxygen limitation increases the TEX₈₆ values (Qin et al. 2015). (Zhang et al. 2016) even suggested that the TEX₈₆ values are primarily influenced by oxygen dissolved in the water and not by temperature. The details are still poorly investigated, but due to the redistribution of isoGDGTs, a reassessment of the TEX₈₆ proxies needs to be considered. Since the nutrient content of lake Maninjau has increased due to aquaculture, resulting in increased primary production and its oxygen-depleting degradation, low-oxygen conditions are well possible in lake Maninjau (Komala et al. 2019). Due to the fact that there is no significant increase in the TEX₈₆ values of the sediment samples, there is also no clear increase in GDGT-2 and GDGT-3. On the other hand, (Zhang et al. 2016) found that oxygen depletion promotes a community shift towards methanogenic Euryarchaeota. In the case of lake Maninjau, no increased influence of methanogenic archaea through the methane index could be detected. The predominant anoxic degradation of organic carbon could be sulphate reduction in a volcanic lake like Maninjau, which contains a lot of sulphur. By sulphate reducing bacteria (SRB), sulphur is reduced, and carbon is used as a substrate and oxidised. Nonetheless a bias by the oxygen-influenced isoGDGT distribution of the LST according to the TEX₈₆ proxy is possible but cannot be answered conclusively.

Other influences can also affect the LST according to the TEX₈₆ proxy, such as seasonal influences (Inglis and Tierney 2020). However, the climate, especially the temperatures on Sumatra are not very seasonal and therefore the seasonal influence can be assumed to be small. (Schouten et al. 2004) estimated the effect of membrane lipid degradation on TEX₈₆ proxies to be small. The isoGDGT distribution in the sediment deposits does not reflect the surface temperature but rather the mean annual temperature of the water layer with the highest biological productivity. Since different water temperatures in the lake physically form different layers, it is essential for a temperature reconstruction to know whether the archaea lived in the warm epilimnion near the surface or in the lower colder hypolimnion. For the accuracy of the results, only isoGDGTs formed in the epilimnion would be best, since via the TEX₈₆ proxy reconstructs the surface temperature of the lake. (Qin et al. 2015) found that the most abundant populations of archaea are found near the light-flooded, photic zone and (Zhang et al. 2016) observed the highest biological productivity along the oxycline. This suggests that oxygen content as mentioned above, plays a key role in membrane composition, influencing the reconstructed temperature and therefore representing an inaccuracy of the TEX₈₆ proxy.

(Doose-Rolinski et al. 2001) suggest that SST changes are driven by changes in the monsoon strength and coming to the conclusion that the climate of the past 1500 yr BP infer by increased monsoonal variability, as shown by relative strong fluctuations in temperature and salinity reconstructions (Thompson et al. 1995). Some temperature fluctuations could be observed in the case of lake Maninjau, an influence of the fluctuations of the Monsson is

possible but cannot be verified with the sample resolution of 54 years per measurement on average.

6.3 Constraints on the Results

It should not be forgotten that the results of the HPLC-APCI-MS measurements Man-1 and Man-2 must be viewed critically, especially because only one replicate was made due to time constraints. Since the second measurement, Man-2 with a slightly different method, with an increase in injection volume and temperature, yields different results, it should be repeated. Errors cannot be excluded in the data collection alone. An inaccurate integration of the peaks due to incomplete separation, coelution and different isomers of the GDGTs in the HPLC-APCI-MS results or for the Maninjau lake sediment unsuitable calibrations for MAAT, ALST or pH. Especially with respect to the GDGTs, which are not considered in the proxies, such as 5/6-methyl and 7-methyl isomers. Regarding the proxies comparing isoGDGTs and brGDGTs, it should be noted that the brGDGTs have a higher response factor in the mass spectrometry measurement and thus their abundance through peak integration may be calculated higher than in comparison to the isoGDGTs (according to a personal note from R.H. Smittenberg (2022)).

But of course, it cannot be excluded that the proxies and calibrations used in this work are inaccurate or incorrect. Neither can it be eliminated that the distribution of the GDGTs may change after it has been deposited. Chemical alteration due to maturation or different turnover times of the GDGTs cannot be excluded. The conditions prevailing at the lake bottom also play an influence on the degradation of dead bacteria and archaea. Degradation under oxic or anoxic conditions could influence the turnover time. (Huguet et al. 2017) suggested the highest turnover time in the oxic acrotelm part of peat. Often anoxic conditions are found at the bottom of lakes, especially in the case of high organic production and its oxygen-depleting degradation, which can probably be assumed for lake Maninjau. This indicates good preservation of GDGTs in the lake Maninjau.

6.4 Relevance for the Lake Maninjau

Aquaculture has the highest contribution to the contamination of organic matter in the lake Maninjau (Komala et al. 2019). 400 tonne/year of fish is removed from the lake, which also explains why 95 % of the nutrient waste load, mainly nitrogen and phosphates, enters the lake through fish farming (Henny and Nomosatryo 2016). The low water quality is also characterised by high organic carbon content. There are two different sources, either it comes from the primary production in the lake itself or it enters the lake from the catchment through e.g., erosion, aquaculture, agriculture, or wastewater discharge (Komala et al. 2019). Increased erosion and runoff of surface water with dissolved carbon can result from increased precipitation (Yodfiatfinda 2017).

Increased nutrient contribution increases phytoplankton production, and the algal blooming of cyanobacteria (Microcystis) has been observed in the lake (Sulastris et al. 2016). (Li et al. 2017) revealed that nitrogen and phosphorus were essential nutrients for algae growth. These lead to reduced water clarity and light penetration, which is problematic for photosynthetic organisms, which could subsequently die and be degraded, consuming oxygen. As a result, the sediments become oxygen-free, causing phosphate to be released from the sediments, which increases phytoplankton growth. A reduction in dissolved oxygen content has been observed (Komala et al. 2019). The cycle of increased nutrient input and more organic material leads to eutrophication of the lake. Dead organic material sinks to the bottom of the lake and

is deposited there. If there is a precipitation event that brings cold water into the lake in relation to the water temperature, this sinks downwards due to the higher density, resulting in convection, which brings the nutrients deposited on the bottom back to the upper water layers. The result is an increase in the phytoplankton production. A correlation between precipitation patterns and dissolved oxygen concentration has been established (Yodfiatfinda 2017). However, changes in wind speeds, which are influenced by shifts in large-scale climatic phenomena such as the shift in the ITCZ, are another reason for water mixing.

Maninjau is of volcanic origin, which is why it contains a large amount of sulphur. The increase in organic carbon increases the production of hydrogen sulphide. The degradation of organic carbon can be carried out by sulphate reducing bacteria (SRB). Elevated methane levels were not found, reflecting the results of the Maninjau sediment core. The MI index is low, indicating the presence of non-methanogenic archaea. The results indicate that the pH has increased slightly over the last 2500 years BP. One reason for this could be the increased photosynthesis rate, which releases OH⁻ ions and thereby increases the pH (Killops and Killops 2005). Especially in the last 30 years, this could have been a reason for the pH rise.

7. Conclusion and Future Prospects

In this bachelor thesis, brGDGTs and isoGDGTs from lake sediment (Man-18-44A) of lake Maninjau in Sumatra, Indonesia, were quantified by HPLC-APCI-MS analysis and following peak integration. Tetramethylated were the most abundant brGDGT with a mean relative abundance of 59.92 %, mainly due to 5-methyl uncyclized brGDGTs Ia. Crenarchaeol was the most abundant isoGDGT with a mean relative abundance of 59.12 %. The age of the sediment core was dated to a basal ¹⁴C age of 2660-2340 yr BP.

For a temperature reconstruction the MBT'_{5ME} proxy was used, which is mainly controlled by uncyclized brGDGTs Ia and IIa due to the high correlation with FA, calculated according to the (Raberg et al. 2021) methylation set. The influence of monocyclized brGDGTs Ib and IIb on the MBT'_{5ME} proxy was observed, from which it can be concluded that the MBT'_{5ME} proxy and probably also MAAT are mainly determined by the ratio of un- and monocyclized tetra- to pentamethylated brGDGTs. A significant influence of brGMGTs on MAAT could not be detected by the correlation of FA with the brGMGTI or MBT'_{5ME} proxy. But it should be mentioned that the state of research on GMGTs is still too limited to be able to make precise statements. The reconstructed mean annual air temperature according to MBT'_{5ME} proxy shows a mean fluctuation of over 8 °C with a warming trend of $\bar{x} = 1.63$ °C towards the top of the sediment at recent times. The reconstructed temperature increase should be questioned from a critical perspective, as it is disputable whether a temperature increase in the last 2500 yr BP can be expected in the southern latitudes close to the equator, where Sumatra is located in. The hypothesis put forward at the beginning of the thesis as to whether an SST decrease gradient in the northern hemisphere west of Sumatra can also be transferred to terrestrial temperatures cannot be confirmed by the results achieved. Instead, the results indicate an opposite conclusion.

The CBT proxy and the resulting pH increase in the mean $\bar{x} = 0.79$ is mainly determined by the bicyclized brGDGTs Ib, IIb', which shows the negative correlation between CBT proxy and FA, calculated according to the cyclization set of (Raberg et al. 2021). A correlation with multiple cyclized (bicyclized) brGDGTs cannot be detected. Therefore, the simple relationship between cyclization and CBT, and thus supposedly pH, is not valid due to the different behaviour of monocyclized and bicyclized brGDGTs. All pH reconstructions according to

different CBT proxies show a slight increase of the pH value upwards with an average of 1.36 fluctuation. Correlations between MBT_{5ME} and CBT proxies to the isomerization index IR_{6ME} suggest that 6-methyl brGDGTs have an effect on both temperature and pH. In the further development of such proxies, the influence of 5/6- or 7-methyl isomers could be examined in addition to the influence of 6-methyl isomers. The impact of alkalinity and conductivity on the CBT proxy is recognised and could also be tested for lake Maninjau in the future.

Calibrations of the ALST resulting from the TEX_{86} proxy do not show a significant trend. Presumably, as for MAAT, no real trend for warming in the region of Sumatra and in the period is to be expected. An increase in the BIT index was observed towards the sediment top, which indicates an increased influence of brGDGTs. The increase in brGDGTs may be due to erosion, in lake Maninjau as a result of increased human activity, especially through high aquaculture use. An impact of AOM could not be detected with the help of the MI index but cannot be excluded. The predominant anoxic degradation of organic carbon in a volcanic lake with a lot of sulphur, as in the case of lake Maninjau, could be sulphate reduction by sulphate reducing bacteria (SRB). Further measurements are needed to conclusively answer the question of whether the TEX_{86} proxy are affected by the oxygen content, even more so than by the temperature.

To improve the results presented in this thesis, further HPLC-APCI-MS measurements would have to be carried out to optimise the accuracy of the data. In particular, the replicate measurement (Man-2) with the higher injection and temperature should be repeated, if necessary, as it showed slightly different results than the first measurement (Man-1). Also, a general change in chromatography could possibly result in better separation of the peaks and lower background noise, which would enhance the accuracy of the data. The possible inclusion of other forms of GDGTs, such as OH-GDGTs, GTGT or other isomers could improve proxies and calibrations. Also, for better paleodata, an analysis of the n-alkanes or specific stable isotopes in lake Maninjau could provide a wider insight into the paleoclimate and the paleoenvironmental. Overall, a better understanding of the role of the IPWP in global climate and the history of the ENSO and Indian Monsoon variability is needed to make reliable paleoclimate reconstructions and to estimate possible changes of the IPWP under global warming.

References

- Akmal, F., Rifai, H., Syafriani, S., Bouvet de la Maisonneuve, C., Oalmann, J. A. G., Forni, F., Eisele, S., Phua, M. & Putra, R. (2021). Identification of Elemental Composition and Heavy Metal Content in Maninjau Lake Sediment Using X-Ray Fluorescence (MNJ 18-41B). *JPSE (Journal of Physical Science and Engineering)* 6 (2), 68–76. <https://doi.org/10.17977/um024v6i22021p068>.
- Ayache, M., Swingedouw, D., Mary, Y., Eynaud, F. & Colin, C. (2018). Multi-centennial variability of the AMOC over the Holocene: A new reconstruction based on multiple proxy-derived SST records. *Global and Planetary Change* 170, 172–189. <https://doi.org/10.1016/j.gloplacha.2018.08.016>.
- Bale, N. J., Palatinszky, M., Rijpstra, W. I. C., Herbold, C. W., Wagner, M. & Sinninghe Damsté, J. S. (2019). Membrane Lipid Composition of the Moderately Thermophilic Ammonia-Oxidizing Archaeon "Candidatus Nitrosotenuis uzonensis" at Different Growth Temperatures. *Applied and environmental microbiology* 85 (20). <https://doi.org/10.1128/AEM.01332-19>.
- Baxter, A. J., Hopmans, E. C., Russell, J. M. & Sinninghe Damsté, J. S. (2019). Bacterial GMGTs in East African lake sediments: Their potential as palaeotemperature indicators. *Geochimica et Cosmochimica Acta* 259, 155–169. <https://doi.org/10.1016/j.gca.2019.05.039>.
- Baxter, A. J., Peterse, F., Verschuren, D. & Sinninghe Damsté, J. S. (2021). Anoxic in situ production of bacterial GMGTs in the water column and surficial bottom sediments of a meromictic tropical crater lake: Implications for lake paleothermometry. *Geochimica et Cosmochimica Acta* 306, 171–188. <https://doi.org/10.1016/j.gca.2021.05.015>.
- Beck, C. (2009). "Late Quaternary lacustrine paleo-seismic archives in north-western Alps: Examples of earthquake-origin assessment of sedimentary disturbances". *Earth-Science Reviews* 96 (4), 327–344. <https://doi.org/10.1016/j.earscirev.2009.07.005>.
- Berner, K. S., Koç, N., Godtlielsen, F. & Divine, D. (2011). Holocene climate variability of the Norwegian Atlantic Current during high and low solar insolation forcing. *Paleoceanography* 26 (2), n/a-n/a. <https://doi.org/10.1029/2010PA002002>.
- Błaga, C. I., Reichert, G.-J., Heiri, O. & Sinninghe Damsté, J. S. (2009). Tetraether membrane lipid distributions in water-column particulate matter and sediments: a study of 47 European lakes along a north–south transect. *Journal of Paleolimnology* 41 (3), 523–540. <https://doi.org/10.1007/s10933-008-9242-2>.
- Blome, M. W., Cohen, A. S., Tryon, C. A., Brooks, A. S. & Russell, J. (2012). The environmental context for the origins of modern human diversity: a synthesis of regional variability in African climate 150,000-30,000 years ago. *Journal of human evolution* 62 (5), 563–592. <https://doi.org/10.1016/j.jhevol.2012.01.011>.
- Bouvet de la Maisonneuve, C., Eisele, S., Forni, F., Hamdi, Park, E., Phua, M. & Putra, R. (2019). Bathymetric survey of lakes Maninjau and Diatas (West Sumatra), and lake Kerinci (Jambi). *Journal of Physics: Conference Series* 1185, 12001. <https://doi.org/10.1088/1742-6596/1185/1/012001>.
- Cai, W., Wang, G., Dewitte, B., Wu, L., Santoso, A., Takahashi, K., Yang, Y., Carréric, A. & McPhaden, M. J. (2018). Increased variability of eastern Pacific El Niño under greenhouse warming. *Nature* 564 (7735), 201–206. <https://doi.org/10.1038/s41586-018-0776-9>.
- Cai, W., Wu, L., Lengaigne, M., Li, T., McGregor, S., Kug, J.-S., Yu, J.-Y., Stuecker, M. F., Santoso, A., Li, X., Ham, Y.-G., Chikamoto, Y., Ng, B., McPhaden, M. J., Du, Y., Dommenges, D., Jia, F., Kajtar, J. B., Keenlyside, N., Lin, X., Luo, J.-J., Martín-Rey, M., Ruprich-Robert, Y., Wang, G., Xie, S.-P., Yang, Y., Kang, S. M., Choi, J.-Y., Gan, B.,

- Kim, G.-I., Kim, C.-E., Kim, S., Kim, J.-H. & Chang, P. (2019). Pantropical climate interactions. *Science (New York, N.Y.)* 363 (6430).
<https://doi.org/10.1126/science.aav4236>.
- Castañeda, I. S. & Schouten, S. (2011). A review of molecular organic proxies for examining modern and ancient lacustrine environments. *Quaternary Science Reviews* 30 (21-22), 2851–2891. <https://doi.org/10.1016/j.quascirev.2011.07.009>.
- Chabangborn, A. & Wohlfarth, B. (2014). Climate over mainland Southeast Asia 10.5-5 ka. *Journal of Quaternary Science* 29 (5), 445–454. <https://doi.org/10.1002/jqs.2715>.
- Chabangborn, A., Yamoah, K. K., Phantuwoongraj, S. & Choowong, M. (2018). Climate in Sundaland and Asian monsoon variability during the last deglaciation. *Quaternary International* 479, 141–147. <https://doi.org/10.1016/j.quaint.2017.04.017>.
- Chappe, B., Michaelis, W., Albrecht, P. & Ourisson, G. (1979). Fossil evidence for a novel series of archaeobacterial lipids. *Naturwissenschaften* 66 (10), 522–523.
<https://doi.org/10.1007/BF00404868>.
- Chen, Y., Zheng, F., Yang, H., Yang, W., Wu, R., Liu, X., Liang, H., Chen, H., Pei, H., Zhang, C., Pancost, R. D. & Zeng, Z. (2022). The production of diverse brGDGTs by an *Acidobacterium* allows a direct test of temperature and pH controls on their distribution.
- Climate-data Bukittinggi (2022). Bukittinggi climate: Average Temperature, weather by month, Bukittinggi weather averages - Climate-Data.org. Available online at <https://en.climate-data.org/asia/indonesia/west-sumatra/bukittinggi-32982/> (accessed 8/31/2022).
- Climate-data Maninjau (2022). Maninjau climate: Average Temperature, weather by month, Maninjau weather averages - Climate-Data.org. Available online at <https://en.climate-data.org/asia/indonesia/west-sumatra/maninjau-570079/> (accessed 8/31/2022).
- Cohen, A. S. (2003). *Paleolimnology. The History and Evolution of Lake Systems*. Oxford University Press.
- Coviaga, C., Cusminsky, G., Pérez, A. P., Schwalb, A., Markgraf, V. & Ariztegui, D. (2018). Paleoenvironmental changes during the last 3000 years in Lake Cari-Laufquen (Northern Patagonia, Argentina), inferred from ostracod paleoecology, petrophysical, sedimentological and geochemical data. *The Holocene* 28 (12), 1881–1893.
<https://doi.org/10.1177/0959683618798131>.
- Dang, H., Jian, Z., Wang, Y., Mohtadi, M., Rosenthal, Y., Ye, L., Bassinot, F. & Kuhnt, W. (2020). Pacific warm pool subsurface heat sequestration modulated Walker circulation and ENSO activity during the Holocene. *Science advances* 6 (42).
<https://doi.org/10.1126/sciadv.abc0402>.
- De Deckker, P. (2016). The Indo-Pacific Warm Pool: critical to world oceanography and world climate. *Geoscience Letters* 3 (1). <https://doi.org/10.1186/s40562-016-0054-3>.
- De Jonge, C., Hopmans, E. C., Stadnitskaia, A., Rijpstra, W. I. C., Hofland, R., Tegelaar, E. & Sinninghe Damsté, J. S. (2013). Identification of novel penta- and hexamethylated branched glycerol dialkyl glycerol tetraethers in peat using HPLC–MS2, GC–MS and GC–SMB-MS. *Organic Geochemistry* 54, 78–82.
<https://doi.org/10.1016/j.orggeochem.2012.10.004>.
- De Jonge, C., Hopmans, E. C., Zell, C. I., Kim, J.-H., Schouten, S. & Sinninghe Damsté, J. S. (2014). Occurrence and abundance of 6-methyl branched glycerol dialkyl glycerol tetraethers in soils: Implications for palaeoclimate reconstruction. *Geochimica et Cosmochimica Acta* 141, 97–112. <https://doi.org/10.1016/j.gca.2014.06.013>.
- De Jonge, C., Kuramae, E. E., Radujković, D., Weedon, J. T., Janssens, I. A. & Peterse, F. (2021). The influence of soil chemistry on branched tetraether lipids in mid- and high latitude soils: Implications for brGDGT- based paleothermometry. *Geochimica et Cosmochimica Acta* 310, 95–112. <https://doi.org/10.1016/j.gca.2021.06.037>.

- De Jonge, C., Radujković, D., Sigurdsson, B. D., Weedon, J. T., Janssens, I. & Peterse, F. (2019). Lipid biomarker temperature proxy responds to abrupt shift in the bacterial community composition in geothermally heated soils. *Organic Geochemistry* 137, 103897. <https://doi.org/10.1016/j.orggeochem.2019.07.006>.
- Ding, S., Xu, Y., Wang, Y., He, Y., Hou, J., Chen, L. & He, J.-S. (2015). Distribution of branched glycerol dialkyl glycerol tetraethers in surface soils of the Qinghai–Tibetan Plateau: implications of brGDGTs-based proxies in cold and dry regions. *Biogeosciences* 12 (11), 3141–3151. <https://doi.org/10.5194/bg-12-3141-2015>.
- Dommain, R., Couwenberg, J., Glaser, P. H., Joosten, H. & Suryadiputra, I. N. N. (2014). Carbon storage and release in Indonesian peatlands since the last deglaciation. *Quaternary Science Reviews* 97, 1–32. <https://doi.org/10.1016/j.quascirev.2014.05.002>.
- Doose-Rolinski, H., Rogalla, U., Scheeder, G., Lückge, A. & Rad, U. von (2001). High-resolution temperature and evaporation changes during the Late Holocene in the northeastern Arabian Sea. *Paleoceanography* 16 (4), 358–367. <https://doi.org/10.1029/2000PA000511>.
- Halamka, T., Raberg, J., McFarlin, J., Younkin, A., Mulligan, C., Liu, X.-L. & Kopf, S. (2022). Production of diverse brGDGTs by *Acidobacterium Solibacter usitatus* in response to temperature, pH, and O₂ provides a culturing perspective on brGDGT paleoproxies and biosynthesis. <https://doi.org/10.31223/X5WD2C>.
- Hällberg, P. L., Bueno, G. J., Schankat, Y. L., Steinbach, J., Rifai, H., Bouvet de la Maisonneuve, C. & Smittenberg, R. H. (2022b). Lipid biomarker glycerol dialkyl glycerol tetraether (GDGT) distributions from soils, peats and lake sediments on Sumatra. <https://doi.org/10.17043/hallberg-2022-sumatra-1>.
- Hällberg, P. L., Schenk, F., Yamoah, K. A., Kuang, X. & Smittenberg, R. H. (2022a). Seasonal aridity in the Indo-Pacific Warm Pool during the Late Glacial driven by El Niño-like conditions. *Climate of the Past* 18 (7), 1655–1674. <https://doi.org/10.5194/cp-18-1655-2022>.
- Heathcock, C. H., Finkelstein, B. L., Aoki, T. & Poulter, C. D. (1985). Stereostructure of the archaeobacterial C40 diol. *Science (New York, N.Y.)* 229 (4716), 862–864. <https://doi.org/10.1126/science.3927485>.
- Henny, C. & Nomosatryo, S. (2016). Changes in water quality and trophic status associated with cage aquaculture in Lake Maninjau, Indonesia. *IOP Conference Series: Earth and Environmental Science* 31 (1), 12027. <https://doi.org/10.1088/1755-1315/31/1/012027>.
- Hopmans, E. C., Schouten, S. & Sinninghe Damsté, J. S. (2016). The effect of improved chromatography on GDGT-based palaeoproxies. *Organic Geochemistry* 93, 1–6. <https://doi.org/10.1016/j.orggeochem.2015.12.006>.
- Hopmans, E. C., Weijers, J. W., Schefuß, E., Herfort, L., Sinninghe Damsté, J. S. & Schouten, S. (2004). A novel proxy for terrestrial organic matter in sediments based on branched and isoprenoid tetraether lipids. *Earth and Planetary Science Letters* 224 (1–2), 107–116. <https://doi.org/10.1016/j.epsl.2004.05.012>.
- Huguet, A., Wiesenberg, G. L., Gocke, M., Fosse, C. & Derenne, S. (2012). Branched tetraether membrane lipids associated with rhizoliths in loess: Rhizomicrobial overprinting of initial biomarker record. *Organic Geochemistry* 43, 12–19. <https://doi.org/10.1016/j.orggeochem.2011.11.006>.
- Huguet, C., Fietz, S., Rosell-Melé, A., Daura, X. & Costenaro, L. (2017). Molecular dynamics simulation study of the effect of glycerol dialkyl glycerol tetraether hydroxylation on membrane thermostability. *Biochimica et biophysica acta. Biomembranes* 1859 (5), 966–974. <https://doi.org/10.1016/j.bbamem.2017.02.009>.
- Inglis, G. N. & Tierney, J. E. (2020). The TEX86 Paleotemperature Proxy. <https://doi.org/10.1017/9781108846998>.

- Junaidi, A. (2014). Loading and Distribution of Organic Materials in Maninjau Lake West Sumatra Province-Indonesia. *Journal of Aquaculture Research & Development* 05 (07). <https://doi.org/10.4172/2155-9546.1000278>.
- Kaufman, D., McKay, N., Routsom, C., Erb, M., Dätwyler, C., Sommer, P. S., Heiri, O. & Davis, B. (2020). Holocene global mean surface temperature, a multi-method reconstruction approach. *Scientific data* 7 (1), 201. <https://doi.org/10.1038/s41597-020-0530-7>.
- Killops, S. D. & Killops, V. J. (2005). *An introduction to organic geochemistry*. 2nd ed. Malden, MA, Blackwell.
- Kim, J.-G., Jung, M.-Y., Park, S.-J., Rijpstra, W. I. C., Sinninghe Damsté, J. S., Madsen, E. L., Min, D., Kim, J.-S., Kim, G.-J. & Rhee, S.-K. (2012). Cultivation of a highly enriched ammonia-oxidizing archaeon of thaumarchaeotal group I.1b from an agricultural soil. *Environmental microbiology* 14 (6), 1528–1543. <https://doi.org/10.1111/j.1462-2920.2012.02740.x>.
- Kim, J.-H., Schouten, S., Hopmans, E. C., Donner, B. & Sinninghe Damsté, J. S. (2008). Global sediment core-top calibration of the TEX86 paleothermometer in the ocean. *Geochimica et Cosmochimica Acta* 72 (4), 1154–1173. <https://doi.org/10.1016/j.gca.2007.12.010>.
- Kim, J.-H., van der Meer, J., Schouten, S., Helmke, P., Willmott, V., Sangiorgi, F., Koç, N., Hopmans, E. C. & Damsté, J. S. S. (2010). New indices and calibrations derived from the distribution of crenarchaeal isoprenoid tetraether lipids: Implications for past sea surface temperature reconstructions. *Geochimica et Cosmochimica Acta* 74 (16), 4639–4654. <https://doi.org/10.1016/j.gca.2010.05.027>.
- Komala, P. S., Nur, A. & Nazhifa, I. (2019). Distribution of organic contamination based on depth stratification in Maninjau Lake, Indonesia. *IOP Conference Series: Materials Science and Engineering* 602 (1), 12057. <https://doi.org/10.1088/1757-899X/602/1/012057>.
- Kremer, K., Simpson, G. & Girardclos, S. (2012). Giant Lake Geneva tsunami in AD 563. *Nature Geoscience* 5 (11), 756–757. <https://doi.org/10.1038/ngeo1618>.
- Lehmusluoto, P. (1997). National inventory of the major lakes and reservoirs in Indonesia. Expedition Indodanau Technical Report, ... Available online at https://www.academia.edu/1025268/National_inventory_of_the_major_lakes_and_reservoirs_in_Indonesia.
- Li, X., Sha, J. & Wang, Z.-L. (2017). Chlorophyll-A Prediction of Lakes with Different Water Quality Patterns in China Based on Hybrid Neural Networks. *Water* 9 (7), 524. <https://doi.org/10.3390/w9070524>.
- Liang, J., Guo, Y., Richter, N., Xie, H., Vachula, R. S., Lupien, R. L., Zhao, B., Wang, M., Yao, Y., Hou, J., Liu, J. & Russell, J. M. (2022). Calibration and Application of Branched GDGTs to Tibetan Lake Sediments: The Influence of Temperature on the Fall of the Guge Kingdom in Western Tibet, China. *Paleoceanography and Paleoclimatology* 37 (5). <https://doi.org/10.1029/2021PA004393>.
- Liu, X.-L., Summons, R. E. & Hinrichs, K.-U. (2012). Extending the known range of glycerol ether lipids in the environment: structural assignments based on tandem mass spectral fragmentation patterns. *Rapid communications in mass spectrometry : RCM* 26 (19), 2295–2302. <https://doi.org/10.1002/rcm.6355>.
- Liu, Z., Jian, Z., Poulsen, C. J. & Zhao, L. (2019). Isotopic evidence for twentieth-century weakening of the Pacific Walker circulation. *Earth and Planetary Science Letters* 507, 85–93. <https://doi.org/10.1016/j.epsl.2018.12.002>.
- Liu, Z., Zhu, J., Rosenthal, Y., Zhang, X., Otto-Bliesner, B. L., Timmermann, A., Smith, R. S., Lohmann, G., Zheng, W. & Elison Timm, O. (2014). The Holocene temperature conundrum. *Proceedings of the National Academy of Sciences of the United States of America* 111 (34), E3501-5. <https://doi.org/10.1073/pnas.1407229111>.

- Loomis, S. E., Russell, J. M., Verschuren, D., Morrill, C., Cort, G. de, Sinninghe Damsté, J. S., Olago, D., Eggermont, H., Street-Perrott, F. A. & Kelly, M. A. (2017). The tropical lapse rate steepened during the Last Glacial Maximum. *Science advances* 3 (1), e1600815. <https://doi.org/10.1126/sciadv.1600815>.
- Marcott, S. A., Shakun, J. D., Clark, P. U. & Mix, A. C. (2013). A reconstruction of regional and global temperature for the past 11,300 years. *Science* (New York, N.Y.) 339 (6124), 1198–1201. <https://doi.org/10.1126/science.1228026>.
- Marriner, N., Kaniewski, D., Pourkerman, M. & Devillers, B. (2022). Anthropocene tipping point reverses long-term Holocene cooling of the Mediterranean Sea: A meta-analysis of the basin's Sea Surface Temperature records. *Earth-Science Reviews* 227, 103986. <https://doi.org/10.1016/j.earscirev.2022.103986>.
- Milto, K. D. & Bezman-Moseyko, O. S. (2021). Herpetofauna of the Maninjau caldera, West Sumatra, Indonesia, with special account to geckos. *Proceedings of the Zoological Institute RAS* 325 (4), 430–446. <https://doi.org/10.31610/trudyzin/2021.325.4.430>.
- Morii, H., Eguchi, T., Nishihara, M., Kakinuma, K., König, H. & Koga, Y. (1998). A novel ether core lipid with H-shaped C80-isoprenoid hydrocarbon chain from the hyperthermophilic methanogen *Methanothermus fervidus*. *Biochimica et Biophysica Acta (BBA) - Lipids and Lipid Metabolism* 1390 (3), 339–345. [https://doi.org/10.1016/S0005-2760\(97\)00183-5](https://doi.org/10.1016/S0005-2760(97)00183-5).
- Naafs, B., Gallego-Sala, A. V., Inglis, G. N. & Pancost, R. D. (2017b). Refining the global branched glycerol dialkyl glycerol tetraether (brGDGT) soil temperature calibration. *Organic Geochemistry* 106, 48–56. <https://doi.org/10.1016/j.orggeochem.2017.01.009>.
- Naafs, B., Inglis, G. N., Blewett, J., McClymont, E. L., Laurentano, V., Xie, S., Evershed, R. P. & Pancost, R. D. (2019). The potential of biomarker proxies to trace climate, vegetation, and biogeochemical processes in peat: A review. *Global and Planetary Change* 179, 57–79. <https://doi.org/10.1016/j.gloplacha.2019.05.006>.
- Naafs, B., Inglis, G. N., Zheng, Y., Amesbury, M. J., Biester, H., Bindler, R., Blewett, J., Burrows, M. A., Del Castillo Torres, D., Chambers, F. M., Cohen, A. D., Evershed, R. P., Feakins, S. J., Galka, M., Gallego-Sala, A., Gandois, L., Gray, D. M., Hatcher, P. G., Honorio Coronado, E. N., Hughes, P., Huguet, A., Könönen, M., Laggoun-Défarge, F., Lähteenoja, O., Lamentowicz, M., Marchant, R., McClymont, E., Pontevedra-Pombal, X., Ponton, C., Pourmand, A., Rizzuti, A. M., Rochefort, L., Schellekens, J., Vleeschouwer, F. de & Pancost, R. D. (2017a). Introducing global peat-specific temperature and pH calibrations based on brGDGT bacterial lipids. *Geochimica et Cosmochimica Acta* 208, 285–301. <https://doi.org/10.1016/j.gca.2017.01.038>.
- Naafs, B., McCormick, D., Inglis, G. N. & Pancost, R. D. (2018). Archaeal and bacterial H-GDGTs are abundant in peat and their relative abundance is positively correlated with temperature. *Geochimica et Cosmochimica Acta* 227, 156–170. <https://doi.org/10.1016/j.gca.2018.02.025>.
- Naeher, S., Smittenberg, R. H., Gilli, A., Kirilova, E. P., Lotter, A. F. & Schubert, C. J. (2012). Impact of recent lake eutrophication on microbial community changes as revealed by high resolution lipid biomarkers in Rotsee (Switzerland). *Organic Geochemistry* 49, 86–95. <https://doi.org/10.1016/j.orggeochem.2012.05.014>.
- Niedermeyer, E. M., Sessions, A. L., Feakins, S. J. & Mohtadi, M. (2014). Hydroclimate of the western Indo-Pacific Warm Pool during the past 24,000 years. *Proceedings of the National Academy of Sciences of the United States of America* 111 (26), 9402–9406. <https://doi.org/10.1073/pnas.1323585111>.
- Orme, L. C., Miettinen, A., Seidenkrantz, M.-S., Tuominen, K., Pearce, C., Divine, D. V., Oksman, M. & Kuijpers, A. (2021). Mid to late-Holocene sea-surface temperature variability off north-eastern Newfoundland and its linkage to the North Atlantic Oscillation. *The Holocene* 31 (1), 3–15. <https://doi.org/10.1177/0959683620961488>.

- Otto-Bliesner, B. L., Brady, E. C., Clauzet, G., Tomas, R., Levis, S. & Kothavala, Z. (2006). Last Glacial Maximum and Holocene Climate in CCSM3. *Journal of Climate* 19 (11), 2526–2544. <https://doi.org/10.1175/JCLI3748.1>.
- Pancost, R., Hopmans, E. & Sinninghe Damsté, J. (2001). Archaeal lipids in Mediterranean cold seeps: molecular proxies for anaerobic methane oxidation. *Geochimica et Cosmochimica Acta* 65 (10), 1611–1627. [https://doi.org/10.1016/S0016-7037\(00\)00562-7](https://doi.org/10.1016/S0016-7037(00)00562-7).
- Pape, T., Blumenberg, M., Seifert, R., Egorov, V. N., Gulin, S. B. & Michaelis, W. (2005). Lipid geochemistry of methane-seep-related Black Sea carbonates. *Palaeogeography, Palaeoclimatology, Palaeoecology* 227 (1-3), 31–47. <https://doi.org/10.1016/j.palaeo.2005.04.030>.
- Pearson, A. & Ingalls, A. E. (2013). Assessing the Use of Archaeal Lipids as Marine Environmental Proxies. *Annual Review of Earth and Planetary Sciences* 41 (1), 359–384. <https://doi.org/10.1146/annurev-earth-050212-123947>.
- Powers, L., Werne, J. P., Vanderwoude, A. J., Sinninghe Damsté, J. S., Hopmans, E. C. & Schouten, S. (2010). Applicability and calibration of the TEX86 paleothermometer in lakes. *Organic Geochemistry* 41 (4), 404–413. <https://doi.org/10.1016/j.orggeochem.2009.11.009>.
- Prasetyo, I. J., Rifai, H., Syafriani, S. & Putra, R. (2022). Morphological Characteristics and Elemental Composition of Magnetic Minerals from the Volcanic Activity of Lake Maninjau Sediments. *Trends in Sciences* 19 (8), 3428. <https://doi.org/10.48048/tis.2022.3428>.
- Qin, W., Carlson, L. T., Armbrust, E. V., Devol, A. H., Moffett, J. W., Stahl, D. A. & Ingalls, A. E. (2015). Confounding effects of oxygen and temperature on the TEX86 signature of marine Thaumarchaeota. *Proceedings of the National Academy of Sciences of the United States of America* 112 (35), 10979–10984. <https://doi.org/10.1073/pnas.1501568112>.
- Raberg, J. H., Harning, D. J., Crump, S. E., Wet, G. de, Blumm, A., Kopf, S., Geirsdóttir, Á., Miller, G. H. & Sepúlveda, J. (2021). Revised fractional abundances and warm-season temperatures substantially improve brGDGT calibrations in lake sediments. <https://doi.org/10.5194/bg-2021-16>.
- Raberg, J. H., Miller, G. H., Geirsdóttir, Á. & Sepúlveda, J. (2022). Near-universal trends in brGDGT lipid distributions in nature. *Science advances* 8 (20), eabm7625. <https://doi.org/10.1126/sciadv.abm7625>.
- Rattray, J. E. & Smittenberg, R. H. (2020). Separation of Branched and Isoprenoid Glycerol Dialkyl Glycerol Tetraether (GDGT) Isomers in Peat Soils and Marine Sediments Using Reverse Phase Chromatography. *Frontiers in Marine Science* 7, 765. <https://doi.org/10.3389/fmars.2020.539601>.
- Richey, J. N., Hollander, D. J., Flower, B. P. & Eglinton, T. I. (2011). Merging late Holocene molecular organic and foraminiferal-based geochemical records of sea surface temperature in the Gulf of Mexico. *Paleoceanography* 26 (1). <https://doi.org/10.1029/2010PA002000>.
- Rosa, M. de & Gambacorta, A. (1988). The lipids of archaebacteria. *Progress in Lipid Research* 27 (3), 153–175. [https://doi.org/10.1016/0163-7827\(88\)90011-2](https://doi.org/10.1016/0163-7827(88)90011-2).
- Rosa, M. de, Rosa, S. de, Gambacorta, A., Minale, L. & Bu'lock, J. D. (1977). Chemical structure of the ether lipids of thermophilic acidophilic bacteria of the *Caldariella* group. *Phytochemistry* 16 (12), 1961–1965. [https://doi.org/10.1016/0031-9422\(77\)80105-2](https://doi.org/10.1016/0031-9422(77)80105-2).
- Rosenthal, Y., Linsley, B. K. & Oppo, D. W. (2013). Pacific Ocean heat content during the past 10,000 years. *Science (New York, N.Y.)* 342 (6158), 617–621. <https://doi.org/10.1126/science.1240837>.

- Roxy, M. K., Dasgupta, P., McPhaden, M. J., Suematsu, T., Zhang, C. & Kim, D. (2019). Twofold expansion of the Indo-Pacific warm pool warps the MJO life cycle. *Nature* 575 (7784), 647–651. <https://doi.org/10.1038/s41586-019-1764-4>.
- Russell, J. M., Hopmans, E. C., Loomis, S. E., Liang, J. & Sinninghe Damsté, J. S. (2018). Distributions of 5- and 6-methyl branched glycerol dialkyl glycerol tetraethers (brGDGTs) in East African lake sediment: Effects of temperature, pH, and new lacustrine paleotemperature calibrations. *Organic Geochemistry* 117, 56–69. <https://doi.org/10.1016/j.orggeochem.2017.12.003>.
- Santoso, A. B., Triwisesa, E. & Fakhrudin, M. (2021). A Simple Solution for Refining Lake Water Temperature Profiles Data Arrayed from High-Frequency Monitoring Sensors. *OLDI (Oseanologi dan Limnologi di Indonesia)* 6 (1), 25. <https://doi.org/10.14203/oldi.2021.v6i1.324>.
- Schlesinger, W. H. & Bernhardt, E. S. (2020). Inland Waters. In: *Biogeochemistry. The Oceans*. Elsevier, 293–360.
- Schoon, P. L., Kluijver, A. de, Middelburg, J. J., Downing, J. A., Sinninghe Damsté, J. S. & Schouten, S. (2013). Influence of lake water pH and alkalinity on the distribution of core and intact polar branched glycerol dialkyl glycerol tetraethers (GDGTs) in lakes. *Organic Geochemistry* 60, 72–82. <https://doi.org/10.1016/j.orggeochem.2013.04.015>.
- Schouten, S., Baas, M., Hopmans, E. C. & Sinninghe Damsté, J. S. (2008b). An unusual isoprenoid tetraether lipid in marine and lacustrine sediments. *Organic Geochemistry* 39 (8), 1033–1038. <https://doi.org/10.1016/j.orggeochem.2008.01.019>.
- Schouten, S., Hopmans, E. C. & Sinninghe Damsté, J. S. (2004). The effect of maturity and depositional redox conditions on archaeal tetraether lipid palaeothermometry. *Organic Geochemistry* 35 (5), 567–571. <https://doi.org/10.1016/j.orggeochem.2004.01.012>.
- Schouten, S., Hopmans, E. C. & Sinninghe Damsté, J. S. (2013). The organic geochemistry of glycerol dialkyl glycerol tetraether lipids: A review. *Organic Geochemistry* 54, 19–61. <https://doi.org/10.1016/j.orggeochem.2012.09.006>.
- Schouten, S., Hopmans, E. C., Baas, M., Boumann, H., Standfest, S., Könneke, M., Stahl, D. A. & Sinninghe Damsté, J. S. (2008a). Intact membrane lipids of "Candidatus Nitrosopumilus maritimus," a cultivated representative of the cosmopolitan mesophilic group I Crenarchaeota. *Applied and environmental microbiology* 74 (8), 2433–2440. <https://doi.org/10.1128/AEM.01709-07>.
- Schouten, S., Hopmans, E. C., Pancost, R. D. & Damsté, J. S. (2000). Widespread occurrence of structurally diverse tetraether membrane lipids: evidence for the ubiquitous presence of low-temperature relatives of hyperthermophiles. *Proceedings of the National Academy of Sciences of the United States of America* 97 (26), 14421–14426. <https://doi.org/10.1073/pnas.97.26.14421>.
- Schouten, S., Hopmans, E. C., Schefuß, E. & Sinninghe Damsté, J. S. (2002). Distributional variations in marine crenarchaeotal membrane lipids: a new tool for reconstructing ancient sea water temperatures? *Earth and Planetary Science Letters* 204 (1-2), 265–274. [https://doi.org/10.1016/S0012-821X\(02\)00979-2](https://doi.org/10.1016/S0012-821X(02)00979-2).
- Schouten, S., van der Meer, M. T. J., Hopmans, E. C., Rijpstra, W. I. C., Reysenbach, A.-L., Ward, D. M. & Sinninghe Damsté, J. S. (2007). Archaeal and bacterial glycerol dialkyl glycerol tetraether lipids in hot springs of yellowstone national park. *Applied and environmental microbiology* 73 (19), 6181–6191. <https://doi.org/10.1128/AEM.00630-07>.
- Schouten, S., Wakeham, S. G., Hopmans, E. C. & Sinninghe Damsté, J. S. (2003). Biogeochemical evidence that thermophilic archaea mediate the anaerobic oxidation of methane. *Applied and environmental microbiology* 69 (3), 1680–1686. <https://doi.org/10.1128/AEM.69.3.1680-1686.2003>.
- Sinninghe Damsté, J. S., Hopmans, E. C., Pancost, R. D., Schouten, S. & Geenevasen, J. A. J. (2000). Newly discovered non-isoprenoid glycerol dialkyl glycerol tetraether lipids in

- sediments. *Chemical Communications* (17), 1683–1684.
<https://doi.org/10.1039/b004517i>.
- Sinninghe Damsté, J. S., Ossebaar, J., Abbas, B., Schouten, S. & Verschuren, D. (2009). Fluxes and distribution of tetraether lipids in an equatorial African lake: Constraints on the application of the TEX86 palaeothermometer and BIT index in lacustrine settings. *Geochimica et Cosmochimica Acta* 73 (14), 4232–4249.
<https://doi.org/10.1016/j.gca.2009.04.022>.
- Sinninghe Damsté, J. S., Ossebaar, J., Schouten, S. & Verschuren, D. (2012). Distribution of tetraether lipids in the 25-ka sedimentary record of Lake Challa: extracting reliable TEX86 and MBT/CBT palaeotemperatures from an equatorial African lake. *Quaternary Science Reviews* 50, 43–54. <https://doi.org/10.1016/j.quascirev.2012.07.001>.
- Sinninghe Damsté, J. S., Rijpstra, W. I. C., Hopmans, E. C., Uijl, M. J. den, Weijers, J. W. & Schouten, S. (2018). The enigmatic structure of the crenarchaeol isomer. *Organic Geochemistry* 124, 22–28. <https://doi.org/10.1016/j.orggeochem.2018.06.005>.
- Sinninghe Damsté, J. S., Schouten, S., Hopmans, E. C., van Duin, A. C. T. & Geenevasen, J. A. J. (2002). Crenarchaeol: the characteristic core glycerol dibiphytanyl glycerol tetraether membrane lipid of cosmopolitan pelagic crenarchaeota. *Journal of lipid research* 43 (10), 1641–1651. <https://doi.org/10.1194/jlr.M200148-JLR200>.
- Smith, V. C., Staff, R. A., Blockley, S. P., Bronk Ramsey, C., Nakagawa, T., Mark, D. F., Takemura, K. & Danhara, T. (2013). Identification and correlation of visible tephras in the Lake Suigetsu SG06 sedimentary archive, Japan: chronostratigraphic markers for synchronising of east Asian/west Pacific palaeoclimatic records across the last 150 ka. *Quaternary Science Reviews* 67, 121–137.
<https://doi.org/10.1016/j.quascirev.2013.01.026>.
- Sulastri, Hartoto, D. I. & Yuniarti, I. (2016). Environmental condition, fish resources and management of Maninjau lake of west Sumatera. *Indonesian Fisheries Research Journal* 18 (1), 1. <https://doi.org/10.15578/ifrj.18.1.2012.1-12>.
- Thompson, L. G., Mosley-Thompson, E., Davis, M. E., Lin, P. N., Dai, J., Bolzan, J. F. & Yao, T. (1995). A 1000 year climate ice-core record from the Guliya ice cap, China: its relationship to global climate variability. *Annals of Glaciology* 21, 175–181.
<https://doi.org/10.3189/S0260305500015780>.
- Tierney, J. E. & Russell, J. M. (2009). Distributions of branched GDGTs in a tropical lake system: Implications for lacustrine application of the MBT/CBT paleoproxy. *Organic Geochemistry* 40 (9), 1032–1036. <https://doi.org/10.1016/j.orggeochem.2009.04.014>.
- Tierney, J. E., Russell, J. M., Eggermont, H., Hopmans, E. C., Verschuren, D. & Sinninghe Damsté, J. S. (2010). Environmental controls on branched tetraether lipid distributions in tropical East African lake sediments. *Geochimica et Cosmochimica Acta* 74 (17), 4902–4918. <https://doi.org/10.1016/j.gca.2010.06.002>.
- Tierney, J. E., Schouten, S., Pitcher, A., Hopmans, E. C. & Sinninghe Damsté, J. S. (2012). Core and intact polar glycerol dialkyl glycerol tetraethers (GDGTs) in Sand Pond, Warwick, Rhode Island (USA): Insights into the origin of lacustrine GDGTs. *Geochimica et Cosmochimica Acta* 77, 561–581.
<https://doi.org/10.1016/j.gca.2011.10.018>.
- UNESCO World Heritage (2022). Messel Pit Fossil Site. Available online at <https://whc.unesco.org/en/list/720> (accessed 8/31/2022).
- Van Bree, L. G. J., Peterse, F., Baxter, A. J., Crop, W. de, van Grinsven, S., Villanueva, L., Verschuren, D. & Sinninghe Damsté, J. S. (2020). Seasonal variability and sources of in situ brGDGT production in a permanently stratified African crater lake. *Biogeosciences* 17 (21), 5443–5463. <https://doi.org/10.5194/bg-17-5443-2020>.
- Verschuren, D., Sinninghe Damsté, J. S., Moernaut, J., Kristen, I., Blaauw, M., Fagot, M. & Haug, G. H. (2009). Half-precessional dynamics of monsoon rainfall near the East African Equator. *Nature* 462 (7273), 637–641. <https://doi.org/10.1038/nature08520>.

- Waldmann, N., Anselmetti, F. S., Ariztegui, D., Austin Jr, J. A., Pirouz, M., Moy, C. M. & Dunbar, R. (2011). Holocene mass-wasting events in Lago Fagnano, Tierra del Fuego (54°S): implications for paleoseismicity of the Magallanes-Fagnano transform fault. *Basin Research* 23 (2), 171–190. <https://doi.org/10.1111/j.1365-2117.2010.00489.x>.
- Weatherspark Maninjau (2022). Maninjau Climate, Weather By Month, Average Temperature (Indonesia) - Weather Spark. Available online at <https://weatherspark.com/y/113272/Average-Weather-in-Maninjau-Indonesia-Year-Round> (accessed 8/30/2022).
- Weber, Y., De Jonge, C., Rijpstra, W. I. C., Hopmans, E. C., Stadnitskaia, A., Schubert, C. J., Lehmann, M. F., Sinninghe Damsté, J. S. & Niemann, H. (2015). Identification and carbon isotope composition of a novel branched GDGT isomer in lake sediments: Evidence for lacustrine branched GDGT production. *Geochimica et Cosmochimica Acta* 154, 118–129. <https://doi.org/10.1016/j.gca.2015.01.032>.
- Weber, Y., Sinninghe Damsté, J. S., Zopfi, J., De Jonge, C., Gilli, A., Schubert, C. J., Lepori, F., Lehmann, M. F. & Niemann, H. (2018). Redox-dependent niche differentiation provides evidence for multiple bacterial sources of glycerol tetraether lipids in lakes. *Proceedings of the National Academy of Sciences of the United States of America* 115 (43), 10926–10931. <https://doi.org/10.1073/pnas.1805186115>.
- Weijers, J. W. H., Schouten, S., Hopmans, E. C., Geenevasen, J. A. J., David, O. R. P., Coleman, J. M., Pancost, R. D. & Sinninghe Damsté, J. S. (2006a). Membrane lipids of mesophilic anaerobic bacteria thriving in peats have typical archaeal traits. *Environmental microbiology* 8 (4), 648–657. <https://doi.org/10.1111/j.1462-2920.2005.00941.x>.
- Weijers, J. W., Schouten, S., Spaargaren, O. C. & Sinninghe Damsté, J. S. (2006b). Occurrence and distribution of tetraether membrane lipids in soils: Implications for the use of the TEX86 proxy and the BIT index. *Organic Geochemistry* 37 (12), 1680–1693. <https://doi.org/10.1016/j.orggeochem.2006.07.018>.
- Weijers, J. W., Schouten, S., van den Donker, J. C., Hopmans, E. C. & Sinninghe Damsté, J. S. (2007). Environmental controls on bacterial tetraether membrane lipid distribution in soils. *Geochimica et Cosmochimica Acta* 71 (3), 703–713. <https://doi.org/10.1016/j.gca.2006.10.003>.
- Wu, J., Yang, H., Pancost, R. D., Naafs, B. D. A., Qian, S., Dang, X., Sun, H., Pei, H., Wang, R., Zhao, S. & Xie, S. (2021). Variations in dissolved O₂ in a Chinese lake drive changes in microbial communities and impact sedimentary GDGT distributions. *Chemical Geology* 579, 120348. <https://doi.org/10.1016/j.chemgeo.2021.120348>.
- Yang, H., Ding, W., Zhang, C. L., Wu, X., Ma, X., He, G., Huang, J. & Xie, S. (2011). Occurrence of tetraether lipids in stalagmites: Implications for sources and GDGT-based proxies. *Organic Geochemistry* 42 (1), 108–115. <https://doi.org/10.1016/j.orggeochem.2010.11.006>.
- Yang, H., Lü, X., Ding, W., Lei, Y., Dang, X. & Xie, S. (2015). The 6-methyl branched tetraethers significantly affect the performance of the methylation index (MBT') in soils from an altitudinal transect at Mount Shennongjia. *Organic Geochemistry* 82, 42–53. <https://doi.org/10.1016/j.orggeochem.2015.02.003>.
- Yodfiatfinda, Y. (2017). Impact of Climate Change on Floating Net Fish Farming in Maninjau Lake, West Sumatera.
- Zhang, Y. G., Zhang, C. L., Liu, X.-L., Li, L., Hinrichs, K.-U. & Noakes, J. E. (2011). Methane Index: A tetraether archaeal lipid biomarker indicator for detecting the instability of marine gas hydrates. *Earth and Planetary Science Letters* 307 (3-4), 525–534. <https://doi.org/10.1016/j.epsl.2011.05.031>.
- Zhang, Z., Smittenberg, R. H. & Bradley, R. S. (2016). GDGT distribution in a stratified lake and implications for the application of TEX86 in paleoenvironmental reconstructions. *Scientific reports* 6, 34465. <https://doi.org/10.1038/srep34465>.

Appendix

The raw data of the Man-18-44A HPLC-APCI-MS measurements are stored in an electronic appendix (Hällberg et al. 2022b).

Table 3: MBT'_{5ME} proxy (De Jonge et al. 2014) calculated for two HPLC-APCI-MS measurements of the sediment core Man-18-44A of Lake Maninjau, west Sumatra, Indonesia. To see is the average of both analyses Man-1 and Man-2 and standard deviations (SD).

Depth [cm]		MBT'_{5ME} Run 1	MBT'_{5ME} Run 2	MBT'_{5ME} average	MBT'_{5ME} SD
0	0.3	0.8448	-	0.8448	-
0.3	1.3	0.8293	0.8424	0.8359	0.00927
1.3	2.3	0.8137	0.8037	0.8087	0.00705
2.3	3.3	0.9008	0.9033	0.902	0.001764
3.3	3.7	0.9069	0.9184	0.9127	0.00817
3.7	4.5	0.9193	0.9285	0.9239	0.006502
4.5	5.5	0.8993	0.908	0.9037	0.006117
5.5	6.5	0.8812	0.8706	0.8759	0.007502
6.5	7.5	0.8727	0.876	0.8744	0.00227
7.5	8.5	0.8808	0.8816	0.8812	0.0005673
8.5	9.5	0.8715	0.8803	0.8759	0.006218
9.5	10.5	0.7891	0.7914	0.7903	0.001657
10.5	11.5	0.8431	0.8484	0.8457	0.003715
11.5	12.4	0.834	0.8454	0.8397	0.008121
12.4	13	0.85	0.8574	0.8537	0.005199
13	14	0.8179	0.831	0.8244	0.009294
14	15	0.8555	0.8532	0.8544	0.001579
15	15.5	0.9626	0.8117	0.8871	0.1068
15.5	16.3	0.817	0.827	0.822	0.007103
16.3	17.3	0.8044	0.8052	0.8048	0.0005221
17.3	17.9	0.7742	0.7819	0.7781	0.005387
17.9	18.9	0.796	0.8027	0.7994	0.004772
18.9	19.9	0.8525	0.8611	0.8568	0.006058
19.9	20.9	0.8333	0.8367	0.835	0.002418
20.9	21.4	0.8478	0.8413	0.8445	0.004559
21.4	21.8	0.8159	0.8261	0.821	0.007165
21.8	22.8	0.8355	0.8373	0.8364	0.001255
22.8	23.8	0.8287	0.8269	0.8278	0.001296
23.8	24.8	0.8587	0.8653	0.862	0.004723
24.8	25.8	0.9548	0.8949	0.9249	0.04238
25.8	26.3	0.8501	0.8336	0.8419	0.01169
26.3	26.6	0.7794	0.7851	0.7823	0.004076
26.6	27.6	0.7885	0.7847	0.7866	0.002649
27.6	28.6	0.8147	0.8164	0.8156	0.001218
28.6	29	0.8153	0.8116	0.8134	0.002613
29	29.5	0.668	0.8308	0.7494	0.1151
29.5	30.5	0.8262	0.8331	0.8296	0.004827
30.5	31.5	0.7832	0.7893	0.7862	0.004361

31.5	32.5	0.8207	0.825	0.8229	0.003051
32.5	33.4	0.7914	0.7984	0.7949	0.00492
33.4	34.1	0.8151	0.8183	0.8167	0.00226
34.1	35.1	0.7713	0.8418	0.8066	0.04989
35.1	36.1	0.842	0.8406	0.8413	0.0009529
36.1	36.8	0.7861	0.7867	0.7864	0.000451
36.8	37.7	0.6324	0.7773	0.7048	0.1024
37.7	38.7	0.8341	0.8293	0.8317	0.003372
38.7	39.2	0.7616	0.7613	0.7615	0.0002604
39.2	40	0.8069	0.8244	0.8156	0.01237
40	41	0.8088	0.8228	0.8158	0.009907
41	42	0.7994	0.8069	0.8031	0.0053
Mean				0.8311	0.02886

Table 4: brGMGTI proxy (Baxter et al. 2019) calculated for two HPLC-APCI-MS measurements of the sediment core Man-18-44A of Lake Maninjau, west Sumatra, Indonesia. To see is the average of both analyses Man-1 and Man-2 and standard deviations (SD).

Depth [cm]		brGMGTI Man-1	brGMGTI Man-2	brGMGTI average	brGMGTI SD
0	0.3	-	-	-	-
0.3	1.3	0.8168	0.8348	0.8258	0.01275
1.3	2.3	0.842	0.8221	0.8321	0.01408
2.3	3.3	0.8278	0.8491	0.8384	0.01508
3.3	3.7	0.8345	0.7913	0.8129	0.0305
3.7	4.5	0.8011	0.8201	0.8106	0.01341
4.5	5.5	0.8152	0.8341	0.8247	0.01336
5.5	6.5	0.8295	0.8195	0.8245	0.007102
6.5	7.5	0.8352	0.7854	0.8103	0.03524
7.5	8.5	0.8259	0.8365	0.8312	0.007518
8.5	9.5	0.8518	0.8445	0.8481	0.0052
9.5	10.5	0.8108	0.7938	0.8023	0.01202
10.5	11.5	0.8374	0.8047	0.821	0.0231
11.5	12.4	0.8267	0.778	0.8024	0.03443
12.4	13	0.8232	0.7687	0.7959	0.03852
13	14	0.8381	0.8159	0.827	0.01577
14	15	0.8355	0.8318	0.8336	0.002585
15	15.5	0.8522	0.8316	0.8419	0.01455
15.5	16.3	0.8084	0.8085	0.8085	0.00001389
16.3	17.3	0.847	0.8612	0.8541	0.01002
17.3	17.9	0.8357	0.8023	0.819	0.02362
17.9	18.9	0.8517	0.8538	0.8527	0.001536
18.9	19.9	0.8477	0.8209	0.8343	0.01891
19.9	20.9	0.8359	0.7895	0.8127	0.03278
20.9	21.4	0.8655	0.8293	0.8474	0.02555
21.4	21.8	0.8756	0.8595	0.8675	0.01137
21.8	22.8	0.8498	0.8157	0.8327	0.02414
22.8	23.8	0.8473	0.8673	0.8573	0.0142

23.8	24.8	0.8228	0.7832	0.803	0.02796
24.8	25.8	0.8242	0.8176	0.8209	0.004633
25.8	26.3	0.9223	0.8466	0.8844	0.05352
26.3	26.6	0.8524	0.8212	0.8368	0.02203
26.6	27.6	0.8125	0.8009	0.8067	0.008231
27.6	28.6	0.8113	0.8212	0.8163	0.006989
28.6	29	0.8827	0.8674	0.875	0.01084
29	29.5	0.8067	0.8539	0.8303	0.03341
29.5	30.5	0.8486	0.8307	0.8397	0.0126
30.5	31.5	0.8598	0.8164	0.8381	0.0307
31.5	32.5	0.8463	0.8607	0.8535	0.01019
32.5	33.4	0.8155	0.7836	0.7995	0.02252
33.4	34.1	0.819	0.7891	0.804	0.02116
34.1	35.1	0.8172	0.8151	0.8161	0.001452
35.1	36.1	0.7936	0.7616	0.7776	0.02259
36.1	36.8	0.8049	0.7993	0.8021	0.003996
36.8	37.7	0.8509	0.8719	0.8614	0.01478
37.7	38.7	0.8125	0.8175	0.815	0.00358
38.7	39.2	0.7547	0.7183	0.7365	0.02571
39.2	40	0.8272	0.7941	0.8107	0.0234
40	41	0.8215	0.8316	0.8265	0.00716
41	42	0.8265	0.7906	0.8085	0.02534
Mean				0.8251	0.02073

Table 5: CBT proxy (Weijers et al. 2007) calculated for two HPLC-APCI-MS measurements of the sediment core Man-18-44A of Lake Maninjau, west Sumatra, Indonesia. To see is the average of both analyses Man-1 and Man-2 and standard deviations (SD).

Depth [cm]		CBT Man-1	CBT Man-2	CBT average	CBT SD
0	0.3	0.1922	-	0.1922	-
0.3	1.3	0.2109	0.215	0.2129	0.002902
1.3	2.3	0.4802	0.4673	0.4738	0.009126
2.3	3.3	0.2988	0.2841	0.2915	0.01043
3.3	3.7	0.3267	0.3097	0.3182	0.01202
3.7	4.5	0.3031	0.31	0.3066	0.004917
4.5	5.5	0.3291	0.3376	0.3334	0.00602
5.5	6.5	0.2621	0.2718	0.267	0.006913
6.5	7.5	0.2165	0.2312	0.2239	0.01042
7.5	8.5	0.3099	0.3121	0.311	0.001517
8.5	9.5	0.2842	0.3079	0.296	0.01671
9.5	10.5	0.5729	0.6062	0.5895	0.02349
10.5	11.5	0.3957	0.3957	0.3957	4.634E-06
11.5	12.4	0.3575	0.3624	0.36	0.003447
12.4	13	0.3171	0.3375	0.3273	0.0144
13	14	0.4645	0.477	0.4707	0.00886
14	15	0.4331	0.4404	0.4367	0.00517
15	15.5	0.4819	0.4382	0.46	0.03091

15.5	16.3	0.4369	0.4613	0.4491	0.01721
16.3	17.3	0.5034	0.5081	0.5057	0.003329
17.3	17.9	0.6024	0.6187	0.6105	0.01149
17.9	18.9	0.5823	0.6011	0.5917	0.0133
18.9	19.9	0.4853	0.4884	0.4868	0.002171
19.9	20.9	0.5197	0.5697	0.5447	0.03535
20.9	21.4	0.4475	0.4783	0.4629	0.02176
21.4	21.8	0.4895	0.548	0.5188	0.04135
21.8	22.8	0.4803	0.5498	0.5151	0.04915
22.8	23.8	0.4583	0.4987	0.4785	0.02854
23.8	24.8	0.5616	0.5622	0.5619	0.0004183
24.8	25.8	0.7314	0.6905	0.711	0.02891
25.8	26.3	0.4877	0.4859	0.4868	0.001259
26.3	26.6	0.5497	0.5156	0.5326	0.02412
26.6	27.6	0.7339	0.6275	0.6807	0.07521
27.6	28.6	0.5244	0.5394	0.5319	0.01066
28.6	29	0.5232	0.4994	0.5113	0.01687
29	29.5	0.532	0.543	0.5375	0.007794
29.5	30.5	0.5399	0.5575	0.5487	0.01246
30.5	31.5	0.5237	0.5746	0.5491	0.03602
31.5	32.5	0.6215	0.6378	0.6297	0.01152
32.5	33.4	0.4739	0.5042	0.4891	0.02137
33.4	34.1	0.5685	0.5827	0.5756	0.01009
34.1	35.1	0.5058	0.548	0.5269	0.02984
35.1	36.1	0.4684	0.4708	0.4696	0.001679
36.1	36.8	0.4151	0.4428	0.429	0.01958
36.8	37.7	0.6386	0.4423	0.5404	0.1388
37.7	38.7	0.4807	0.4796	0.4802	0.0007956
38.7	39.2	0.3605	0.4071	0.3838	0.03297
39.2	40	0.4482	0.4576	0.4529	0.006632
40	41	0.5151	0.5167	0.5159	0.001137
41	42	0.4748	0.493	0.4839	0.01287
Mean				0.4612	0.0291

Table 6: CBT'_{5ME} proxy (De Jonge et al. 2014) calculated for two HPLC-APCI-MS measurements of the sediment core Man-18-44A of Lake Maninjau, west Sumatra, Indonesia. To see is the average of both analyses Man-1 and Man-2 and standard deviations (SD).

Depth [cm]		CBT'_{5ME} Man-1	CBT'_{5ME} Man-2	CBT'_{5ME} average	CBT'_{5ME} SD
0	0.3	0.4724	-	0.4724	-
0.3	1.3	0.4657	0.4611	0.4634	0.003235
1.3	2.3	0.6537	0.6334	0.6435	0.0144
2.3	3.3	0.4533	0.4338	0.4435	0.0138
3.3	3.7	0.4659	0.4481	0.457	0.01262
3.7	4.5	0.4496	0.4481	0.4488	0.001051
4.5	5.5	0.451	0.4776	0.4643	0.01876
5.5	6.5	0.4284	0.4389	0.4337	0.007411

6.5	7.5	0.3732	0.3752	0.3742	0.001412
7.5	8.5	0.4142	0.4118	0.413	0.001671
8.5	9.5	0.3762	0.3902	0.3832	0.009868
9.5	10.5	0.6588	0.699	0.6789	0.02841
10.5	11.5	0.4979	0.5013	0.4996	0.002415
11.5	12.4	0.4743	0.4611	0.4677	0.009367
12.4	13	0.4354	0.4397	0.4375	0.003013
13	14	0.5758	0.5742	0.575	0.001094
14	15	0.5227	0.5377	0.5302	0.01062
15	15.5	0.4497	0.5308	0.4903	0.05735
15.5	16.3	0.5129	0.5407	0.5268	0.01962
16.3	17.3	0.5624	0.5584	0.5604	0.002869
17.3	17.9	0.6339	0.6437	0.6388	0.006927
17.9	18.9	0.6562	0.6779	0.6671	0.01538
18.9	19.9	0.5841	0.5794	0.5817	0.003299
19.9	20.9	0.5819	0.633	0.6074	0.03616
20.9	21.4	0.5377	0.5466	0.5421	0.006292
21.4	21.8	0.5478	0.5871	0.5675	0.02775
21.8	22.8	0.6846	0.5772	0.6309	0.07591
22.8	23.8	0.5559	0.5677	0.5618	0.008328
23.8	24.8	0.6302	0.6046	0.6174	0.0181
24.8	25.8	0.7314	0.7255	0.7285	0.004197
25.8	26.3	0.5682	0.5412	0.5547	0.01914
26.3	26.6	0.5713	0.5388	0.5551	0.02293
26.6	27.6	0.6222	0.6619	0.6421	0.02803
27.6	28.6	0.59	0.609	0.5995	0.01349
28.6	29	0.609	0.5599	0.5844	0.03469
29	29.5	0.7299	0.6164	0.6731	0.08023
29.5	30.5	0.5912	0.6002	0.5957	0.006366
30.5	31.5	0.572	0.6063	0.5891	0.02421
31.5	32.5	0.6557	0.6738	0.6647	0.01276
32.5	33.4	0.5539	0.556	0.5549	0.001507
33.4	34.1	0.6009	0.6136	0.6073	0.008968
34.1	35.1	0.3948	0.6222	0.5085	0.1608
35.1	36.1	0.5577	0.5504	0.5541	0.005154
36.1	36.8	0.4923	0.5137	0.503	0.01518
36.8	37.7	0.623	0.4718	0.5474	0.1069
37.7	38.7	0.5348	0.5365	0.5357	0.001155
38.7	39.2	0.4475	0.4685	0.458	0.01488
39.2	40	0.5184	0.5205	0.5194	0.001456
40	41	0.575	0.5719	0.5734	0.002208
41	42	0.55	0.5619	0.5559	0.008418
Mean				0.5457	0.03574

Table 7: CBT_{peat} proxy (Naafs et al. 2017a) calculated for two HPLC-APCI-MS measurements of the sediment core Man-18-44A of Lake Maninjau, west Sumatra, Indonesia. To see is the average of both analyses Man-1 and Man-2 and standard deviations (SD).

Depth [cm]		CBT_{peat} Man-1	CBT_{peat} Man-2	CBT_{peat} average	CBT_{peat} SD
0	0.3	0.1836	-	0.1836	-
0.3	1.3	0.1741	0.1902	0.1821	0.01141
1.3	2.3	-0.141	-0.1331	-0.137	0.005567
2.3	3.3	0.05137	0.06689	0.05913	0.01098
3.3	3.7	0.04631	0.05195	0.04913	0.003988
3.7	4.5	0.09169	0.07803	0.08486	0.009658
4.5	5.5	0.0653	0.05888	0.06209	0.004543
5.5	6.5	0.07525	0.08252	0.07889	0.005138
6.5	7.5	0.1444	0.1256	0.135	0.01325
7.5	8.5	0.04073	0.008624	0.02468	0.02271
8.5	9.5	-0.03148	-0.03862	-0.03505	0.005045
9.5	10.5	-0.2682	-0.3019	-0.2851	0.02383
10.5	11.5	-0.1363	-0.137	-0.1366	0.000501
11.5	12.4	-0.1017	-0.1341	-0.1179	0.02292
12.4	13	-0.0671	-0.07908	-0.07309	0.008468
13	14	-0.1983	-0.2005	-0.1994	0.001525
14	15	-0.1493	-0.1449	-0.1471	0.003102
15	15.5	-0.2212	-0.1439	-0.1825	0.05464
15.5	16.3	-0.1175	-0.149	-0.1333	0.02231
16.3	17.3	-0.1829	-0.1789	-0.1809	0.002839
17.3	17.9	-0.275	-0.2943	-0.2847	0.01361
17.9	18.9	-0.2838	-0.3119	-0.2979	0.01985
18.9	19.9	-0.1846	-0.1917	-0.1881	0.004979
19.9	20.9	-0.1825	-0.2313	-0.2069	0.03451
20.9	21.4	-0.1328	-0.1463	-0.1396	0.009514
21.4	21.8	-0.1431	-0.1404	-0.1417	0.00188
21.8	22.8	-0.4426	-0.1344	-0.2885	0.2179
22.8	23.8	-0.1418	-0.1435	-0.1426	0.001173
23.8	24.8	-0.167	-0.1549	-0.161	0.008547
24.8	25.8	-0.6739	-0.1512	-0.4125	0.3696
25.8	26.3	-0.1233	-0.1312	-0.1273	0.005549
26.3	26.6	-0.1543	-0.1442	-0.1493	0.007137
26.6	27.6	-0.2143	-0.2183	-0.2163	0.002833
27.6	28.6	-0.1867	-0.2107	-0.1987	0.01699
28.6	29	-0.2027	-0.1809	-0.1918	0.01542
29	29.5	-0.5037	-0.1541	-0.3289	0.2472
29.5	30.5	-0.2301	-0.2536	-0.2418	0.01662
30.5	31.5	-0.1774	-0.1987	-0.188	0.01509
31.5	32.5	-0.3007	-0.3127	-0.3067	0.008471
32.5	33.4	-0.1837	-0.1688	-0.1762	0.01056
33.4	34.1	-0.2165	-0.2458	-0.2311	0.02072
34.1	35.1	-0.1433	-0.2065	-0.1749	0.04473

35.1	36.1	-0.1379	-0.133	-0.1354	0.003405
36.1	36.8	-0.1108	-0.1517	-0.1312	0.02892
36.8	37.7	-0.5409	-0.1767	-0.3588	0.2575
37.7	38.7	-0.1913	-0.2026	-0.197	0.007981
38.7	39.2	-0.1143	-0.1249	-0.1196	0.007491
39.2	40	-0.1801	-0.1866	-0.1833	0.004593
40	41	-0.2384	-0.2309	-0.2347	0.005307
41	42	-0.2245	-0.2143	-0.2194	0.0072
Mean				-0.1428	0.08133

Table 8: CBT' proxy (De Jonge et al. 2014) calculated for two HPLC-APCI-MS measurements of the sediment core Man-18-44A of Lake Maninjau, west Sumatra, Indonesia. To see is the average of both analyses Man-1 and Man-2 and standard deviations (SD).

Depth [cm]		CBT' Man-1	CBT' Man-2	CBT' average	CBT' SD
0	0.3	0.07709	-	0.07709	-
0.3	1.3	0.06459	0.08705	0.07582	0.01588
1.3	2.3	-0.2935	-0.2922	-0.2929	0.0009235
2.3	3.3	-0.1072	-0.09102	-0.09909	0.01142
3.3	3.7	-0.1076	-0.1066	-0.1071	0.0007088
3.7	4.5	-0.05053	-0.07035	-0.06044	0.01402
4.5	5.5	-0.08963	-0.0818	-0.08571	0.005542
5.5	6.5	-0.08115	-0.06249	-0.07182	0.0132
6.5	7.5	-0.004905	-0.03051	-0.01771	0.0181
7.5	8.5	-0.1377	-0.1869	-0.1623	0.03485
8.5	9.5	-0.2764	-0.2706	-0.2735	0.004111
9.5	10.5	-0.475	-0.5058	-0.4904	0.02177
10.5	11.5	-0.3652	-0.3666	-0.3659	0.001002
11.5	12.4	-0.3165	-0.3876	-0.3521	0.05025
12.4	13	-0.2933	-0.3118	-0.3026	0.01309
13	14	-0.418	-0.4238	-0.4209	0.004077
14	15	-0.3703	-0.3483	-0.3593	0.01557
15	15.5	-0.5695	-0.3551	-0.4623	0.1516
15.5	16.3	-0.3244	-0.3572	-0.3408	0.0232
16.3	17.3	-0.3953	-0.3887	-0.392	0.004686
17.3	17.9	-0.5031	-0.5284	-0.5158	0.0179
17.9	18.9	-0.5029	-0.5303	-0.5166	0.01936
18.9	19.9	-0.3847	-0.4016	-0.3932	0.01199
19.9	20.9	-0.3848	-0.4322	-0.4085	0.03355
20.9	21.4	-0.3254	-0.3374	-0.3314	0.008501
21.4	21.8	-0.3473	-0.3188	-0.333	0.02014
21.8	22.8	-0.7672	-0.3074	-0.5373	0.3251
22.8	23.8	-0.341	-0.329	-0.335	0.008496
23.8	24.8	-0.333	-0.3304	-0.3317	0.001795
24.8	25.8	-1.327	-0.2736	-0.8001	0.7445
25.8	26.3	-0.3149	-0.3221	-0.3185	0.005109
26.3	26.6	-0.3521	-0.3453	-0.3487	0.004812

26.6	27.6	-0.4116	-0.3965	-0.404	0.01068
27.6	28.6	-0.3872	-0.4094	-0.3983	0.01569
28.6	29	-0.4045	-0.3915	-0.398	0.009208
29	29.5	-0.8532	-0.3228	-0.588	0.375
29.5	30.5	-0.4571	-0.487	-0.472	0.02114
30.5	31.5	-0.3867	-0.3922	-0.3895	0.003885
31.5	32.5	-0.527	-0.5358	-0.5314	0.006209
32.5	33.4	-0.3976	-0.374	-0.3858	0.01668
33.4	34.1	-0.4135	-0.4518	-0.4326	0.02709
34.1	35.1	-0.4618	-0.3919	-0.4268	0.04941
35.1	36.1	-0.3278	-0.3263	-0.327	0.00102
36.1	36.8	-0.3259	-0.3757	-0.3508	0.03515
36.8	37.7	-1.113	-0.4396	-0.7765	0.4764
37.7	38.7	-0.3958	-0.4195	-0.4076	0.01674
38.7	39.2	-0.3628	-0.3662	-0.3645	0.002419
39.2	40	-0.4177	-0.4313	-0.4245	0.009654
40	41	-0.4786	-0.4673	-0.4729	0.007933
41	42	-0.4789	-0.4428	-0.4609	0.0255
Mean				-0.3537	0.1475

Table 9: TEX_{86} proxy (Schouten et al. 2002) calculated for two HPLC-APCI-MS measurements of the sediment core Man-18-44A of Lake Maninjau, west Sumatra, Indonesia. To see is the average of both analyses Man-1 and Man-2 and standard deviations (SD).

Depth [cm]		TEX_{86} Man-1	TEX_{86} Man-2	TEX_{86} average	TEX_{86} SD
0	0.3	-	-	-	-
0.3	1.3	0.31	0.1043	0.2071	0.2071
1.3	2.3	0.5507	0.6578	0.6043	0.6043
2.3	3.3	0.6291	0.7018	0.6655	0.6655
3.3	3.7	0.7069	0.7748	0.7408	0.7408
3.7	4.5	0.724	0.7524	0.7382	0.7382
4.5	5.5	0.7939	0.7985	0.7962	0.7962
5.5	6.5	0.7362	0.7775	0.7568	0.7568
6.5	7.5	0.5828	0.7002	0.6415	0.6415
7.5	8.5	0.7675	0.797	0.7823	0.7823
8.5	9.5	0.7732	0.7875	0.7803	0.7803
9.5	10.5	0.7474	0.7546	0.751	0.751
10.5	11.5	0.767	0.8202	0.7936	0.7936
11.5	12.4	0.8143	0.8104	0.8123	0.8123
12.4	13	0.8045	0.8334	0.819	0.819
13	14	0.793	0.8199	0.8065	0.8065
14	15	0.7764	0.8188	0.7976	0.7976
15	15.5	0.8172	0.8151	0.8161	0.8161
15.5	16.3	0.8326	0.834	0.8333	0.8333
16.3	17.3	0.7869	0.7707	0.7788	0.7788
17.3	17.9	0.7102	0.7458	0.728	0.728
17.9	18.9	0.7199	0.7793	0.7496	0.7496

18.9	19.9	0.7915	0.8176	0.8045	0.8045
19.9	20.9	0.7816	0.7942	0.7879	0.7879
20.9	21.4	0.8136	0.8219	0.8178	0.8178
21.4	21.8	0.7883	0.8071	0.7977	0.7977
21.8	22.8	0.7925	0.8273	0.8099	0.8099
22.8	23.8	0.7567	0.8049	0.7808	0.7808
23.8	24.8	0.7949	0.812	0.8034	0.8034
24.8	25.8	0.8324	0.8586	0.8455	0.8455
25.8	26.3	0.8115	0.844	0.8278	0.8278
26.3	26.6	0.7402	0.7896	0.7649	0.7649
26.6	27.6	0.7612	0.7947	0.7779	0.7779
27.6	28.6	0.7884	0.8142	0.8013	0.8013
28.6	29	0.8109	0.8293	0.8201	0.8201
29	29.5	0.7888	0.8389	0.8139	0.8139
29.5	30.5	0.7413	0.8173	0.7793	0.7793
30.5	31.5	0.8001	0.8141	0.8071	0.8071
31.5	32.5	0.772	0.8152	0.7936	0.7936
32.5	33.4	0.7503	0.7928	0.7715	0.7715
33.4	34.1	0.8024	0.8275	0.8149	0.8149
34.1	35.1	0.7602	0.8273	0.7938	0.7938
35.1	36.1	0.7807	0.8126	0.7966	0.7966
36.1	36.8	0.6136	0.7656	0.6896	0.6896
36.8	37.7	0.6643	0.8077	0.736	0.736
37.7	38.7	0.6475	0.7431	0.6953	0.6953
38.7	39.2	0.5883	0.6673	0.6278	0.6278
39.2	40	0.6812	0.7319	0.7066	0.7066
40	41	0.6938	0.7786	0.7362	0.7362
41	42	0.7126	0.7812	0.7469	0.7469
Mean				0.7581	0.04468

Declaration

I hereby declare that I have written this thesis independently and have not used any sources or aids other than those acknowledged. This thesis has not previously been submitted for the award of an academic degree.

Hiermit erkläre ich, dass ich die vorliegende Arbeit selbstständig verfasst und keine anderen als die angegebenen Quellen und Hilfsmittel benutzt habe. Diese Arbeit wurde zuvor noch nicht zur Erlangung eines akademischen Grades eingereicht.

Bayreuth, 15.09.2022

A handwritten signature in blue ink that reads "Yolanda Schankat". The signature is written in a cursive style and is underlined.

Yolanda Liane Schankat